Behavior of Horizontally Curved Steel I-Girders During Lifting

by

Andrew Clayton Schuh, B.S.C.E

Thesis

Presented to the Faculty of the Graduate School of

The University of Texas at Austin

in Partial Fulfillment

of the Requirements

for the Degree of

Master of Science in Engineering

The University of Texas at Austin

May 2008

Behavior of Horizontally Curved Steel I-Girders During Lifting

APPROVED BY
SUPERVISING COMMITTEE:

Karl H. Frank, Supervisor

Todd A. Helwig

Dedication

To my parents, whose love and support have made this possible.

Acknowledgements

I would like to thank the Texas Department of Transportation for providing the funding for my project and graduate education. I have enjoyed my time at UT immensely, and am very thankful for it.

I am grateful to all involved with the research project and who helped along the way. Thank you to Karl Frank and Todd Helwig for their guidance over the course of the project. Dr. Frank's advice and recommendations during the writing of this thesis were invaluable. I would like to thank those involved with the field work performed during my time at the lab. Team Helwig set a new standard for field testing efficiency. To my PhD student, Jason Stith, thank you for your patience, guidance, and hard work on all aspects of the project. I have learned a great deal from you.

Finally, thank you to my family. Their love and support have made me who I am today, and I owe them everything.

Andrew C. Schuh

May 2, 2008

Behavior of Horizontally Curved Steel I-Girders During Lifting

Andrew Clayton Schuh, M.S.E.

The University of Texas at Austin, 2008

SUPERVISOR: Karl Frank

The analysis of curved I-girders can be challenging because of the interaction of torsional and bending stresses. The St. Venant torsional stiffness of I-shaped girders is relatively small due to the open section. The warping stiffness of the girder therefore plays an important part in resisting the torques that can result from horizontal curvature. In highly curved girders, the warping stresses can become large and perhaps even greater than the bending stresses. There is little guidance, however, from AASHTO or other literature regarding how to account for these stresses or how to consider girder safety and serviceability during critical stages for girder stability such as the early stages of construction when all of the bracing is not installed. The potentially critical construction stage covered in this thesis is the lifting of curved I-girders. Field studies were conducted where data was collected for the validation of a 3-D finite element

model. The model was used to improve understanding of curved girder behavior during lifting.

Upon validation, the finite element model was used to conduct a parametric study of the buckling behavior of a curved girder during lifting. Specifically, the effect of the locations where the crane's lifting apparatus is attached along the girder length is investigated. The serviceability aspect of this parameter i.e. potentially excessive rotations is also discussed. Recommendations are presented to provide guidance for the safe lifting of horizontally curved steel I-girders.

Table of Contents

List of Tables

List of Figures

CHAPTER 1

Introduction

1.1 MOTIVATION

The contents of this thesis are intended to be referenced by engineers needing information on the behavior of horizontally curved steel I-girders during the lifting process. Very little information is available from AASHTO or other literature on this subject; a deficiency that this document aims to correct.

Individual horizontally curved girders see a wide range of support conditions and loading during various stages during construction. Girder stability during erection is often critical due to the variability in the bracing that is present during the process. Recent failures during construction on bridges in Illinois and Colorado have been blamed on inadequate installation of the bracing. Figure 1.1 shows the failure of the bridge in Illinois.

Figure 1.1 Curved Bridge Collapse

In the early 1990s, approximately a quarter of the steel bridges being constructed in the United States were curved [Structural Stability Research Council (SSRC) 1991]; a statistic that further highlights the need for adequate guidelines for curved girder lifting and analysis. The purpose of this document is to provide recommendations and guidelines for lifting curved I-girders.

1.2 ISSUES AND CHALLENGES OF LIFTING CURVED I-GIRDERS

The interaction between bending and torsional stresses presents a unique challenge to the analysis of curved I-girders. The torsional stiffness of I-shaped girders can be divided into two components: 1) the St. Venant stiffness, and 2) the warping stiffness. The St. Venant stiffness is not sensitive to the support boundary conditions, nor the girder span. The warping term, on the other hand, is sensitive to the boundary conditions and girder span, and is often referred to as the non-uniform torsional stiffness. Due to the presence of cross frames that reduce the unbraced length of the girders, the warping stiffness of I-shaped girders often dominates the total torsional stiffness compared to the St. Venant stiffness in the fully erected bridge. During girder erection when limited bracing is present, the warping stiffness may be significantly reduced and torsional stresses may become relatively large. The torsionally-induced warping stresses in horizontally curved girders can often equal or exceed the girder's bending stresses, which are better understood and typically of primary concern during analysis and design. This thesis presents results from field tests where both bending and warping stresses were monitored. These results and their discussion are presented in Chapter 3.

Another challenge presented by curved I-girders is presented by their geometry. The curvature creates a geometrically unstable situation where a lone girder's tendency is to tip over or rotate. This geometric instability occurs as an attempt to satisfy static equilibrium, since the center of gravity of a curved girder is eccentric to the girder centerline. As a result, when curved girders are staged prior to erection or once a single girder is erected into place, additional supports or bracing is required. Typically, a

2

minimum of three support locations is necessary to satisfy equilibrium. Figure 1.2 shows a bridge where the girders were not appropriately supported, causing a failure.

Figure 1.2 Girder Instability

The girder geometry and static equilibrium must also be addressed during curved girder lifting. Large rotations can be caused by the eccentricity between the girder's center of gravity and the line of support formed by the lifting points. The line of support and eccentricity is shown in Figure 1.3. If these rigid body rotations are not accounted for or controlled, the girders can become very difficult to maneuver and place correctly. Additionally, stress data from lift tests presented in Chapter 3 demonstrates that the rotations cause weak axis bending. The rotation of curved I-girders during lifting is

covered more thoroughly in Chapter 4, where a process for predicting and controlling these rotations is presented.
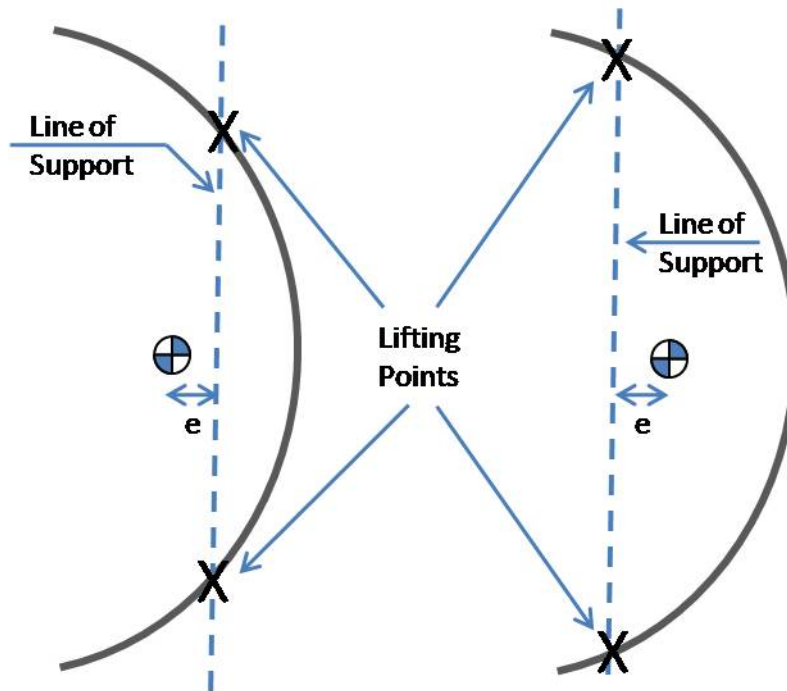
Figure 1.3 Line of Support Formed By Lift Points

1.3 BACKGROUND ON I-GIRDER STABILITY: LATERAL-TORSIONAL BUCKLING

This section details the background and theory regarding girder structural stability during lifting. Structural stability issues include lateral-torsional buckling and adjustment factors that account for moment gradient, curvature, lift point location, etc. Structural stability should not be confused with the geometric stability of curved girders discussed earlier. Because the bracing system assumed during curved bridge design is not yet present during the girder lift, it is crucial to understand girder stability and its effect on curved girder lifting.

The understanding of the limit state of lateral-torsional buckling is very important in the design and analysis of curved I-girders during lifting. Lateral-torsional buckling of a girder occurs when a critical moment is reached, causing both a translation and twisting

4

of the girder section. Figure 1.4 illustrates this buckling mode for a curved I-girder during simulated lifting.
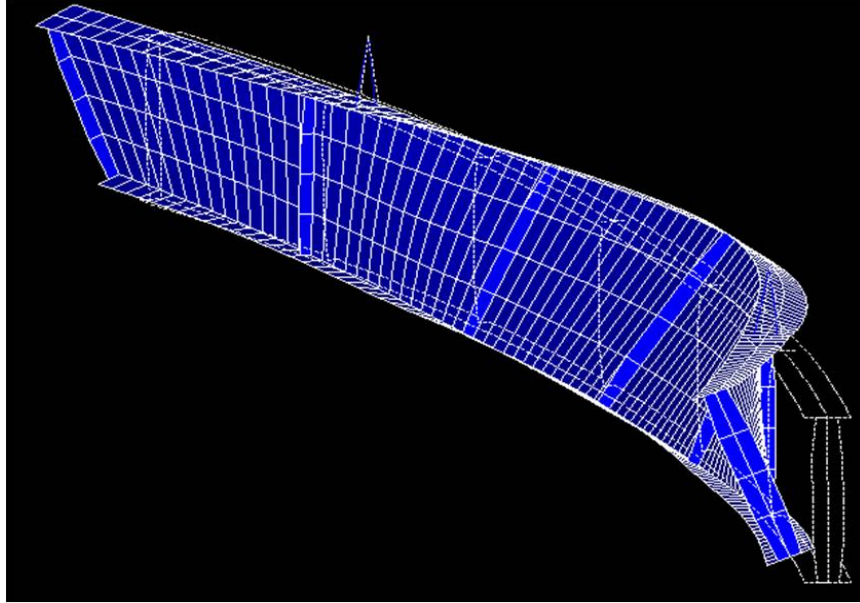
Figure 1.4 Lateral-Torsional Buckling Mode for a Curved I-Girder

The critical moment required to induce lateral-torsional buckling of a beam is given by Timoshenko's equation, given below as Equation 1.1 (Timoshenko 1961).

$$M_o = \frac{\pi}{L_b}\sqrt{EI_y GJ + E^2 I_y C_w \left(\frac{\pi^2}{L_b^2}\right)} \qquad \textbf{\textit{Equation 1.1}}$$

$$L_b = Unbraced\ Length\ of\ Girder\ (in)$$

$$E = Modulus\ of\ Elasticity\ (ksi)$$

$$I_y = Weak\ Axis\ Moment\ of\ Inertia\ (in^4)$$

$$G = Shear\ Modulus\ (ksi)$$

$$J = Torsional\ Constant\ (in^4) = \sum \frac{bt^3}{3}$$

$$C_w = Warping\ Constant\ (in^6) = \frac{I_y h^2}{4}$$

$$h = Distance\ Between\ Flange\ Centroids\ (in)$$

Equation 1.1 and other solutions for lateral-torsional buckling moment provided by most design specifications assume uniform moment acting along the length of the beam. The American Association of State Highway and Transportation Officials (AASHTO) *LRFD Bridge Design Specifications* (AASHTO 2007) uses an equation for the lateral-torsional buckling resistance of the compression flange given in AASHTO Section 6.10.8.2.3.

Equation 1.1 if applicable for the beams subjected to uniform moment loading. Although solutions can be derived for cases with variable moment along the beam length, most specifications make use of a moment modification factor, C_b, to account for moment gradient. The C_b factor is directly applied to the uniform moment solution. In this way, a girder's critical buckling moment can be calculated, as shown in Equation 1.2. For the purposes of this document, M_o will be taken as the Timoshenko solution given by Equation 1.1. Moment gradient factors have been tabulated for common cases and can also be found using expressions in design specifications, provided the girder boundary conditions are satisfied.

$$M_{cr} = C_b M_o \qquad\qquad \textit{Equation 1.2}$$

$$C_b = Adjustment\ Factor\ Derived\ Computationally$$

$$M_o = Critical\ Buckling\ Moment\ for\ Uniform\ Moment$$

The C_b factor can also be determined from a finite element analysis (FEA) on a beam with specific support and load conditions using Equation 1.3. The moment M_{cr} is the maximum moment along the beam length determined from a finite element analysis on the beam with the desired support and loading conditions. The moment M_o represents the buckling capacity for uniform moment loading on a beam and can be determined either from a FEA analysis with constant bending moment or from Equation 1.1.

6

$$C_b = \frac{M_{cr}}{M_o} \qquad\qquad \textbf{\textit{Equation 1.3}}$$

$$M_{cr} = Critical\ Buckling\ Moment\ Determined\ Analytically$$

$$M_o = Critical\ Buckling\ Moment\ for\ Uniform\ Moment$$

A number of expressions have been presented for calculating this adjustment factor to account for different load cases or support conditions. Accounting for moment gradient along a girder's unbraced length is a typical use for the adjustment factor. The American Institute of Steel Construction (AISC) *Load and Resistance Factor Design* (LRFD) specification (*Load* 13th 2005) has incorporated the expression for C_b given in Equation 1.4. The *AASHTO-LRFD Bridge Design Specifications* (AASHTO 2007) uses an equation for C_b to account for moment gradient given in AASHTO Section 6.10.8.2.3.

$$C_b = \frac{12.5 M_{max}}{2.5 M_{max} + 3 M_A + 4 M_B + 3 M_C} \qquad\qquad \textbf{\textit{Equation 1.4}}$$

$$M_{max} = Maximum\ Moment\ Along\ L_b$$

$$M_A = Moment\ at\ .25 L_b$$

$$M_B = Moment\ at\ .5 L_b$$

$$M_C = Moment\ at\ .75 L_b$$

The AISC and AASHTO equations for C_b are suitable for adjusting a critical buckling moment to account for moment gradient along the girder length. However, little guidance has been provided on how to evaluate the lateral-torsional buckling capacity of a curved I-girder during lifting. Current formulations are not appropriate even for the lifting of straight girders. The following section presents formulation of a proper adjustment factor to account for girder lifting. Chapter 5 explains the parametric study and the results that are used along with the process presented in the following section to establish a new adjustment factor, C_L, to account for the lifting of curved I-girders.

1.4 C_L FORMULATION

C_L is formulated in the same manner as the C_b adjustment factor presented earlier. The expression is given in Equation 1.5 below.

$$C_L = \frac{M_{cr}}{M_o}$$ **Equation 1.5**

$M_{cr} = Critical\ Buckling\ Moment\ Determined\ Analytically$

$M_o = Buckling\ Moment\ from\ Equation\ 1.1$

M_{cr} can be determined from an eigenvalue buckling analysis on the curved girder to find the eigenvalue associated with the self-weight, and the maximum moment under the given loading from a static analysis. The relationship is shown in Equation 1.6 below. Equation 1.7 gives the expression for evaluating the maximum static moment for use in Equation 1.6.

$$M_{cr} = \lambda M_{max}$$ **Equation 1.6**

$\lambda = Eigenvalue\ Obtained\ From\ Buckling\ Analysis$

$M_{max} = Maximum\ Moment\ From\ Static\ Analysis$

$$M_{max} = \frac{wa^2}{2} \geq \left| \frac{w(L_{LIFT})^2}{8} - \frac{wa^2}{2} \right|$$ **Equation 1.7**

$w = Factored\ Girder\ Self\ Weight\ (k/ft)$

$a = Cantilever\ Length\ (ft)$

$L_{LIFT} = Span\ Between\ Lift\ Points\ (ft)$
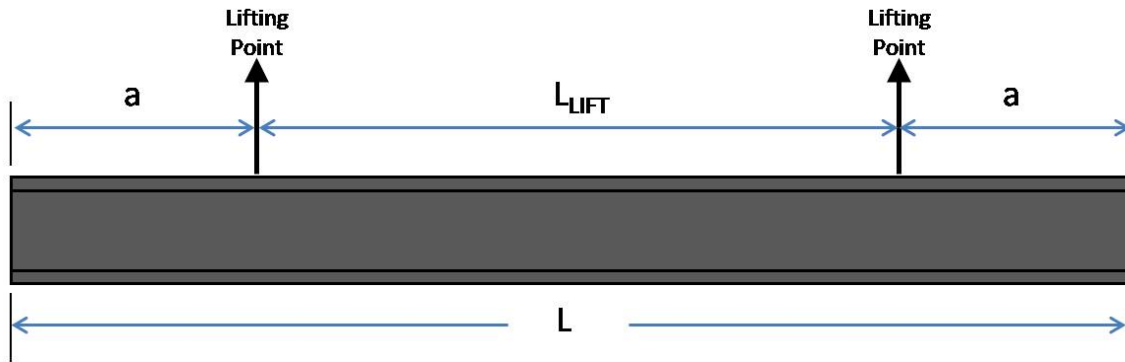
Figure 1.5 Dimension Definitions for Girder Lifting

The calculation of M_{max} was simplified by using a straight girder static analysis to calculate the moments presented in Equation 1.7. Figure 1.6 shows a plan view of a curved girder cantilever (from lift point to girder edge of length a) with the resultant of the self-weight acting at the center of gravity of the curved girder section. The twisting moment induced by the eccentricity can be ignored in this justification for using the straight girder bending moment in lieu of the curved girder bending moment. The calculated curved cantilever moment is equal to the moment at the lift point of a symmetrically lifted curved girder. The equations below can be used to calculate and compare the straight girder bending moment and the curved girder bending moment.
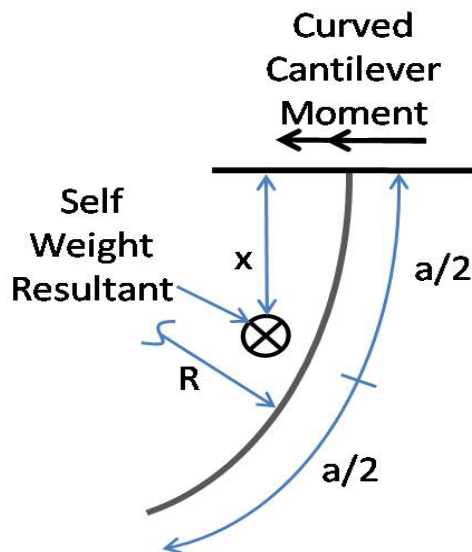
$$M_{straight} = \frac{wa^2}{2}$$

$$M_{curved} = wa * x$$

$$where \; x = R \sin \left[\frac{180° * \frac{a}{2}}{\pi * R} \right]$$

Figure 1.6 Straight vs. Curved Girder Moment

9

For all practical radius of curvatures, the difference in calculated moment using the curved geometry versus the straight geometry is less than .5%. The percent difference reaches 5% when the girder's subtended angle reaches 150 degrees, which is an unrealistic subtended angle for bridges. Refer to Appendix C for tables summarizing the comparison between straight versus curved geometry for moment calculation. Since the difference is negligible for practical cases, the curved girder was treated as straight for the purpose of determining the maximum bending moment.

Once M_{cr} is calculated using Equation 1.6, C_L can be evaluated from Equation 1.5. From observing trends in C_L, an expression for the adjustment factor accounting for lifting curved I-girders can be formulated. C_L can then be applied to M_o to calculate the critical buckling moment for a curved I-girder during lifting. The formulation of C_L and its use in calculating the critical buckling moment is covered in Chapter 5.

1.5   INFLUENCE OF PARAMETERS ON C_L AND CURVED I-GIRDER STABILITY

A number of parameters influence the trends in C_L and curved I-girder stability. The magnitude of the maximum moment is dependent upon the self weight of the girder and the lifting dimensions shown in Figure 1.5. It follows that the lift point locations (given by the ratio of a/L) is significant parameter to explore, since it affects both the max moment and the eigenvalue buckling of the girder. In addition, the effect of radius of curvature, flange width to depth ratio, and span to depth ratio are investigated. These parameters and their effect on girder stability are covered extensively in Chapter 5.

1.6   THESIS OUTLINE

This chapter has provided an introduction and background to the behavior of curved I-girders during lifting. A discussion of geometric and structural stability issues was given. The process of formulating the adjustment factor to account for the lifting of curved I-girders was presented, as well as how this factor would be applied to yield the critical buckling moment of the girder.

Chapter 2 covers the instrumentation and implementation of data acquisition systems for two field tests. The first test involves monitoring the lifting and erection of curved girders and cross frames comprising the direct connector from east-bound US 71 to north-bound SH 130 near Austin-Bergstrom International Airport in Austin, Texas. The second test consisted of girder lift tests performed at the Hirschfeld Steel Company in San Angelo, Texas. Chapter 3 explains the tests in detail and gives the method by which the collected data was analyzed. Results are presented and discussed.

Chapter 4 delves in to the issue of curved I-girder rotation during lifting. The curved girder geometric stability is discussed with influential parameters explained. A process is outlined to calculate and predict the rigid body rotation of a curved I-girder during lifting. The use of this process and collected data to validate a 3-D finite element model is discussed.

In Chapter 5, the finite element model is used to perform a parametric study of lateral-torsional buckling of a curved I-girder during lifting. Discussion of the parameters and results of the study are given. The process by which these results were utilized to formulate recommendations regarding the adjustment factor, C_L, and its use in calculating curved I-girder stability during lifting is detailed.

Chapter 6 summarizes recommendations and guidelines for lifting curved I-girders. Appendix A supplements these guidelines with design examples showing how the equations and processes presented in this thesis are used to predict the behavior of curved I-girders during lifting.

CHAPTER 2

Data Acquisition System and Instrumentations

2.1 INTRODUCTION

This chapter details the data acquisition system and instrumentations performed to collect data from two field studies. The purpose of obtaining this data was to validate analytical models used to enhance the understanding of curved I-girders during construction. As seen in the review of past research conducted on curved I-girders presented in Appendix B, a lack of field studies on curved I-girders during various construction phases exists. This chapter describes the steps taken to correct this deficiency.

2.2 DATA ACQUISITION SYSTEM

2.2.1 Strain Gages

Changes in strain during girder lifting and erection were monitored using strain gages. The purpose of measuring strain changes was to monitor bending and warping stresses in the girders and axial forces in the cross frames during early stages of construction. The method by which bending and warping stresses were calculated is described in detail in Chapter 3.

The foil strain gages that were used were Vishay Micromeasurements' model CEA-06-250UN-350/P2. The gages have 350 ohm resistance and a strain range of ±3% as listed on the data sheet. The Vishay CEA-06-250UN-350/P2 foil strain gage with covered lead wires is shown in Figure 2.1. As shown in the figure, the gages have covered lead wires, which improve the ease of installation. Using gages with covered lead wires circumvented the need to insulate the wires with electrical tape, and saved time and effort during instrumentation.
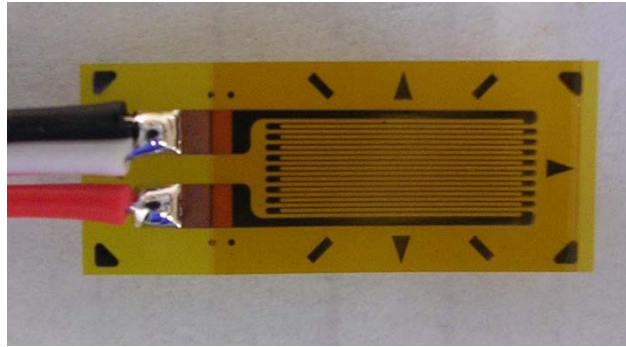
Figure 2.1 CEA-06-250UN-350/P2 Foil Strain Gage

2.2.2 Tilt Sensors

Tilt sensors were used to measure the rotations of the girder over the course of the tests. These rotations were important for the verification of the finite element model and for comparisons with static calculations.

The tilt sensors used were Crossbow Technology's CXTLA01-T single axis tilt sensor. The sensor has a range of ±20° and a resolution of 0.03° with a cross-axis error of less than 5%. The CXTLA01-T tilt sensor is shown in Figure 2.2.

Figure 2.2 CXTLA01-T Tilt Sensor

2.2.3 CR5000 Datalogger

To collect and store the strain gage data and convert it into strains, an on-site computer system was required. The CR5000 Datalogger manufactured by Campbell Scientific was used, as it has proven in past projects to be suitable for the tasks of field data collection. It is capable of taking measurements at a rate of up to 5,000 samples/second with a 16-bit resolution. Voltage measurements of up to 5V can be read with the datalogger. A ±200 mV range was used to improve resolution. The CR5000 Datalogger is shown in Figure 2.3.

13

The software PC9000 is provided by Campbell Scientific to organize and process commands for the CR5000's data acquisition. The CR5000 can connect and read 40 single ended connections or 20 differential connections. Each foil gage requires one differential channel connection, making the CR5000's capacity 20 gages. Each tilt sensor requires two differential channel connections, allowing the CR5000 to read 10 tilt sensors if no other sensors are connected. To limit the number of dataloggers needed for the instrumentation, these capacities were increased using AM416 multiplexers (shown in Figure 2.3), discussed below.

CR5000 Datalogger
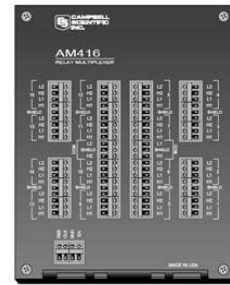
AM416 Relay Multiplexer

Figure 2.3 CR5000 Datalogger & AM416 Multiplexer

2.2.4   AM416 Multiplexer

To increase the number of gages and tilt sensors able to be processed by one datalogger, the AM416 Multiplexer was used. The multiplexer essentially acts as a router for the datalogger, allowing 16 foil gages or 8 tilt sensors (16 total available differential channels) to be read by only one differential channel of the datalogger. The AM416 Multiplexer is shown in Figure 2.3. In addition to increasing the number of readable gages for the data acquisition system, the use of multiplexers reduces the length of wires from the gages since the multiplexer can be placed close to the gages. This is especially important if gage locations are far apart or a significant distance from a datalogger. Figure 2.4 illustrates this situation.
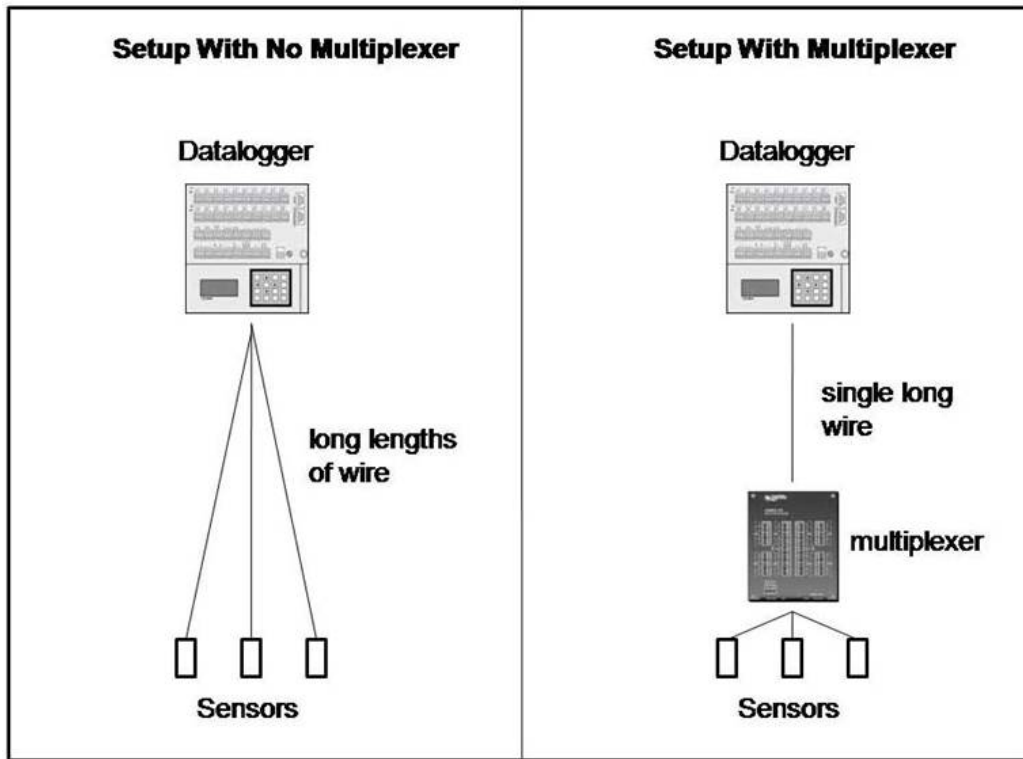
Figure 2.4 Multiplexer Scenarios

2.2.5 4WFB350 4 Wire Full Bridge Terminal Input Module

The 4WFB350 4 Wire Full Bridge Terminal Input Module is used to complete the strain gage bridge circuit. Foil gages are quarter-bridge circuits, whereas the datalogger must read full-bridge circuits. This necessitates the use of completion bridges to allow the datalogger to read the strain gages. A completion bridge module is shown in Figure 2.5.

Figure 2.5 Completion Bridge Module

15

2.2.6   Implementation

The data acquisition system described above was used for two separate field applications. The system was first used to monitor two steel girders and two cross frames from a curved bridge on the direct connector from SH 130 to US 71. Strain changes were collected during the lifting and erection of the girders and cross frames. The second instrumentation was of two girders at the Hirschfeld Steel Company in San Angelo, TX. The acquisition system was used to monitor girder stresses and twists during lifting from well established support conditions. These instrumentations are discussed in detail in the following sections.

2.3   SH 130/US 71 DIRECT CONNECTOR INSTRUMENTATION

The curved bridge selected for instrumentation was Unit 6 of Bridge 88, the direct connector for east-bound US 71 to north-bound SH 130 near Austin-Bergstrom International Airport. Unit 6 is a three span, continuous bridge comprised of a four girder system. The three spans, labeled Span 14, 15, and 16 on the engineering drawings (Span F, G, and H on the shop drawings provided by Hirschfeld Steel Company) have exterior girder span lengths of 185, 210, and 158 feet respectively. The center to center spacing of the girders is 10'-4". The radius of curvature of the fascia girders is 1235.727 feet. Figure 2.6 shows the plan layout of the bridge, with Span 14 magnified to show the location of the instrumented girders and cross frames. The fascia girder, Girder 4, and the adjacent inside girder, Girder 3, of Span 14 were selected for instrumentation. In addition, two cross frames (X1 and X2) connecting the two instrumented girders were gaged. Also pictured is the elevation view of Girder 4 and Girder 3 with the instrumented cross sections detailed.
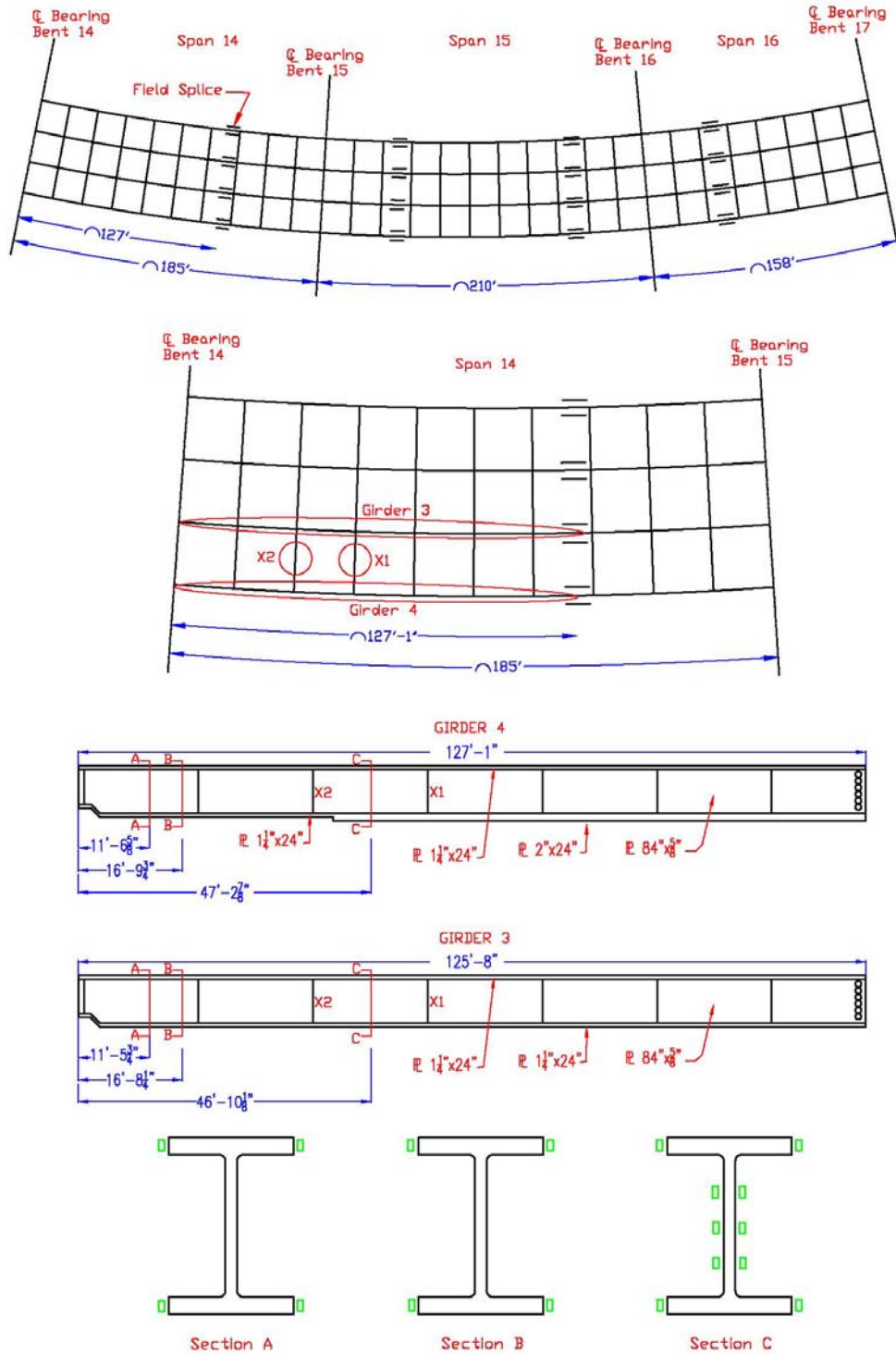
Figure 2.6 Unit 6 Bridge Layout & Girder Elevations w/ Gage Locations

17

2.3.1 Girder and Cross Frame Description

Girder 4 is 127'-1" long, with an 84" deep web plate that is 5/8" thick, constant along the entire girder length. The top flange has a uniform thickness along the girder length of 1.25", while the bottom flange has a thickness transition approximately 40' from bearing of 1.25" to 2". Both the top and bottom flanges have a uniform width of 24". The radius of curvature is 1235.727'

Two gage locations were chosen at Section A-A and Section B-B. The third location was selected at Section C-C, to provide data from near the midspan location and between the two instrumented cross frames, X1 and X2. Gages were installed at mid-thickness of the four flange tips. Collecting strain data from both sides of the top and bottom flange allow bending and warping stresses to be isolated during the data analysis. At the Section C-C, additional gages were placed down the height of the web to track bending stresses through the girder cross section. These gages were placed with uniform spacing down the depth of the web, giving a spacing of about 1'-9". Figures presenting data collected from these gages is presented in Appendix D.

Girder 3 is 125'-8" long, with an 84" deep web plate with a thickness of 5/8". The top and bottom flange have a uniform thickness along the girder length of 1.25" and a uniform width of 24". Girder 3 has a radius of curvature of 1225.394'. The gage locations for Girder 3 are the same as Girder 4. Gage locations for Girder 3 and Girder 4 are shown in Figure 2.6.

The cross frames consist of two diagonals with top and bottom struts composed of 5x5x1/2 angles. The two diagonal members measure 9'-11" in length, and the strut members measure 8'-7" in length. Four gages were placed on each of the four angle members of the cross frame, as shown in Figure 2.7. A gage was placed on each side of the two legs, 1" from the edge. By placing four gages on each cross frame member, axial forces can be isolated to track forces through the bracing and between the Girder 3 and Girder 4.

18
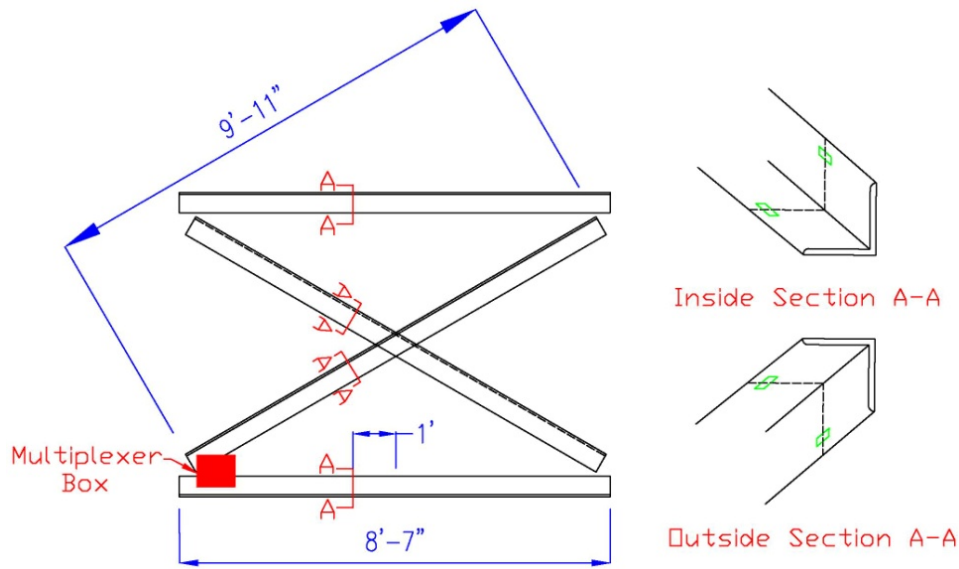
Figure 2.7 X1 & X2 Elevation View w/ Gage Locations

2.3.2 Data Acquisition System Setup

In total, 18 gages were installed on each of the two girders, and 16 gages were installed on each of the two cross frames. This yielded a total of 68 gages to monitor strain changes during the erection. The lifting sequence for the girders consisted of first lifting Girder 4 followed by Girder 3. All of the cross frames were lifted with Girder 3. Two multiplexers and one datalogger were installed on each girder. Each cross frame was outfitted with a multiplexer for its gages, which was wired to the datalogger on Girder 3.

A paramount concern of the instrumentation plan was installing adequate protection of the wiring and the data acquisition system. A number of steps were taken to minimize the possibility of damage to the system during girder lifting and erection. The following two subsections discuss the methods employed to protect the gages and data acquisition system on the cross frames and girders during their lifting and erection.

2.3.2.1 Cross Frames

The two cross frames were transported from the fabricator to the Phil M. Ferguson Structural Engineering Laboratory located at the J.J. Pickle Research Center campus in Austin, TX to be instrumented. Once the strain gages were installed upon each cross frame member as shown in Figure 2.7, three layers of protection were provided. The first was a microcrystalline wax that served as protection against the moisture and humidity that occurs in a field setting. The second was a silicone adhesive that provided a layer of mechanical protection once it dried and hardened. Cross frame gages with these two layers of protection are shown in Figure 2.8. For the third layer of protection, wood blocks were fabricated and attached with hose clamps over the outside gages of each leg of the horizontal members of the cross frames. The blocks provided a buffer in case the cross frames were placed on the ground, which would likely result in gages and wiring being damaged from crushing or contact with the ground. The hose clamps also served to provide the inside gages with some amount of protection from potential foot traffic from the iron workers in the field. The wood blocks attached with hose clamps are shown in Figure 2.9. The gages were positioned within the cutouts in the wood blocking, as seen in the photos.

Steps were taken to ensure wires would not be severed during transportation or erection of the cross frames. The wires from the gages were spliced to shielded wires to complete the connection to the multiplexer. Heat shrink wrap was used to insulate the spliced length from any moisture penetration, and electrical tape was wrapped around the finished splice. Figure 2.10 shows the finished splice before electrical tape secures it.

Figure 2.8 Cross Frame Gages w/ Wax and Silicone Protection

Cutout for Gages
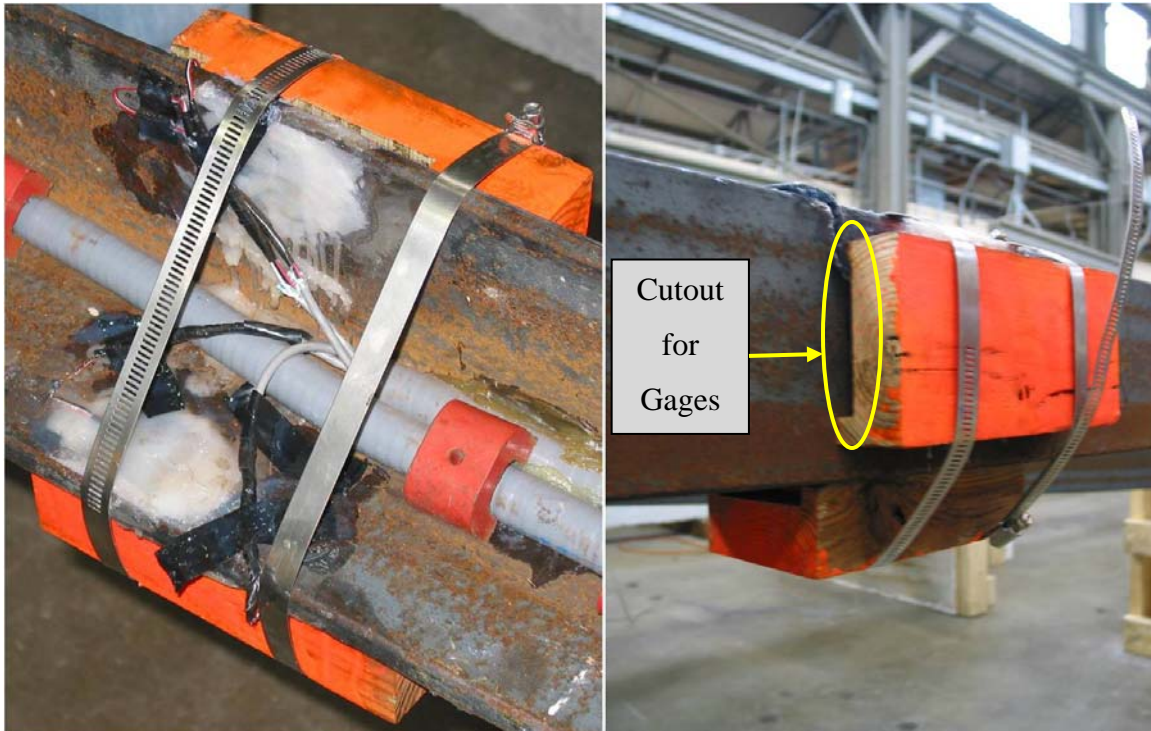
Figure 2.9 Wood Blocks Attached w/ Hose Clamps to Horizontal Members

Also pictured in Figure 2.10 is the flexible metal conduit that was used to run the spliced wire lengths along the cross frame members. This provided a compact, organized, and safe method for running the wire lengths from the gage locations to the multiplexer located in the corner of the cross frame. In addition to Loctite H4500 Speedbonder structural adhesive, hose clamps and wood blocks were used to attach the conduit to the cross frame, as shown in Figure 2.11.

Metal boxes were used to protect the multiplexers and mount them on the cross frames. The boxes were attached to a plate and placed in the corner of each cross frame. Conduit and wires were run to the box, which had holes for wire entry. Figure 2.12 shows the metal boxes mounted on the cross frame with wires in place.
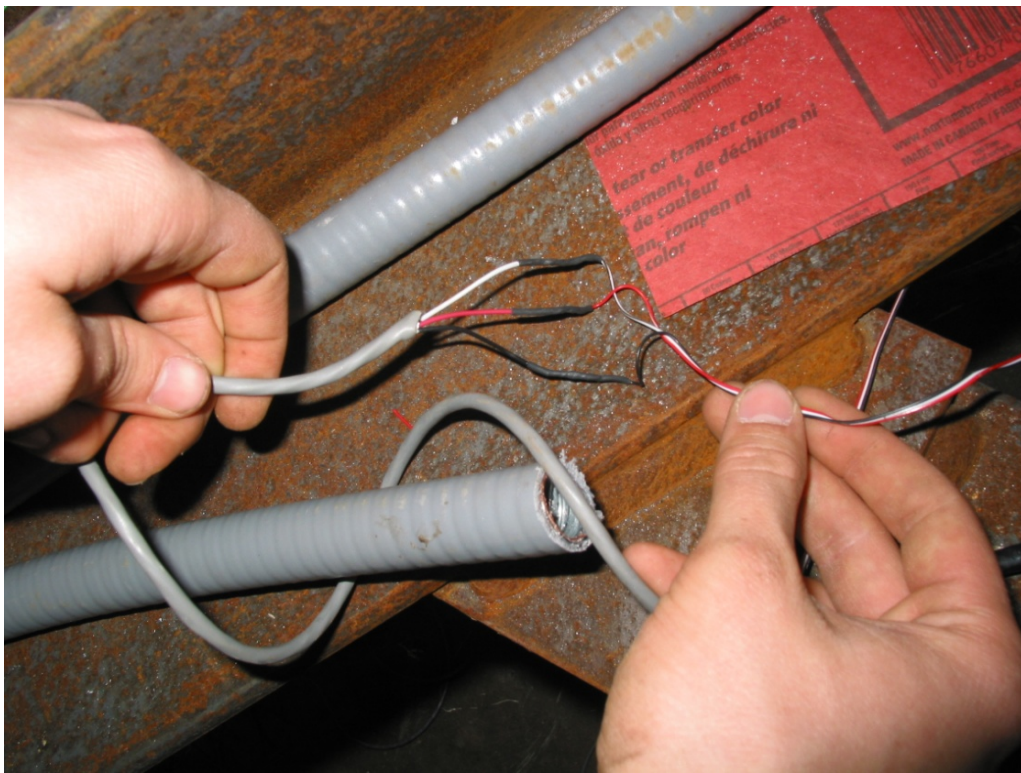
Figure 2.10 Wire Splice w/ Heat Shrink Wrap

Figure 2.11 Conduit Braced w/ Wood Blocks on Cross Frame

Figure 2.12 Multiplexer in Metal Box Mounted on Cross Frame

2.3.2.2 Girders

The two girders, Girder 3 and Girder 4, were instrumented on the job site prior to their erection. Steel channels were fabricated to cover the gages located on the flange tips. They were clamped to the flange using the two bolts shown in Figure 2.13. Similar fabricated channels were used to attach the metal boxes containing dataloggers or multiplexers to the bottom flanges. Figure 2.13 and Figure 2.14 show these fabricated steel channels and their attachments to the girder bottom flange.
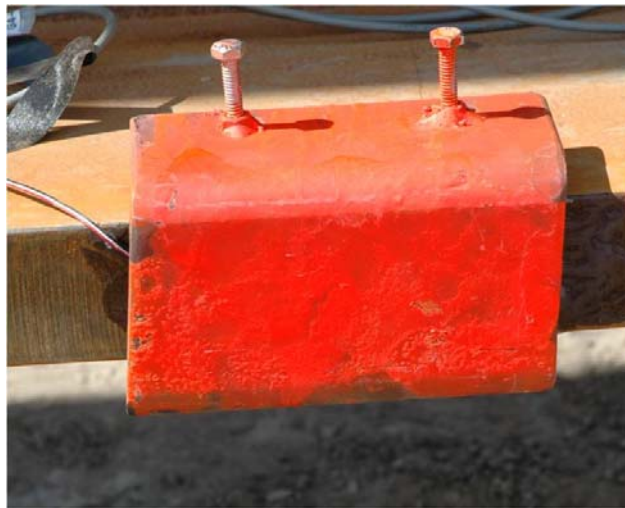
Figure 2.13 Girder Flange Gage Protection

Figure 2.14 Metal Boxes Attached To Girder Flange

Gage wires were spliced at the lab before the field instrumentation similar to the splicing used for the wiring on the cross frames. Conduit was placed on the girder to organize and protect the wires running to the multiplexers and dataloggers. Figure 2.15 shows a side of the fully instrumented girder cross section (Section C-C), as well as flange protection and mounted boxes containing a datalogger and a multiplexer.

Figure 2.15 Instrumented Girder Cross Section

2.4 HIRSCHFELD LIFT TEST INSTRUMENTATION

Two curved girders were instrumented at the Hirschfeld Steel Company in San Angelo, TX. The girders were moved into a staging area in the steel yard where they were instrumented with strain gages, tilt sensors, and the data acquisition system. Figure 2.16 shows the elevation view of Girders 16C4 and 14C2 with the instrumented cross section detailed. These girders are part of the same direct connector as Girder 4 and Girder 3, which lead to the girders bearing similarities with regard to their geometry.
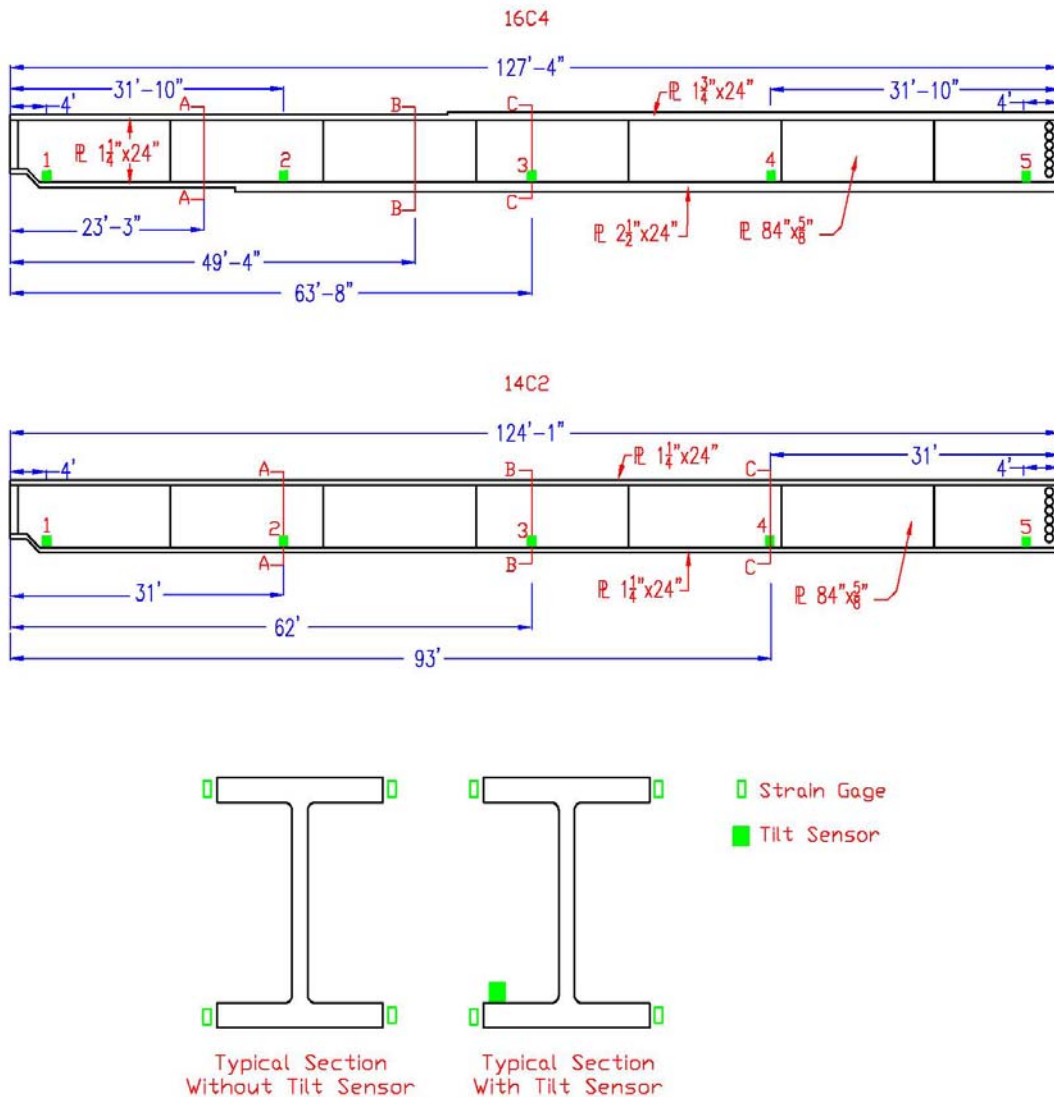
Figure 2.16 Hirschfeld Girder Elevations w/ Gage and Tilt Sensor Locations

26

2.4.1 Girder Description

2.4.1.1 Girder 16C4 – Nonprismatic

Girder 16C4 is 127'-4" long, with an 84" deep web plate that is 5/8" thick, constant along the entire girder length. The top flange has a thickness transition 53'-4" from the dapped end from 1.25" to 1.75". The bottom flange has a thickness transition 27'-3" from the dapped end from 1.25" to 2.5". Both the top and bottom flanges have a uniform width of 24". The radius of curvature is 1235.727'.

Three gage locations were chosen at Section A, Section B, and Section C. Gages were installed at mid-thickness of the four flange tips. The flange gages were used to measure bending and warping stresses. Section A consisted of a doubly symmetric section, while Section B provided data for a singly symmetric section. Section C was chosen to obtain stresses near midspan.

Five tilt sensor locations were selected at sections denoted by 1, 2, 3, 4, and 5. These locations were intended to capture rotation changes at the ends, quarter points, and midspan of the girder. The tilt sensors were located on the inside, bottom flange with respect to the girder's horizontal curvature.

2.4.1.2 Girder 14C2 – Prismatic

Girder 14C2 is 124'-1" long, with an 84" deep web plate with a thickness of 5/8". The top and bottom flange have a uniform thickness along the girder length of 1.25" and a uniform width of 24". The radius of curvature is 1215.06'.

The nomenclature for the strain gage and tilt sensor locations were kept consistent between 14C2 and 16C4. However, the gage locations were located at the quarter points and midspan, since the girder was prismatic and symmetric. The tilt sensor locations remained at the ends, quarter points, and midspan, which coincided with the gage locations at 2, 3, and 4. Figure 2.16 shows the strain gage and tilt sensor locations for 14C2 and 16C4.

2.4.2 Data Acquisition System Setup

Twelve gages and five tilt sensors were installed on each girder. One datalogger and two multiplexers (one for gages, one for tilt sensors) were placed on each girder.

Since these lift tests took place in a more controlled environment than the erection of the previously instrumented girders, many of the protection techniques described earlier were not required. The steel channel gage protection and flexible metal conduit was not used. The metal boxes containing the dataloggers and multiplexers were attached to the bottom flange of the girders using C-clamps. As discussed earlier, the gages were insulated using the microcrystalline wax and silicone adhesive. Strain gage wires were spliced to the shielded wire lengths at Ferguson Laboratory to expedite their application at the Hirschfeld steel yard. The tilt sensors were mounted on 1" x 6" wood boards and attached to the bottom flange of the girders, shown in Figure 2.17.
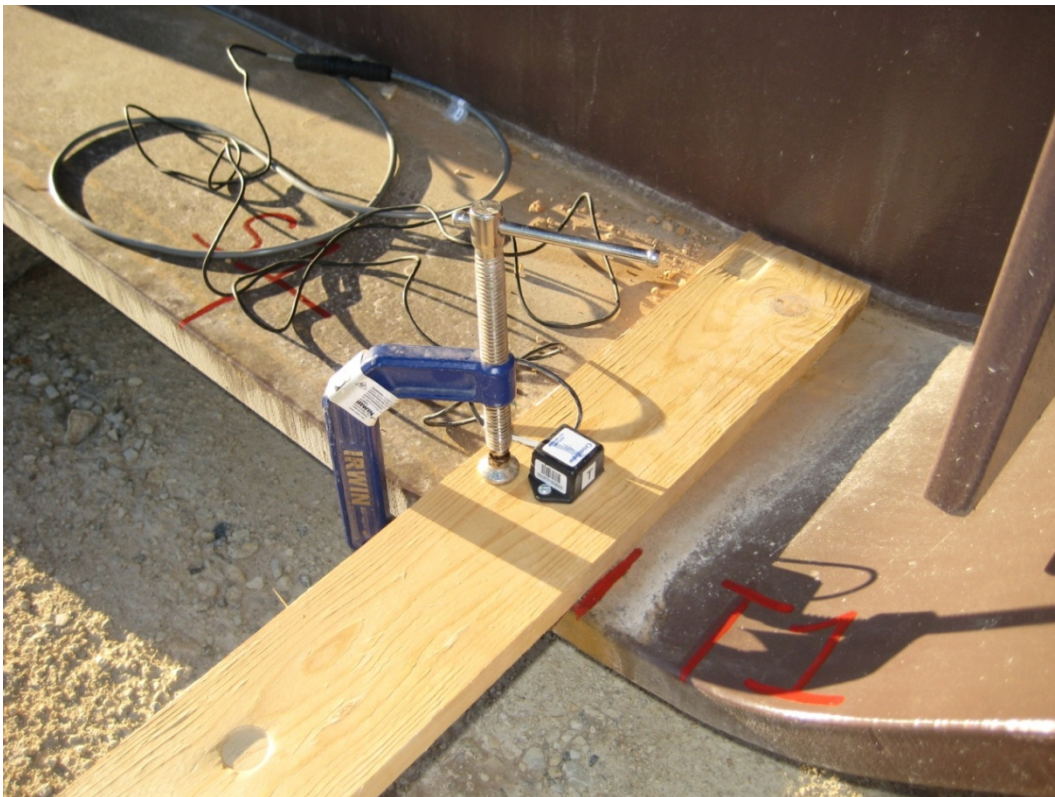
Figure 2.17 Tilt Sensor Installed on Girder

28

2.5 SUMMARY

This chapter discussed the details of the data acquisition system and its components used to collect data for two field studies. The stress and rotation data monitored in these studies was used to compare with finite element results in an effort to calibrate an analytical model of curved I-girder behavior. This model could then be used to extend the understanding and knowledge of curved I-girders during lifting and erection. The following chapter presents the data and results from the two field tests that were used to validate the finite element model.

CHAPTER 3

Description and Results of SH 130/US 71

Bridge Erection and Hirschfeld Lift Tests

3.1   INTRODUCTION

This chapter explains the time line and process by which the girders and cross frames of Span 14 of the SH 130/US 71 direct connector were lifted and erected into place. Results from the girder lift and erection are presented. The lift tests performed at Hirschfeld Steel Company are also discussed. The test setup and procedure are detailed, as well as the results for the two tested girders. The purpose of the tests was to collect data to calibrate analytical models.

3.2   SH 130/US 71 DIRECT CONNECTOR ERECTION

The girders were initially located in a large staging area and supported on heavy timber dunnage. A 60 foot spreader bar with two lift clamps lifted the girders and supported them during the erection. The spreader bar and lift clamp apparatus are shown in Figure 3.1

Figure 3.1 Spreader Bar and Lift Clamp Apparatus

A timeline for both Girder 4 and Girder 3's lifting and erection is shown in Figure 3.2. The timeline begins when the data acquisition system on Girder 4 was activated at 13:45. For both girders, the dataloggers were programmed to record strain data every 2 minutes. Once the girders were lifted into place on the pier, girder splices were made using half snug tightened bolts. Following typical erection procedures, approximately half of the bolts were installed into the splices before the girders were released from the crane. At this stage, cross frame to girder connections consisted of a single snug tightened bolt at the top and bottom of the cross frame. Girder 4 was lifted first, followed by Girder 3 with cross frames attached. A temporary holding crane (second crane) was used to support Girder 4 until Girder 3 was erected and the cross frames were installed between the girders. The following subsections detail each girders' respective lift.
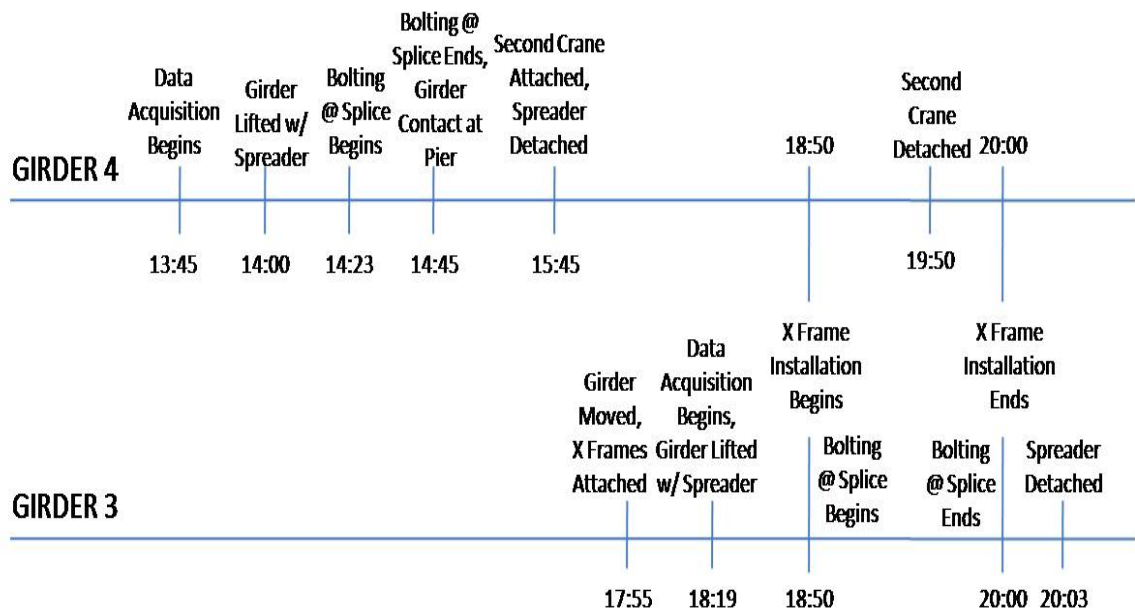
Figure 3.2 Erection Timeline for Girder 4 & 3

31

3.2.1 Girder 4 Lifting and Erection

The data acquisition system was activated approximately 15 minutes before it was lifted at 13:45 while Girder 4 was supported by large timbers on the ground. The spreader bar and lift clamps were attached at the locations shown in Figure 3.3. The girder was then lifted into place as shown in Figure 3.4.
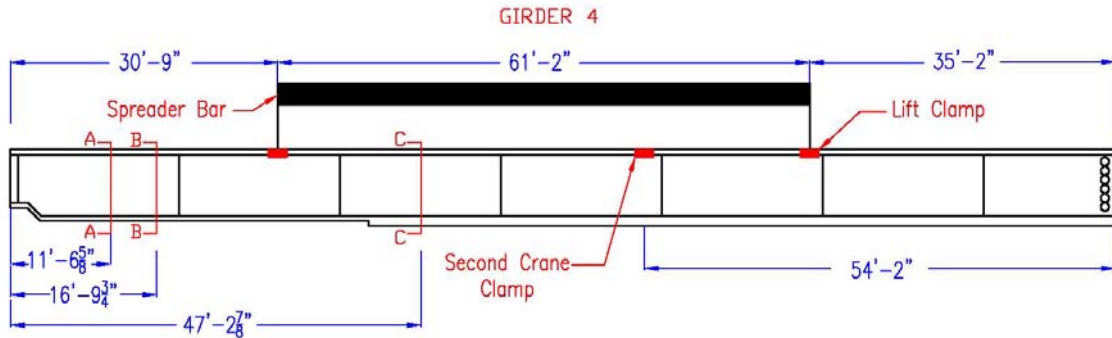
Figure 3.3 Girder 4 Lift Locations w/ Gaged Sections

Figure 3.4 Girder 4 Lifting

Girder 4 was lifted into place and the field splice to the adjacent girder of the girder line was completed at 14:45. The girder was then fully lowered onto the pier and a second crane was brought in at 15:45. The second crane provided an upward reaction at the location labeled "second crane clamp" in Figure 3.3. The second crane was used to stabilize Girder 4 while the larger crane with the spreader bar lifted Girder 3. This method is sometimes necessary during the erection of the first girders when insufficient bracing is present.

Figure 3.5 shows this process. In the left image, the second crane is attached to the girder while the primary crane with the spreader bar is still stabilizing the girder. On the right, the primary crane has been disengaged from Girder 4 and has lowered into place to begin lifting Girder 3, leaving the second crane to provide a stabilizing upward force. According to the crane operator, a load cell in the second crane exerted an upward force of approximately 29 kips on Girder 4.
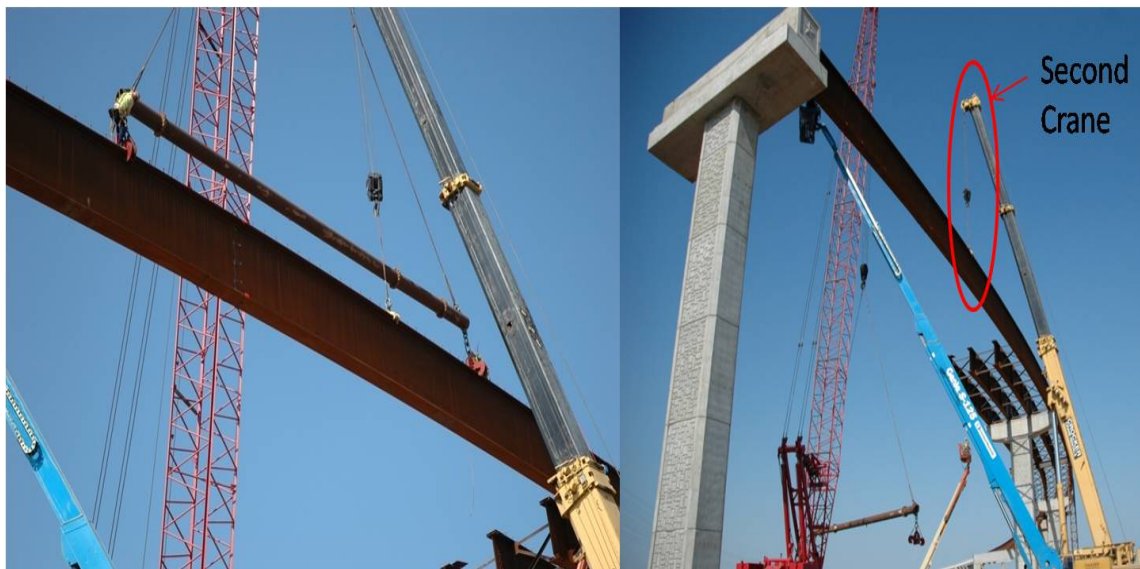
Figure 3.5 Second Crane Stabilizing Girder 4

3.2.2 Girder 3 Lifting and Erection

At 17:55, Girder 3 was initially lifted and moved to a second staging area and placed on large dunnage timbers. Cross frames were attached to both sides of the girder, including the instrumented cross frames, X1 and X2. The data acquisition system was activated at 18:19 immediately before the girder and cross frames were lifted from the second staging area. The lift points were located as shown in Figure 3.6. The girder and cross frames were then lifted as shown in Figure 3.7.
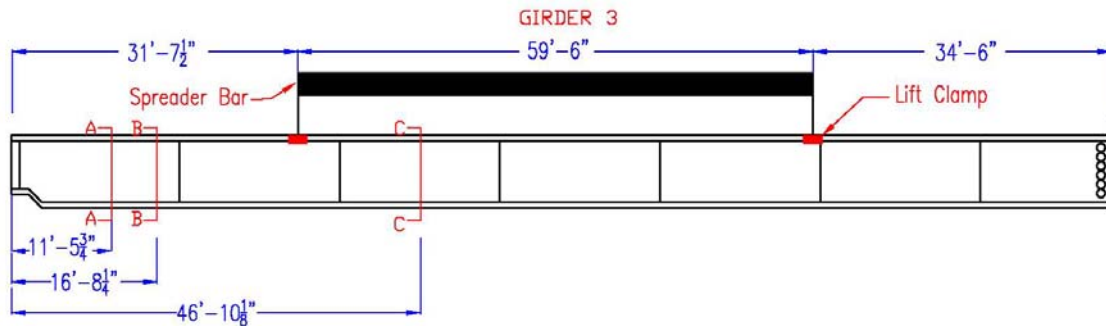
Figure 3.6 Girder 3 Lift Locations w/ Gaged Sections

Figure 3.7 Girder 3 and Cross Frame Lifting

34

Once lifted, the field splice was completed between Girder 3 and the existing girder line and cross frames were attached to Girder 4 (18:50-20:00) using the erection bolts. When most of the cross frames were installed, the second crane was detached from Girder 4 (19:50). The primary lifting crane was removed from Girder 3 after all cross frames were installed (20:03, see Figure 3.2).

Once both girders were erected and all field splices were in place, the data acquisition system was reconfigured to use only one datalogger to collect data from both girders and the cross frames. The multiplexers responsible for the cross frame gages were wired to this datalogger. Wires from Girder 3 were run through the conduit laid on X1 and X2 to the datalogger on Girder 4, which was used to collect the data from the strain gages for the remainder of the field monitoring. Figure 3.8 shows the last phase of the erection of Girder 4 and Girder 3, after which the interior two girders could be erected to complete the erection of Unit 6.

Figure 3.8 Erected Girder 4 & Girder 3 of Span 14-Unit 6

3.3 DATA REDUCTION TECHNIQUE

The purpose of the instrumentation was to measure strains from which bending and warping stresses could be isolated. These stresses could then be used for validating analytical models as well as for improving the general understanding of girder behavior during the early stages of construction. This section illustrates how the bending and warping stresses presented in the results were calculated from the strains collected from the gages during the lifting process.

3.3.1 Bending and Warping Stress Interaction

An important aspect to interpret the strain measurements from the field studies is having a clear understand of the relationship between the bending and warping stress distributions that are present in the flanges of curved I-girders. Bending stresses from vertical bending vary linearly down the depth of the cross section, with the maximum values occurring at the top and bottom flange. The bending stress is assumed to be essentially constant through the relatively small thickness of the flanges. Warping stress varies linearly across the flange width, as it is caused by lateral bending of the flanges. The individual stress components from bending and warping stresses can be isolated using principles of superposition. Figure 3.9 illustrates the bending and warping stress distributions at the flanges, as well as their interaction.

3.3.2 Bending and Warping Stress Isolation

During the girder lifts, stresses at the flange tips were obtained from the strain gages. These stresses are denoted as σ_L and σ_R, referring to the left flange tip stress and right flange tip stress, respectively. For all girders involved with this study, this convention makes σ_L correlate to the inside with respect to horizontal curvature and σ_R with the outside. The characteristics of the combined stress distribution were used to isolate the bending and warping stress components. This process is presented in Figure 3.10, Equation 3.1, and Equation 3.2.

36

Flange Combined Stress Distribution = Flange Bending Stress Distribution + Flange Warping Stress Distribution
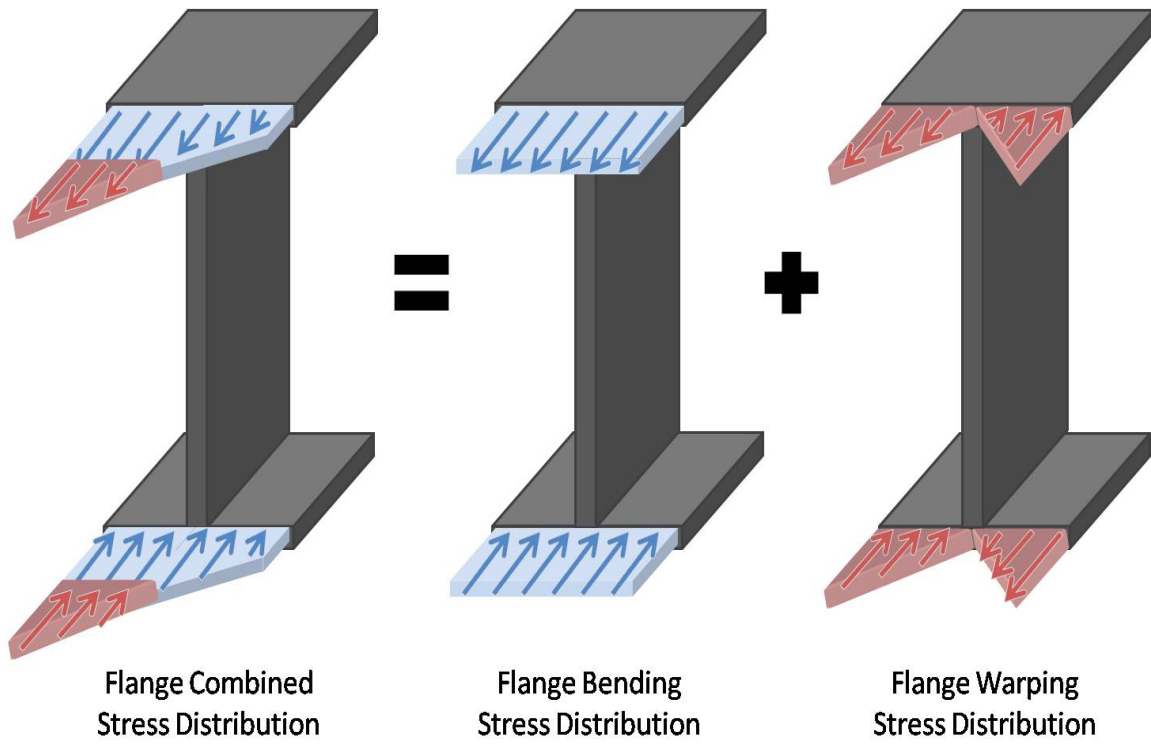
Figure 3.9 Curved I-Girder Flange Stress Distributions
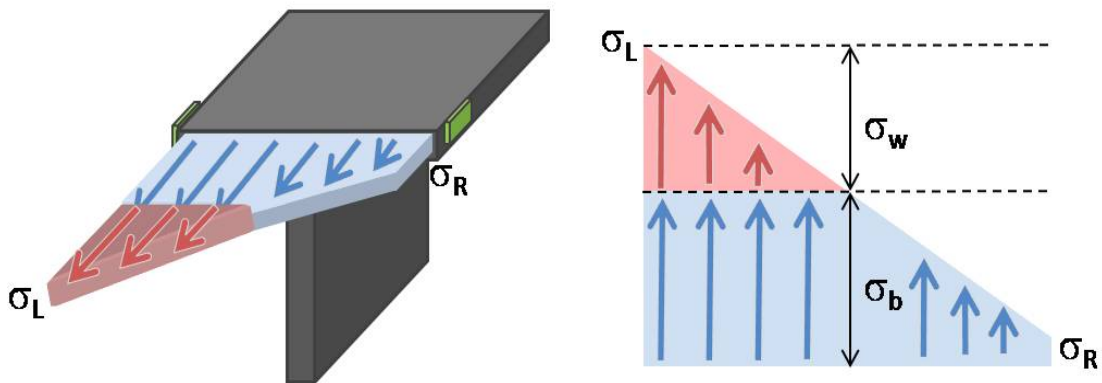
Figure 3.10 Bending and Warping Stress Isolation

$$\sigma_{bending} = \frac{(\sigma_L + \sigma_R)}{2} \qquad \textit{Equation 3.1}$$

$$\sigma_{warping} = \frac{(\sigma_L - \sigma_R)}{2} \qquad \textit{Equation 3.2}$$

The data presented in the following sections gives the bending and warping stress calculated using Equation 3.1 and Equation 3.2. Further discussion of bending and warping stress distributions specific to the tests is also presented. Based upon Equation 3.2, positive warping stress changes indicate higher combined stresses being present on the flange tip located on the inside of the horizontal curvature of the girder.

3.4 SH 130/US 71 GIRDER ERECTION RESULTS

The following section presents figures showing a stress time history of Girder 4 and Girder 3 during their lifting and erection. Each plot shows the bending and warping stresses at a particular gage location (see Figure 3.3 and Figure 3.6 for section locations). Specific events of the lift are highlighted and can be correlated to the timeline presented in Figure 3.2. From these figures, the different states of stress experienced by the girders and the stress changes associated with different operations can be observed.

3.4.1 Girder 4 Results

All stress changes shown for Girder 4 in the following figures were taken relative to the state of stress prior to the lift when the girder was supported by timbers on the ground. Very small changes in stress were recorded at the gage locations during the initial lifting with the spreader bar. The reason for the small changes in stress is that the change in vertical boundary conditions was very small, since the timber support locations were relatively close to the lifting points as shown in Figure 3.11.
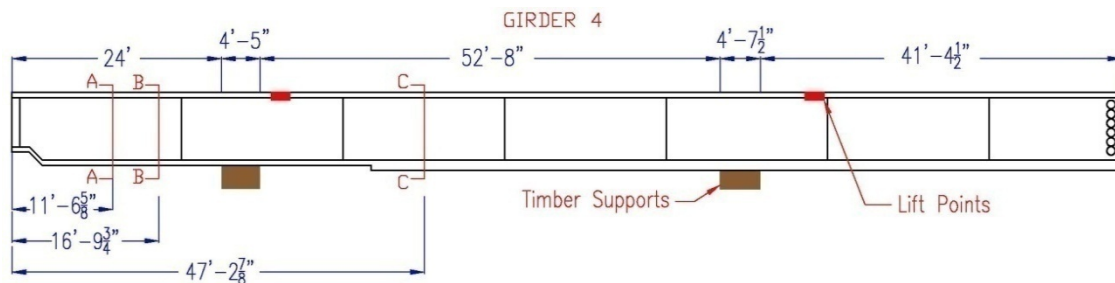
Figure 3.11 Girder 4 Timber Support Locations w/ Gaged Sections

Figure 3.12 shows the graph of Girder 4's bending and warping stress changes at the top flange of Section C during the lifting process. A slight change of less than 1 ksi occurred once the girder was placed on the pier and the splice was completed at 14:45. The first significant stress change occurred when the second crane was attached and the spreader bar was removed from the girder at 15:45. The support conditions changed, causing a significant change in the moment along the girder. Figure 3.12 details the approximate moment expected when the girder was supported by the 60 foot spreader bar during the lift at 14:00 versus the moment once the spreader was detached and the girder was supported at the pier and splice, with a 29 kip stabilizing force provided by the second crane (15:45, see Figure 3.2).

These predicted changes in moment correlate with the observed bending stress changes at the top flange of Section C, shown at the dashed line on the girder detail in Figure 3.12. Once the spreader bar was removed from Girder 4, the bending stress change at this location underwent a brief spike of approximately -2 ksi (negative values denote increasingly compressive stress changes), before settling at about -0.75 ksi. The warping stress change at the top flange of Section C showed a similar brief spike (-6.5 ksi) before settling at approximately -2.5 ksi.
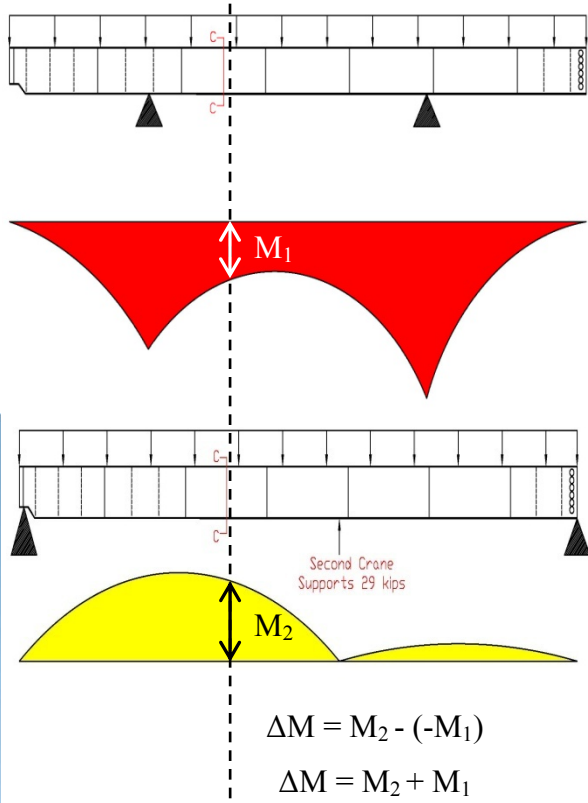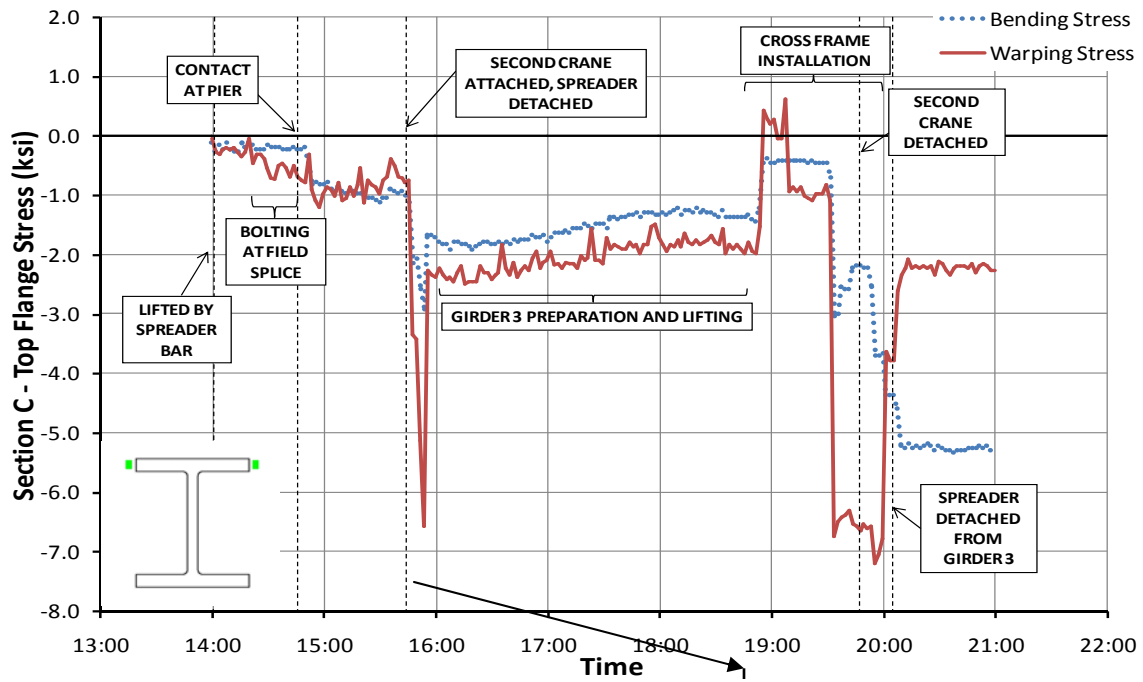
Figure 3.12 Girder 4 Stress Change at Section C Top Flange

$$\Delta M = M_2 - (-M_1)$$

$$\Delta M = M_2 + M_1$$

The second significant stress change occurred during the installation of the cross frames between Girders 4 and 3 from 18:50 to 20:00. The data shows that the bending and warping stress changes during fit-up are significant, with bending stress undergoing maximum changes of 2.5 ksi and warping showing max changes of 7 ksi. The removal of the second crane from Girder 4 and the spreader from Girder 3 at 19:50 and 20:03, respectively, led to the girders acting as a continuous bridge with the rest of Unit 6, though the splices and cross frames were connected with only a small number of bolts, tightened snug at this stage. During this time, bending stresses changed -3 ksi and warping changed +4.5 ksi. These changes associated with this final state can be seen in the data presented in Figure 3.12.

The following figures present the data obtained from the locations instrumented on Girder 4. As in the figures, the stress changes coincide with events given in the timeline of Figure 3.2. Further discussion of the time histories is given in the Girder 4 Summary subsection.
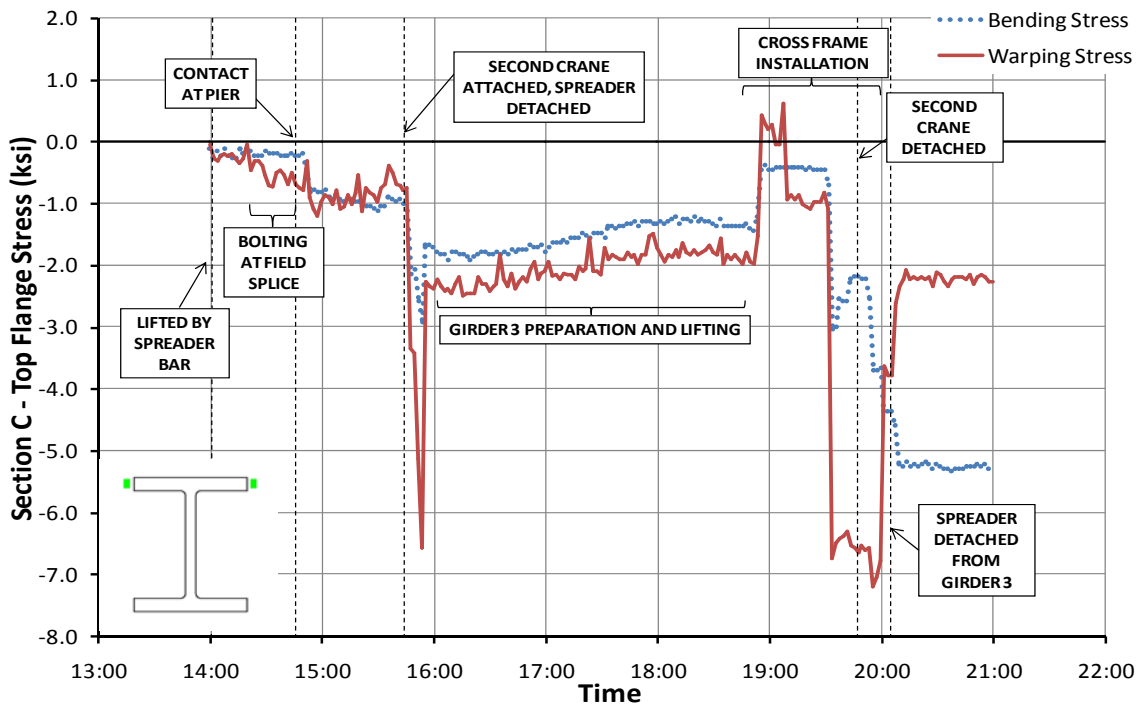
Figure 3.13 Girder 4 Stress Change at Section C Top Flange
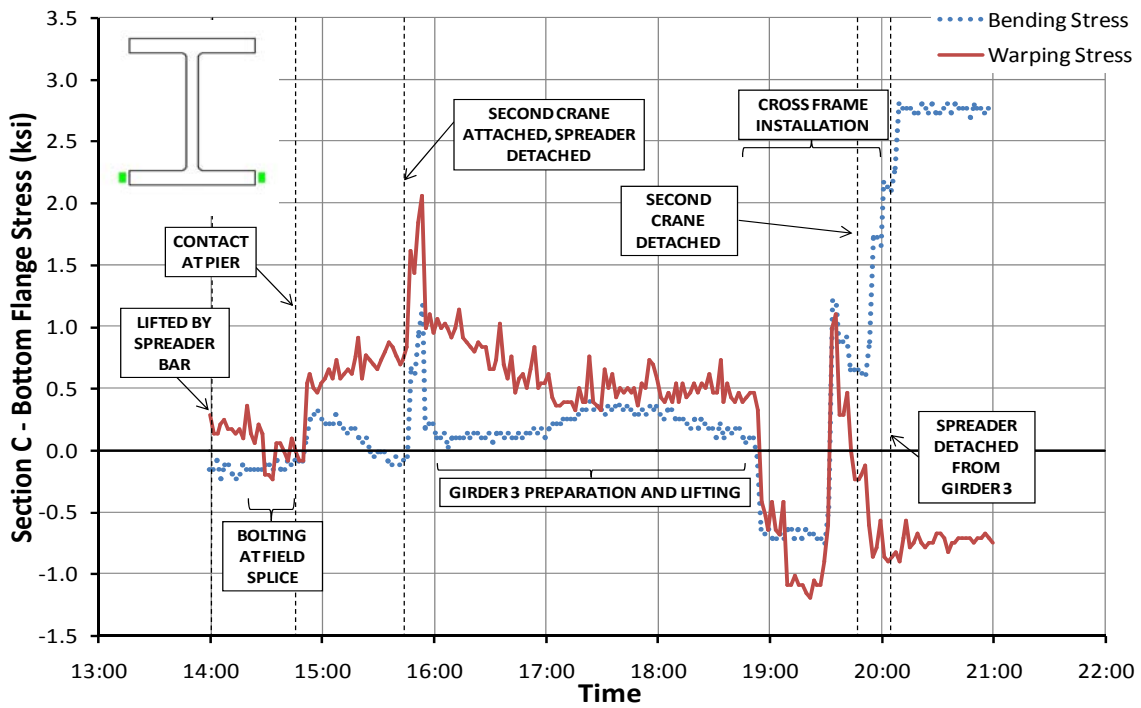
Figure 3.14 Girder 4 Stress Change at Section C Bottom Flange

42
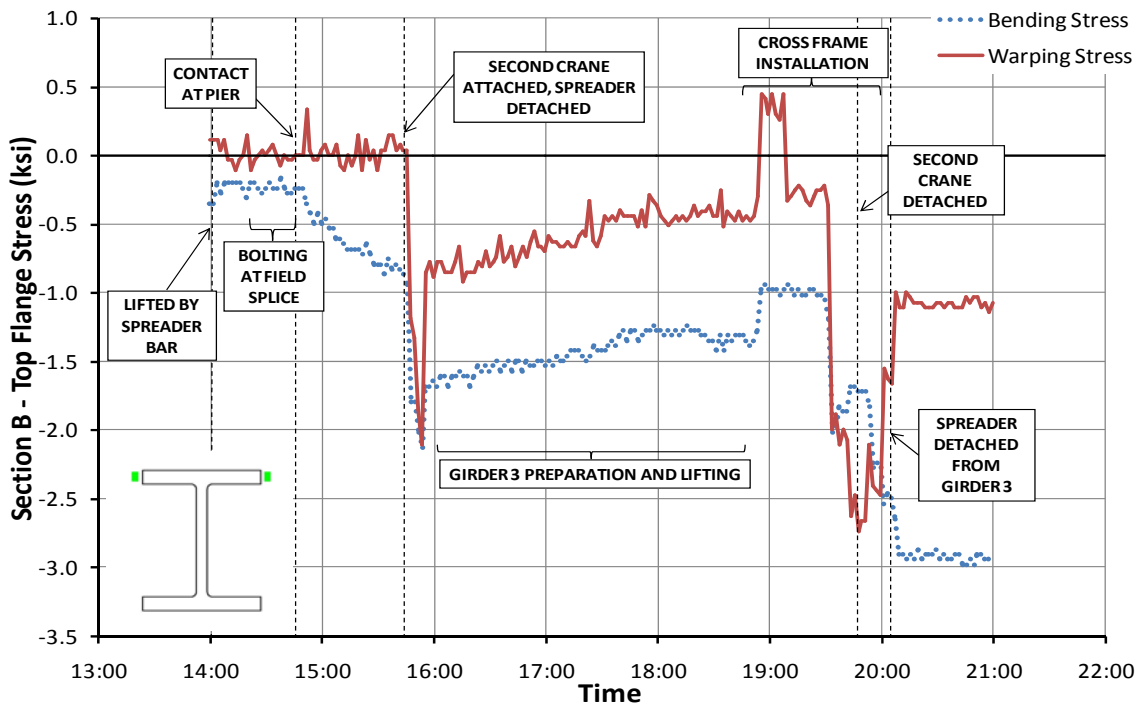
Figure 3.15 Girder 4 Stress Change at Section B Top Flange
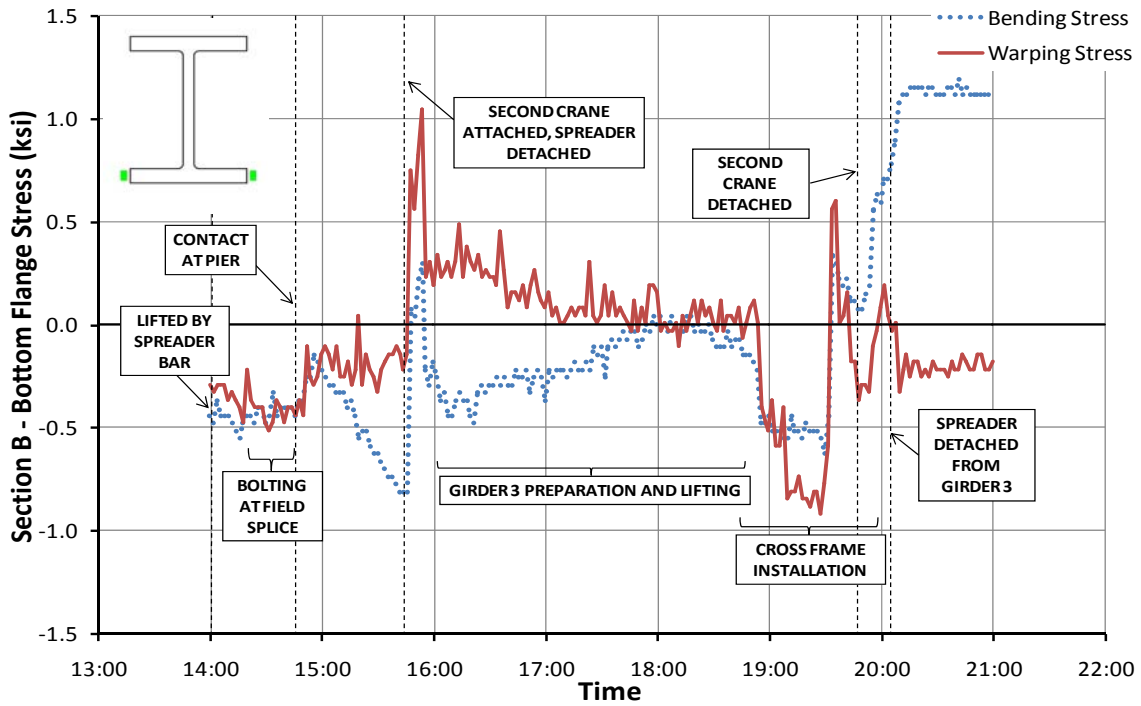
Figure 3.16 Girder 4 Stress Change at Section B Bottom Flange

43
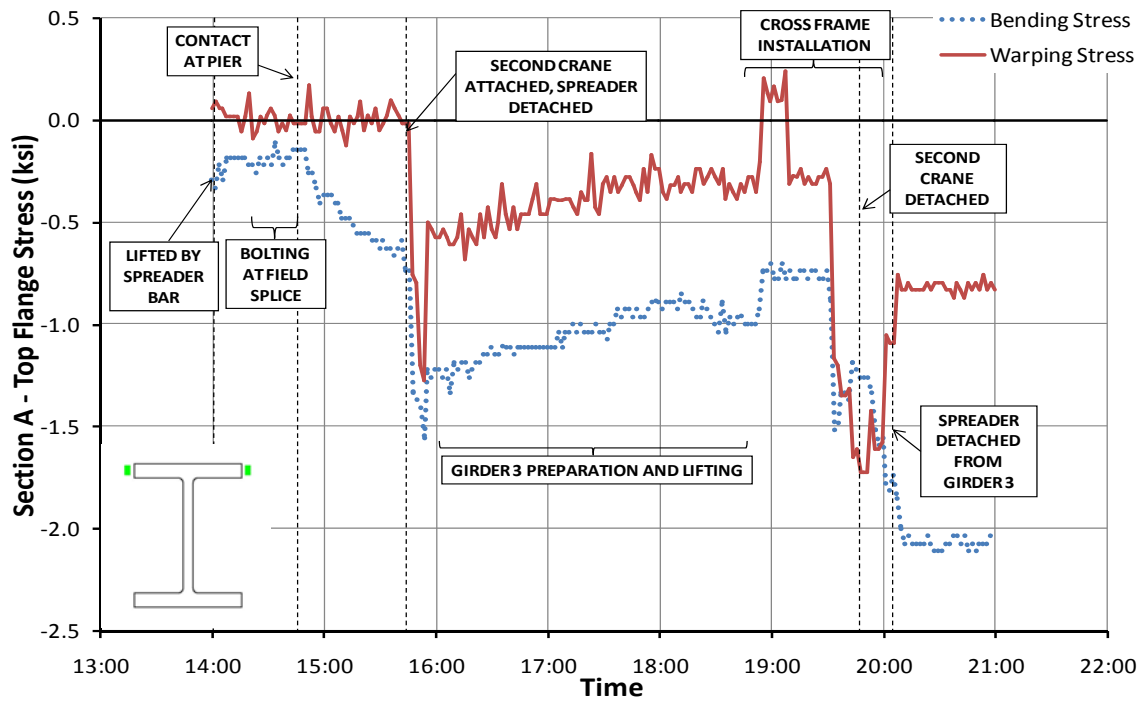
Figure 3.17 Girder 4 Stress Change at Section A Top Flange
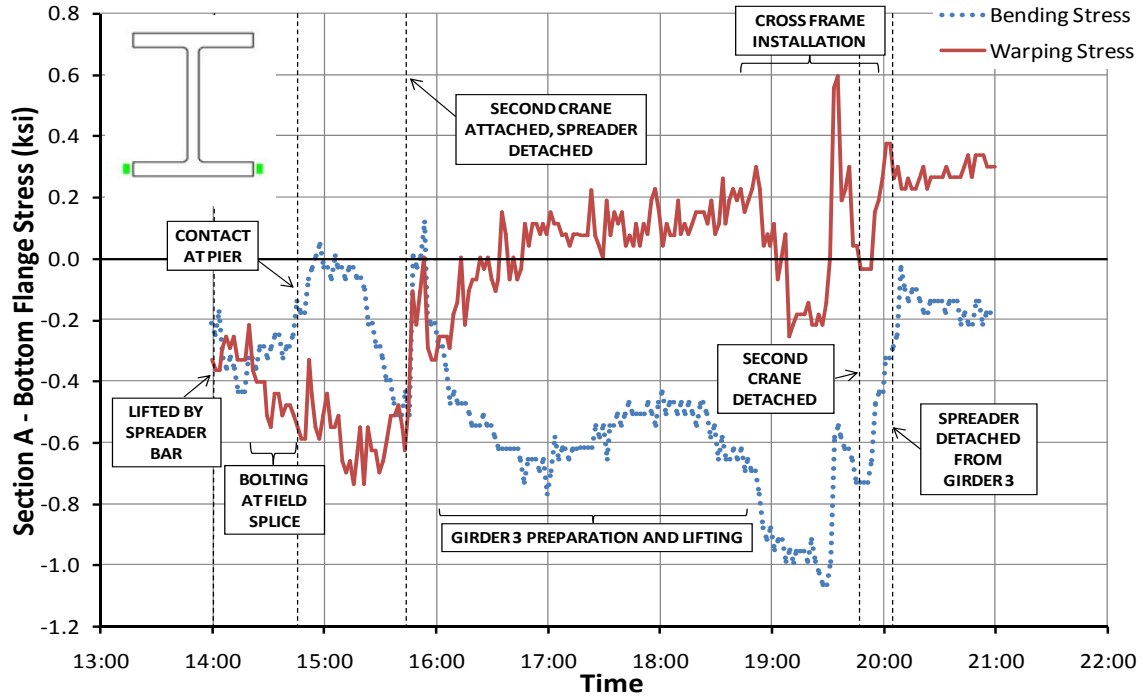
Figure 3.18 Girder 4 Stress Change at Section A Bottom Flange

44

3.4.2 Summary of Girder 4 Results

Location	Stress	Flange	Girder 4 Stress Change During Specified Event (ksi)			
			Second Crane Attached, Spreader Detached (15:45)	Cross Frame Installation* (18:50-20:00)	Second Crane Detached (19:50)	Spreader Detached From Girder 3 (20:03)
Section A	Bending	Top	-0.5 (-0.75)	0.5	-0.5	-0.25
		Bottom	0 (+0.5)	0.5	+0.5	+0.25
	Warping	Top	-0.5 (-1.25)	1.5	+0.75	+0.25
		Bottom	+0.75 (+0.75)	0.75	+0.5	0.0
Section B	Bending	Top	-0.75 (-1.25)	1	-0.75	-0.5
		Bottom	+0.5 (+1.0)	0.75	+0.75	+0.5
	Warping	Top	-0.75 (-2.0)	2.5	+1.0	+0.5
		Bottom	+0.5 (+1.25)	1.25	+0.5	-0.25
Section C	Bending	Top	-0.75 (-2.0)	2.5	-2.5	-0.5
		Bottom	+0.25 (+1.25)	2	+1.5	+0.5
	Warping	Top	-3.0 (-6.0)	7	0.0	+4.5
		Bottom	+0.25 (+1.25)	2.25	0.0	-0.5

*Stress changes during cross frame installation given as max changes independent of sign
( ) denotes initial stress change before values settle once operation is complete

Table 3.1 Girder 4 Stress Change Summary

Table 3.1 tabulates the stress change values observed from the data during the events shown. As mentioned earlier, negative bending stress values denote stress changes of a compressive nature and positive values indicate increasingly tensile stresses. For warping stresses, negative values correlate with higher combined stresses being present on the exterior flange tip of the girder.

The general trends in the stress change time histories were the same for each Section of Girder 4. Around 15:45 when the second crane was attached and the spreader bar was removed, all flanges exhibited pronounced changes in stress (value in parentheses, see note) before settling to values indicative of a more modest change (indicated by the first value in the table). While the cross frames were being installed between Girder 4 and 3 from 18:50 to 20:00, significant stress changes took place, with warping stress changes being more pronounced at all sections. These values were reported as max changes, since multiple fluctuations occurred (see figures), presumably due to ratcheting of the cross frames into place and fit up.

Typically, notable changes in stress occurred near the end of cross frame installation when the second crane was detached at 19:50. Though difficult to fully

dissociate from changes associated with cross frame installation and fit up, the removal of the second crane appeared to correlate with a change in bending and warping stresses. Similarly, the detachment of the spreader bar from Girder 3 at 20:03 caused a final change in stress before the stresses stabilized after all operations were complete.

3.4.2.1   Effects of Cross Section Symmetry

For the symmetric cross sections, Section A and Section B, the magnitude of bending stress changes at the top and bottom flanges were very similar, differing by only 0.25 ksi. This change can be attributed to noise in the data acquisition system. Bending stress changes during the other tabulated events followed this trend dictated by symmetry, with absolute changes at the top and bottom flange being the same when the second crane was detached at 19:50 and when the spreader was detached from Girder 3 at 20:03. As expected, the magnitude of the bending stress changes at the unsymmetric cross section, Section C, showed larger changes at the top flange than at the bottom flange due to the location of the centroid, which was below midheight of the cross section.

3.4.2.2   Maximum Stress Changes

During the important events of Girder 4's lifting and erection, maximum bending stress changes occurred during cross frame installation (absolute max change of 2.5 ksi) and upon the removal of the second crane (compressive stress change of 2.5 ksi). Both of these max stress changes occurred at Section C.

The maximum warping stress change was approximately 7.0 ksi. This was observed at the top flange of Section C during the installation of cross frames. A large change of -6.0 ksi was seen at Section C when the spreader was detached and the second crane was attached.

46

3.4.3 Girder 3 Results

All stresses shown for Girder 3 in the following figures were zeroed using the first ten readings when the girder was lifted from the second staging area because data collection while the girder was supported on the ground by timbers was not possible. The following figures present the data obtained from the locations instrumented on Girder 3.
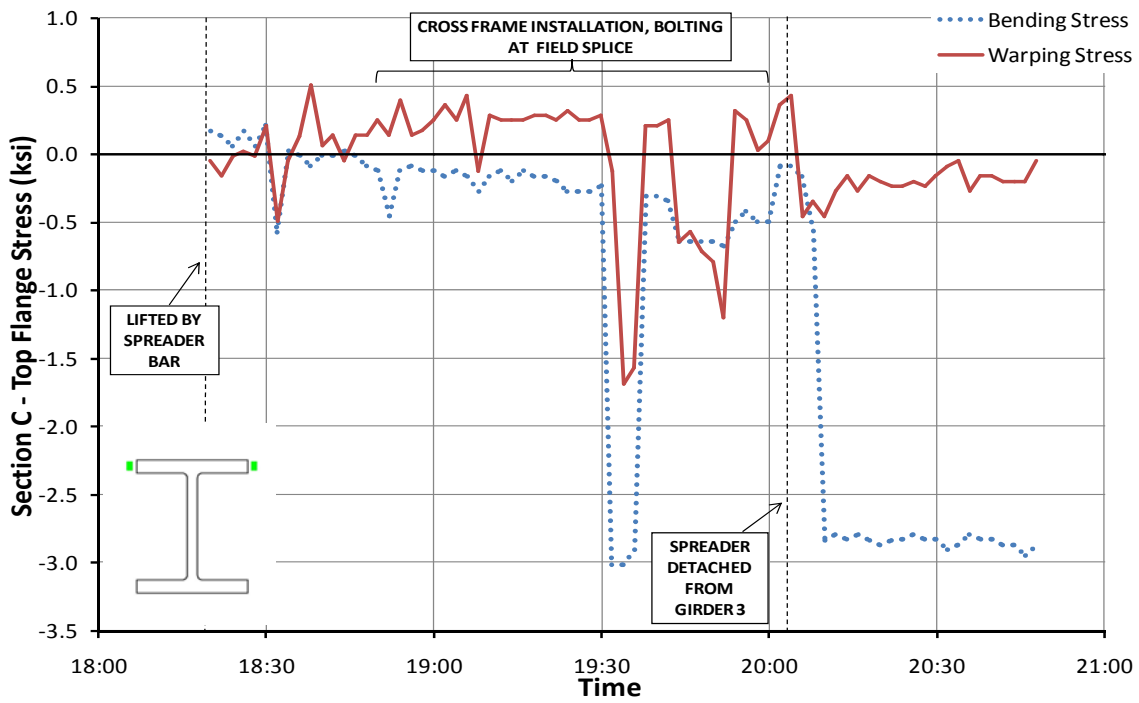
Figure 3.19 Girder 3 Stress Change at Section C Top Flange
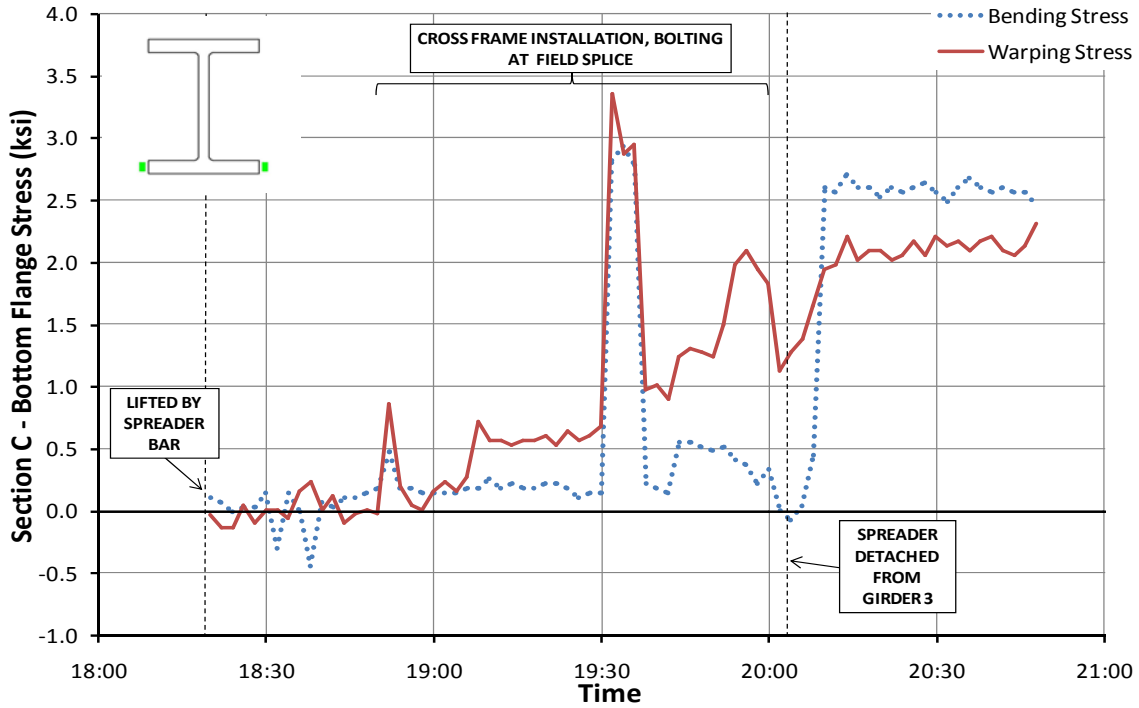
Figure 3.20 Girder 3 Stress Change at Section C Bottom Flange

48
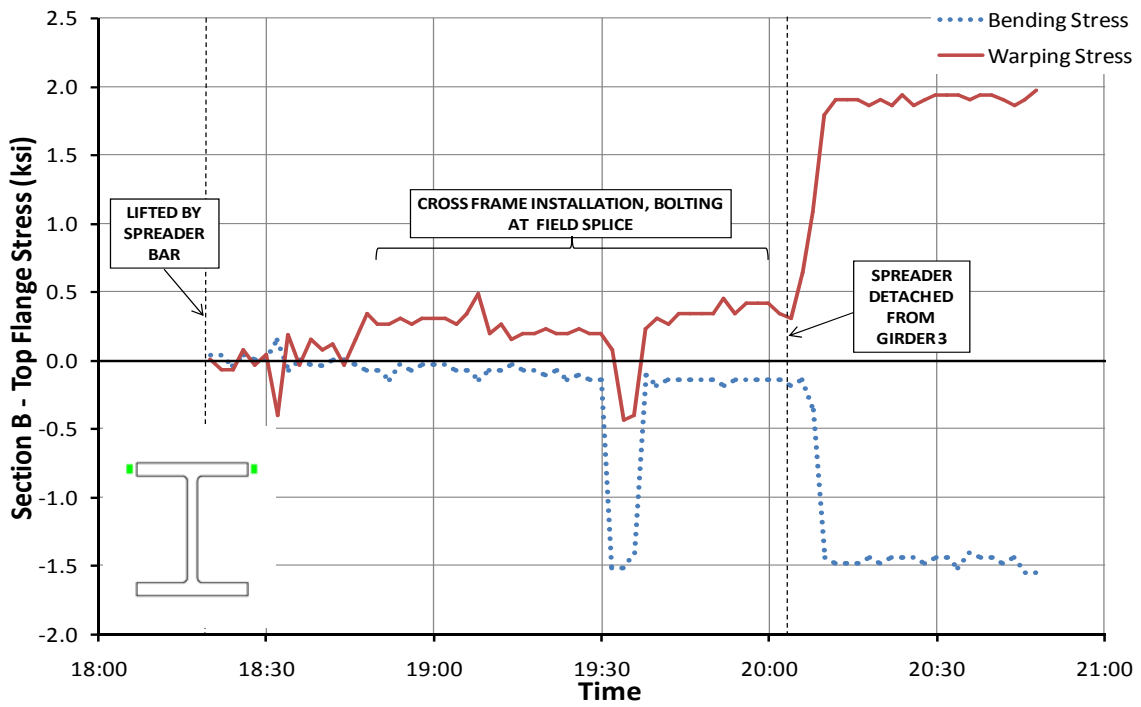
Figure 3.21 Girder 3 Stress Change at Section B Top Flange
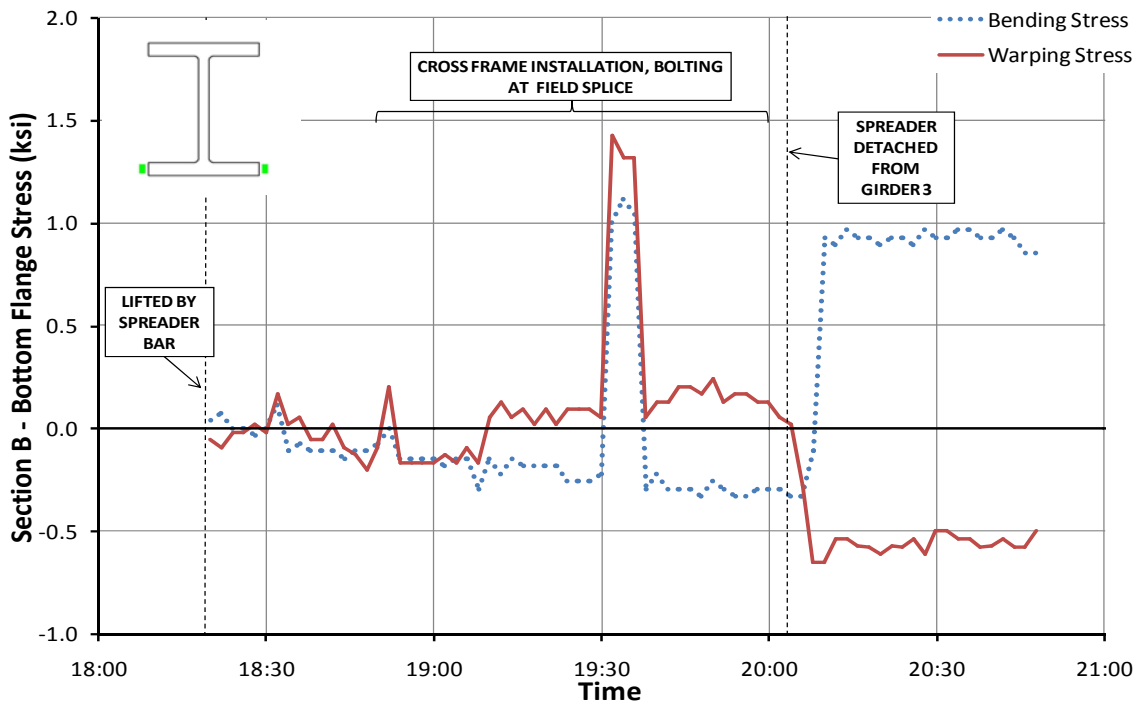
Figure 3.22 Girder 3 Stress Change at Section B Bottom Flange

49
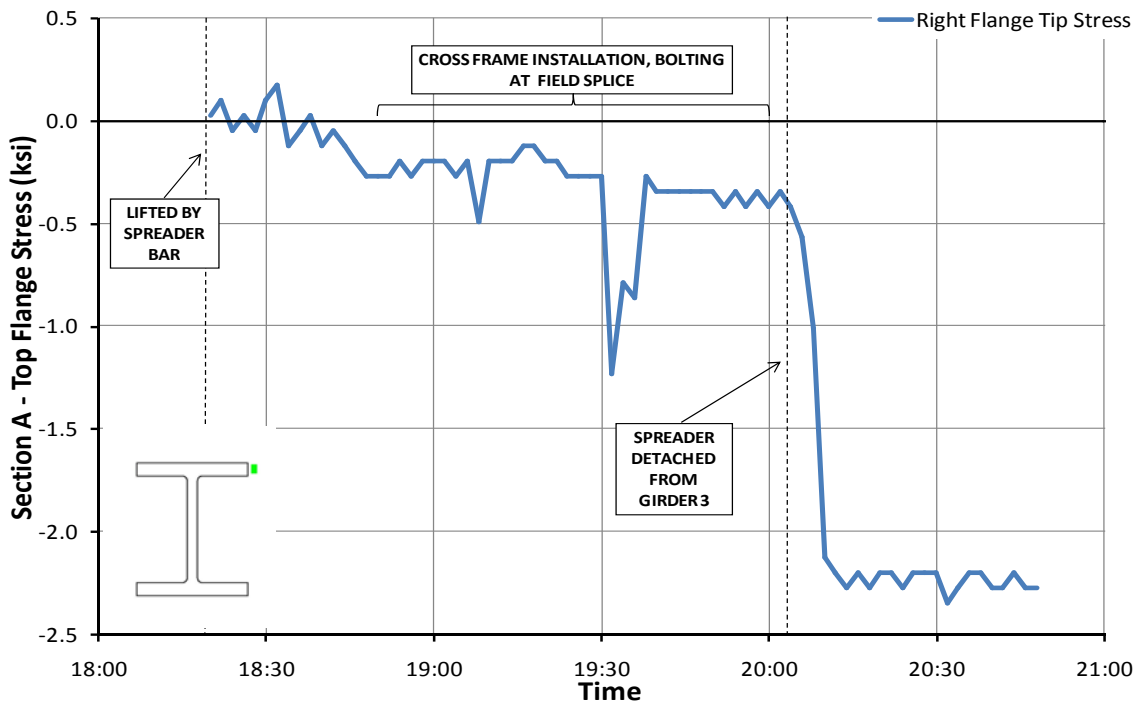
Figure 3.23 Girder 3 Stress Change at Section A Top Flange
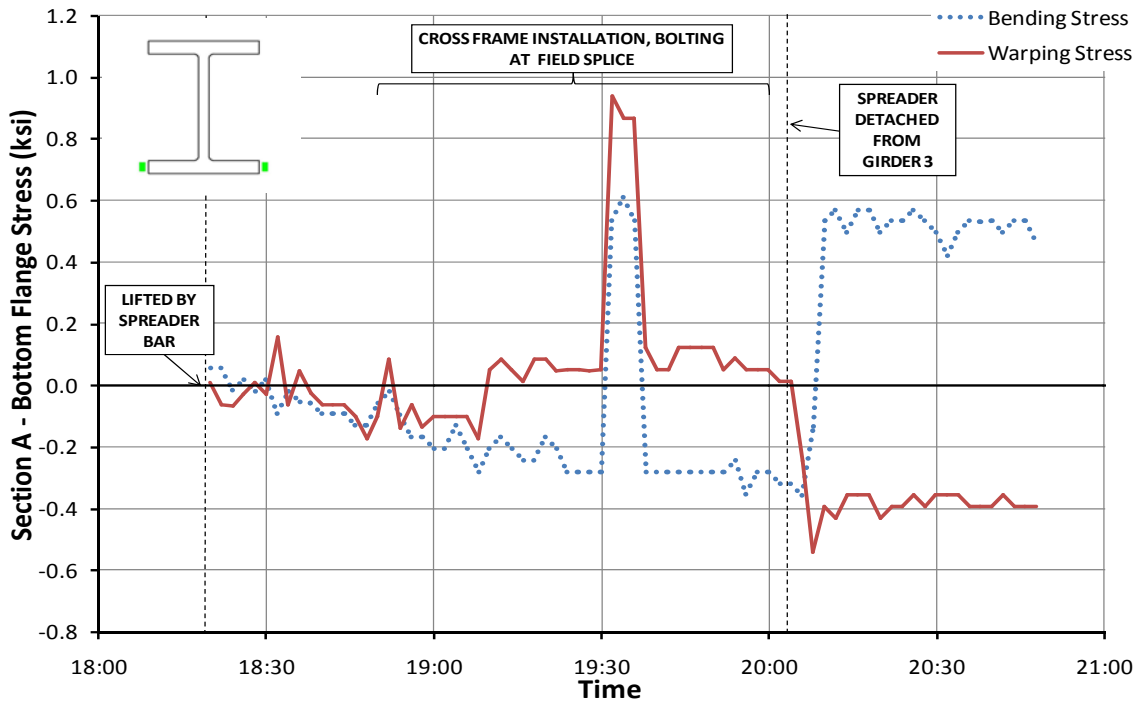
Figure 3.24 Girder 3 Stress Change at Section A Bottom Flange

50

3.4.4 Summary of Girder 3 Results

Location	Stress	Flange	Girder 3 Stress Change During Specified Event (ksi)	
			Cross Frame Installation (18:50-20:00)	Spreader Detached From Girder 3 (20:03)
Section A	Bending	Top	NA	NA
		Bottom	+1.0	+1.0
	Warping	Top	NA	NA
		Bottom	+1.0	-0.5
Section B	Bending	Top	-1.5	-1.25
		Bottom	+1.5	+1.25
	Warping	Top	-0.5	+1.5
		Bottom	+1.25	-0.75
Section C	Bending	Top	-2.75	-2.75
		Bottom	+2.75	+2.75
	Warping	Top	-2.0	-1.0
		Bottom	+2.25	+1.0

Table 3.2 Girder 3 Stress Change Summary

The bending and warping stress changes for each instrumented section during the two primary events are listed in Table 3.2. The same sign convention used with Girder 4's erection applies to Girder 3. Like Girder 4's trends, the trends observed in the stress change time histories of Girder 3 were the same for each section. However, one gage was lost during the erection. As seen in Figure 3.23, data was only collected from the strain gage on the right flange tip, making isolation of bending and warping stresses impossible. However, the stress history of this gage follows the same trends as the other gage sections.

A significant change in bending and warping stress was observed during the cross frame installation between 18:50 and 20:00 at each location. As seen in the figures, the magnitude and direction of this change are very distinguishable, unlike the erratic changes that took place on Girder 4 during cross frame installation. The removal of the spreader bar from Girder 3 led to a stress change in Girder 3, as it did for Girder 4.

3.4.4.1 Effects of Cross Section Symmetry

All of the cross sections of Girder 3 are symmetric. The magnitudes of bending stress changes during both cross frame installation and spreader removal reflect this, with absolute values being the same at the top and bottom flange for Sections B and C.

3.4.4.2 Maximum Stress Changes

Maximum bending stress changes occurred at Section C's top and bottom flange during both cross frame installation and removal of the spreader bar. These max values were approximately -2.75 ksi in the top flange and +2.75 ksi in the bottom flange.

The maximum warping stress change was +2.25 ksi. This value was observed at the bottom flange of Section C during cross frame installation.

3.5   SH 130/US 71 GIRDER ERECTION CONCLUSIONS

The results obtained from the lifting and erection of Girder 4 and Girder 3 can be used to make important conclusions about their general behavior. First, bending and warping stress changes during cross frame installation can be significant. Forcing of the girder into place for fit up purposes or ratcheting of cross frames appears to induce high bending and warping stresses relative to other stages of erection, particularly in the fascia girder, Girder 4. A warping stress change of 7.0 ksi was observed at the top flange of Section C of Girder 4, which was the highest stress change recorded during this study.

Second, locations closer to midspan (Section C in this case) appear to be the more critical sections with regard to bending and warping stresses at all stages of erection. All of the maximum stress values observed for both Girder 4 and Girder 3 occurred at Section C, yielding evidence to this conclusion.

Ultimately, though some results showed relatively large stress change values that led to the conclusions above, most of the observed stress changes were under 3 ksi in magnitude. Noting that reported results are changes in stress from a previous stress state, the magnitude of these changes would make it seem that the possibility of an unpredictably large stress state occurring during erection on this particular bridge is

small. However, since these results are stress changes from an indeterminate state of stress, it is difficult to determine more precise stress magnitudes from this study. The researchers had no control over the support conditions of the girders. The dunnage that was used to support the girders consisted of heavy timbers that were spread over regions of approximately 20' along the girder length in some instances. The actual contact points between the bottom flanges and the wood timbers were very difficult to assess.

Figure 3.25 Dunnage Used for Girder Support

For the purposes of obtaining more appropriate data for the validation of the finite element model used to perform thorough parametric studies of curved I-girder stability during the initial lifting stages of erection, an additional study was needed. The following section details the Hirschfeld lift tests and the results obtained from a more controlled testing environment where the boundary conditions were known.

3.6   HIRSCHFELD LIFT TESTS

The following section details the method by which girders 16C4 and 14C2 were tested at the Hirschfeld Steel Company yard. The lifting setup is discussed, as well as the test procedure and timeline.

3.6.1   Lifting Setup

The Hirschfeld lift tests were undertaken to capture the stresses and rotations associated with placing a curved girder on the ground with known support conditions and lifting it into the air. This process was then repeated to provide repeatable data. Two different girder support locations were tested.

3.6.1.1   Girder Supports

Figure 3.26 Wood Supports

Two identical supports were used, yielding a statically determinate structure and known support conditions. These supports are pictured in Figure 3.26. The supports were fabricated at Phil M. Ferguson Structural Engineering Laboratory. The base consisted of three 2" x 6" timbers bolted together using ½" diameter bolts spaced evenly

along the length. The diagonal struts were composed of 4" x 4" timbers, with a single ¾" diameter bolt connecting them to the base. The single bolt allowed the struts to swivel relative to the base and make girder contact between the top flange and the web. The top ends of the struts were beveled for improved fit up.   These struts were intended to stabilize the curved girder and prevent it from excessive rotation due to its curved geometry while on the supports.

3.6.1.2 Girder Lifting

The girders were lifted using a MI-JACK with a lift clamp spacing of approximately 40 feet. Figure 3.27 and Figure 3.28 show the MI-JACK and lift clamp apparatus.

Figure 3.27 MI-JACK Travelift Provided By Hirschfeld Steel

Figure 3.28 MI-JACK Lift Clamp Apparatus

3.6.2 Test Procedure

The fabricated wood supports were placed at two support locations, S1 and S2, along each girder. Support location S1 was located near the ends of the girder, while S2 was closer to the lift points (see Figure 3.30 and Figure 3.33). The S1 support locations were intended to induce a moment distribution that would maximize the change in moment (and thus stress) during girder lifting. This would alleviate the complicating issue that had been present for the SH 130/US 71 girder erection, where the moment distributions had been very similar during the lift and while it was supported on the ground by timbers; a situation which yielded small changes in stress.

A timeline of this testing procedure is shown in Figure 3.29. Each girder's timeline begins when the data acquisition system was activated and ends when it is placed on timbers and the lift clamps are removed. For both girders, the dataloggers were programmed to scan every 12 seconds. For each location, the girder was placed on the supports for approximately 1-2 minutes, lifted up for approximately 1-2 minutes, replaced on the supports for 1-2 minutes, and lifted again while the supports were moved to the new location.
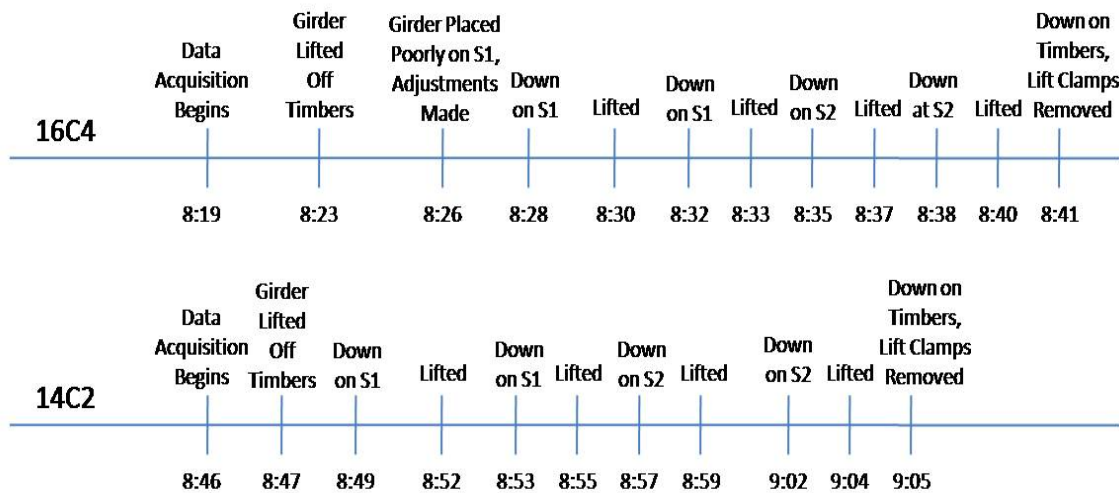
Figure 3.29 Test Timeline for 16C4 & 14C2

3.6.2.1 16C4 Lift Test

For support location S1, each wood support was placed 5 feet from each end of the girder. For support location S2, the wood supports were placed 23'-6" from each end of the girder. Figure 3.30 shows these support locations on 16C4, as well as the location of the lift clamps.
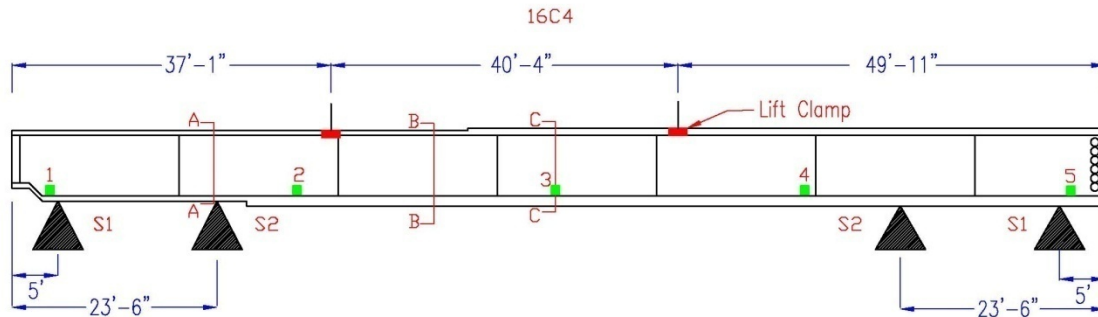
Figure 3.30 16C4 Support and Lift Clamp Locations

During the first attempt at placing the girder on the fabricated supports (8:26 in Figure 3.29), there was difficulty in maneuvering the girder and placing it appropriately. The girder was partially supported by the MI-JACK and the wood supports during this time, until the girder was properly placed at S1 (8:28).

Figure 3.31 16C4 Lifted at S1 (8:30)

Figure 3.32 16C4 Down on S2 (8:35)

Figure 3.31 and Figure 3.32 show 16C4 during the lift tests. Once the lift sequence shown in Figure 3.29 was completed, the lift clamps were detached from 16C4 and the MI-JACK was moved to 14C2 for its lift test.

3.6.2.2 14C2 Lift Test

For support location S1, each wood support was placed 5' from each end of the girder. For support location S2, the wood supports were placed 31' from each end of the girder. Figure 3.33 shows these support locations on 14C2, as well as the location of the lift clamps. The procedure for 14C2's lift test was the same as for 16C4. Figure 3.34 show 14C2 placed on supports located at S2.
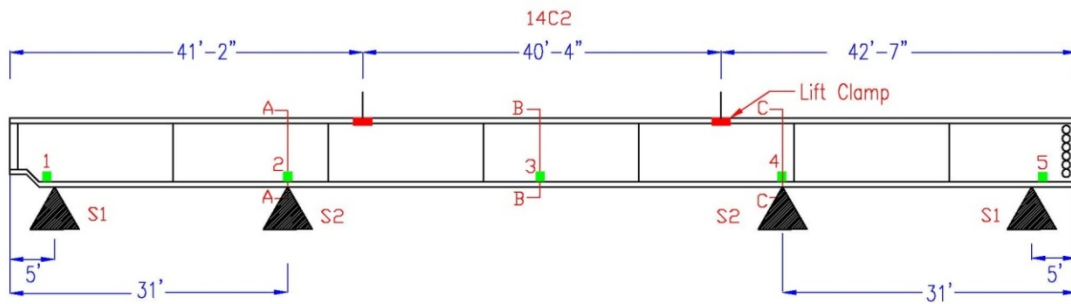
Figure 3.33 14C2 Support and Lift Locations

Figure 3.34 14C2 Down on S2 (8:57)

3.7   HIRSCHFELD LIFT TESTS RESULTS

The following section presents stress and rotation time histories for 16C4 and 14C2's respective lift tests.   For each girder, the data is separated into the graphs associated with the girder supported at S1 and the graphs associated with the girder supported at S2. Bending and warping stresses are shown on separate plots to display the behavior of the instrumented cross section (top and bottom flange). The data was zeroed using the results from the girder while it is supported by the lift clamps in the air. Therefore, the data represents the change in stress or rotation between the ground and lifted positions.

3.7.1   16C4 Results

It is important to note the erratic nature of the stress and rotation data during the initial attempted placement of the girder at S1 (8:26). As mentioned earlier, this data was neglected due to problems placing the girder on the supports properly.   In addition, problems were encountered in placing the girder on timbers after being lifted from S2 at the conclusion of the test (8:40). Adjusting the girder to place it properly prevented the girder's rotations from settling at the typical values exhibited in the air, as shown in Figure 3.36.
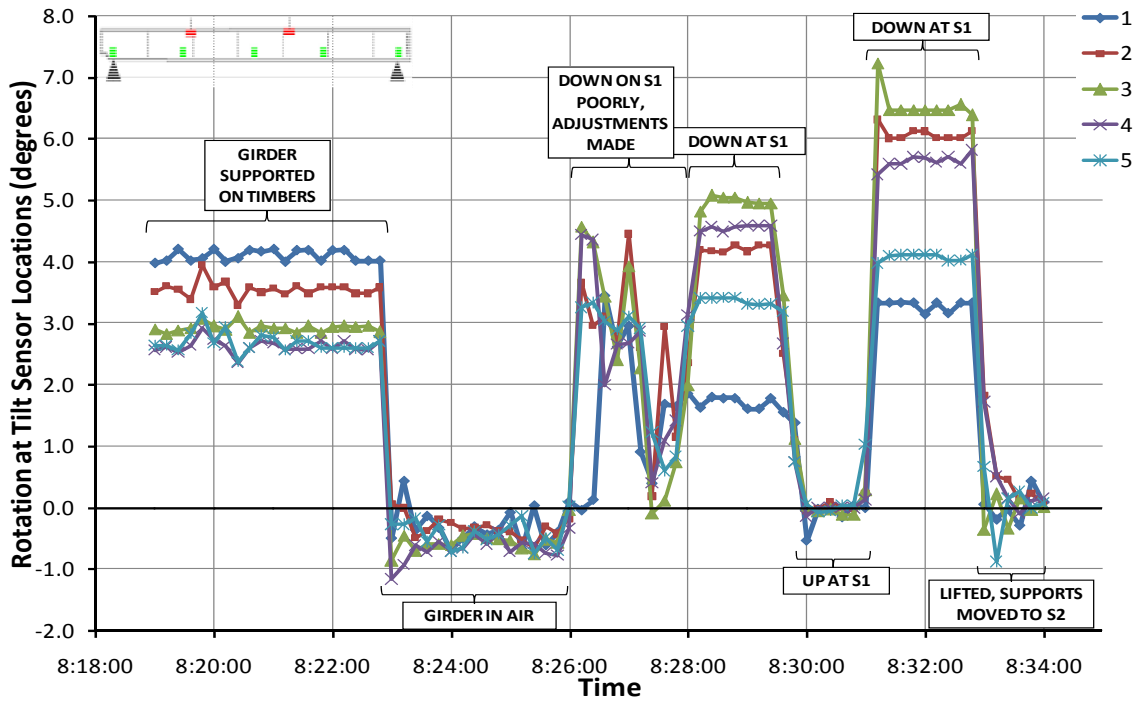
Figure 3.35 16C4 Rotation Changes for Support Location S1
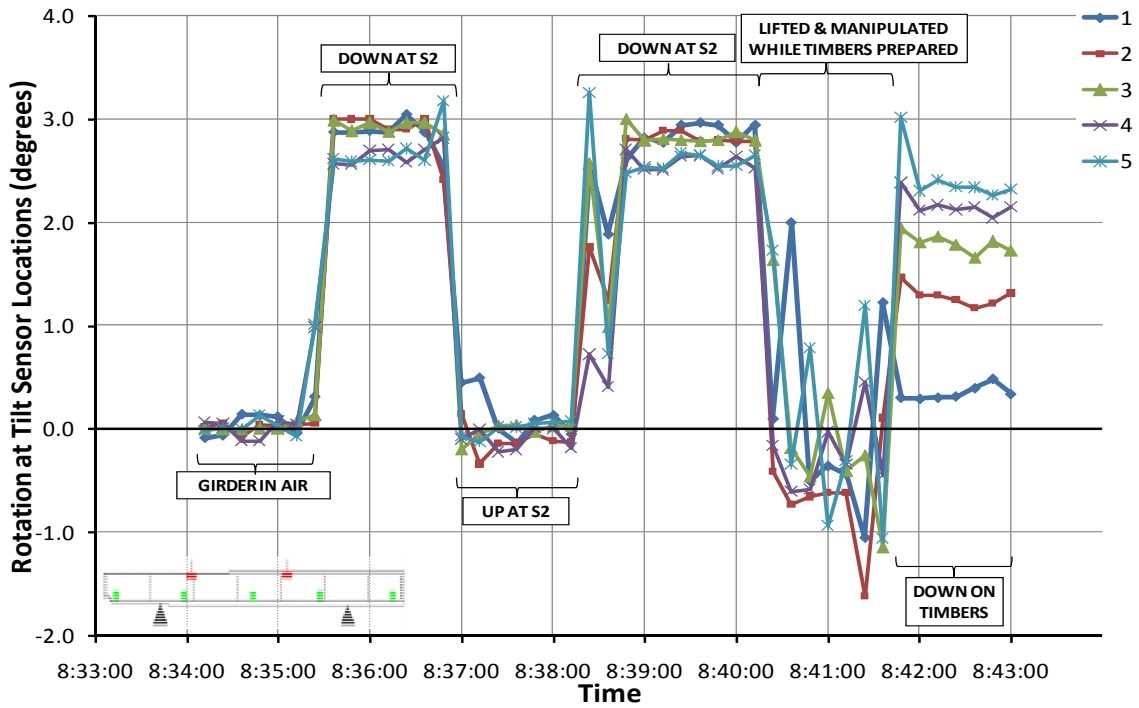
Figure 3.36 16C4 Rotation Changes for Support Location S2

62
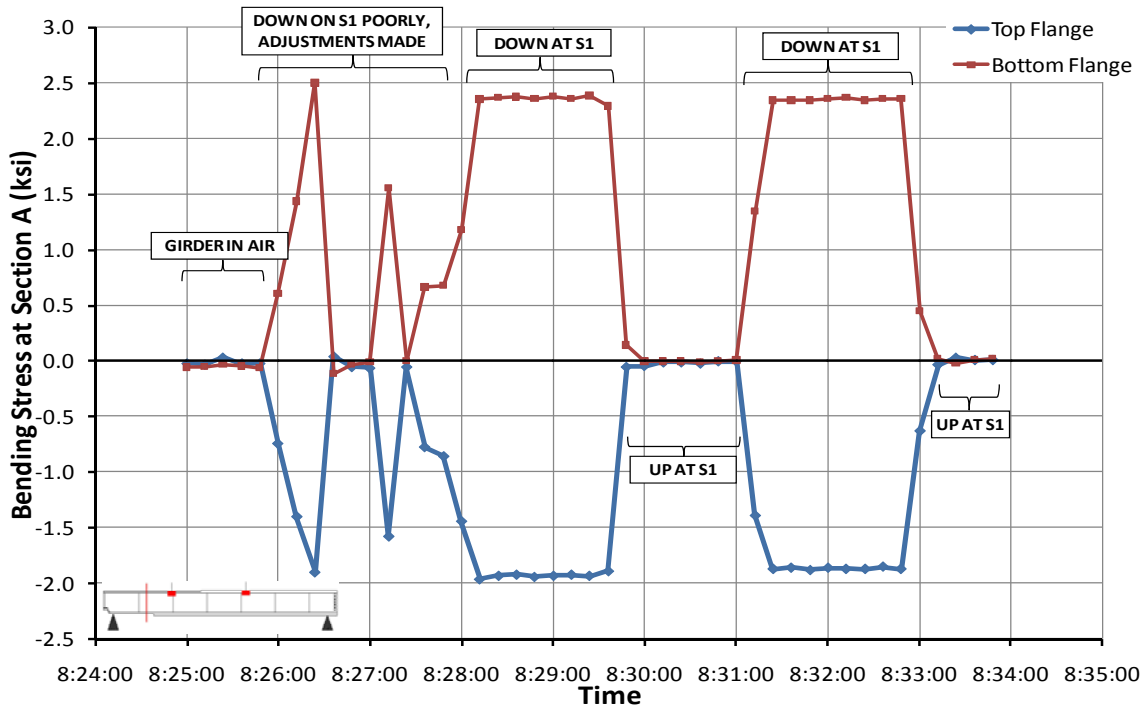
Figure 3.37 16C4 Bending Stress Change at Section A for Support Location S1
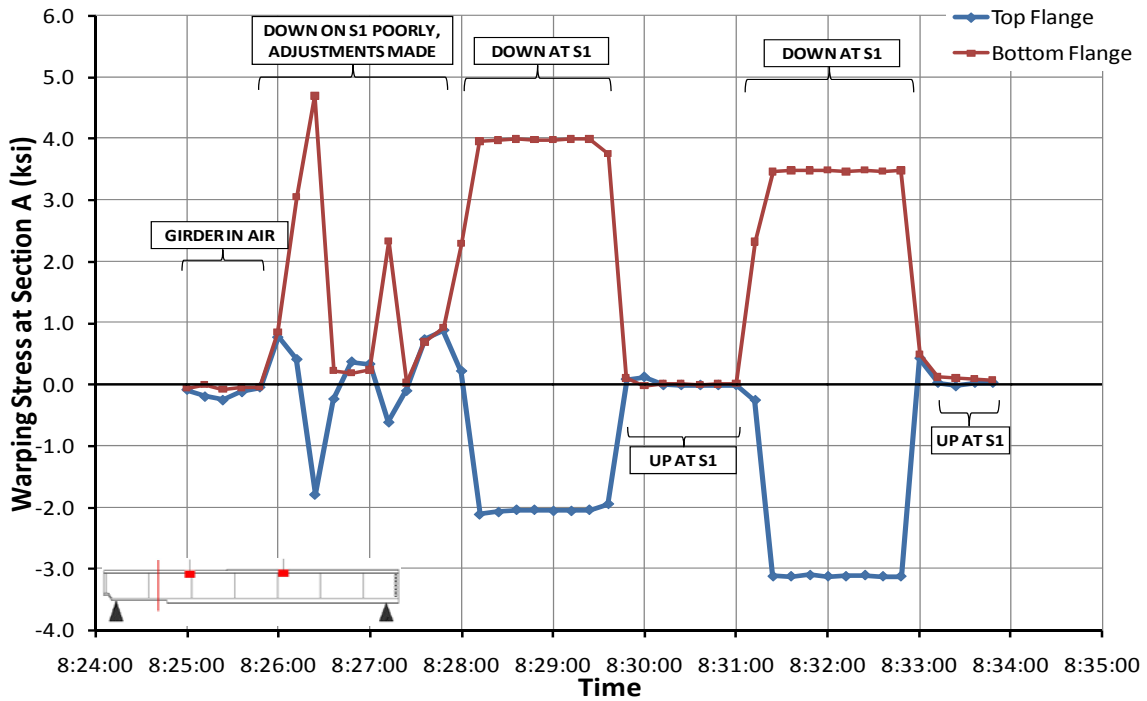
Figure 3.38 16C4 Warping Stress Change at Section A for Support Location S1

63
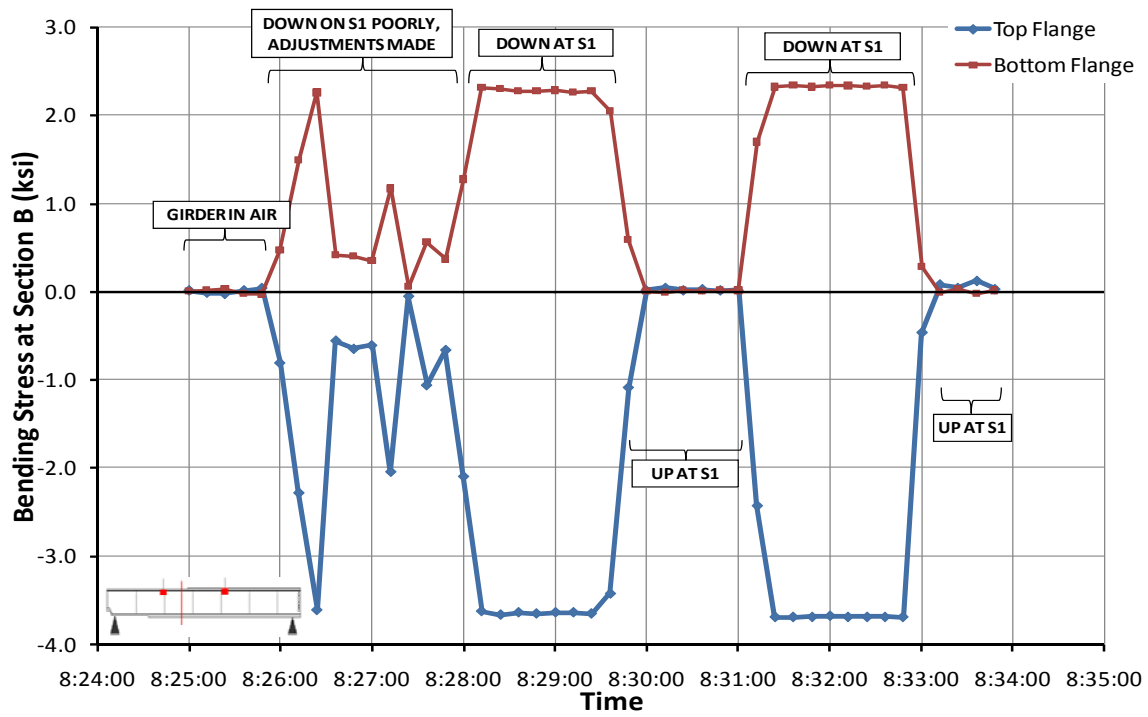
Figure 3.39 16C4 Bending Stress Change at Section B for Support Location S1
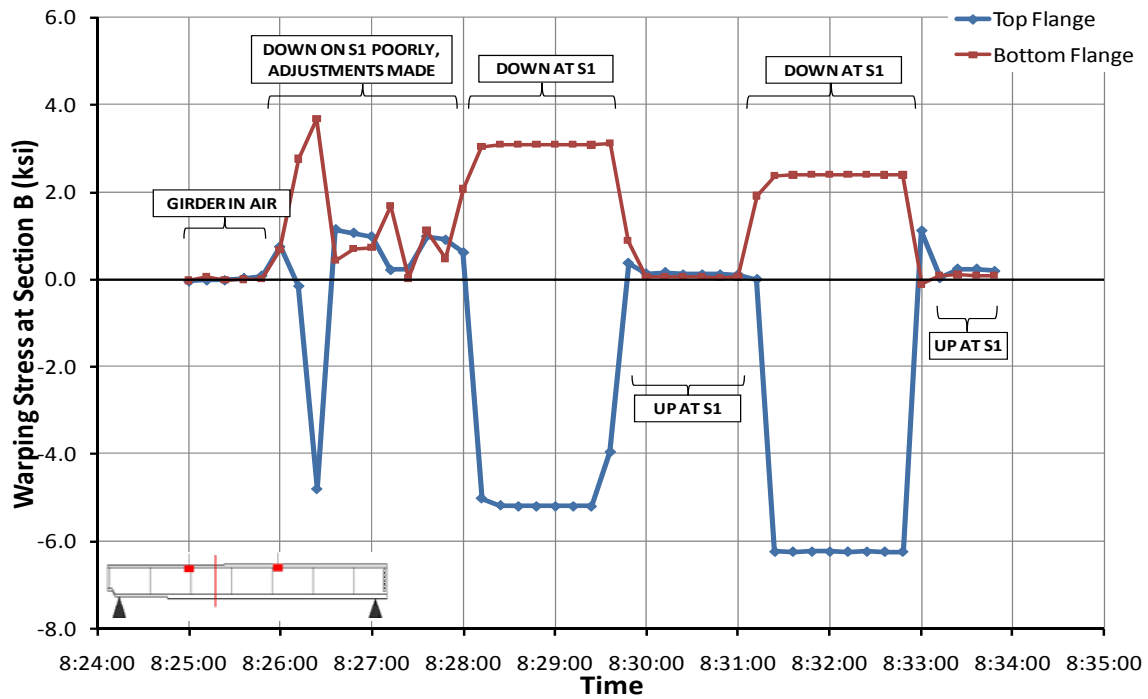
Figure 3.40 16C4 Warping Stress Change at Section B for Support Location S1

64
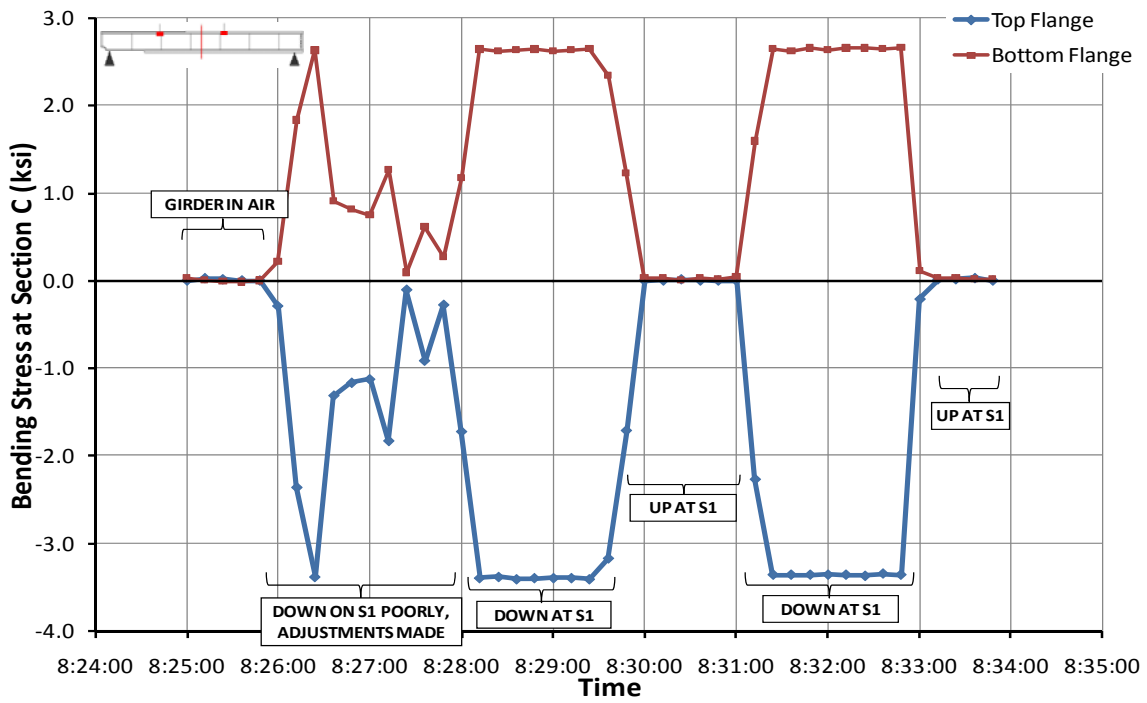
Figure 3.41 16C4 Bending Stress Change at Section C for Support Location S1
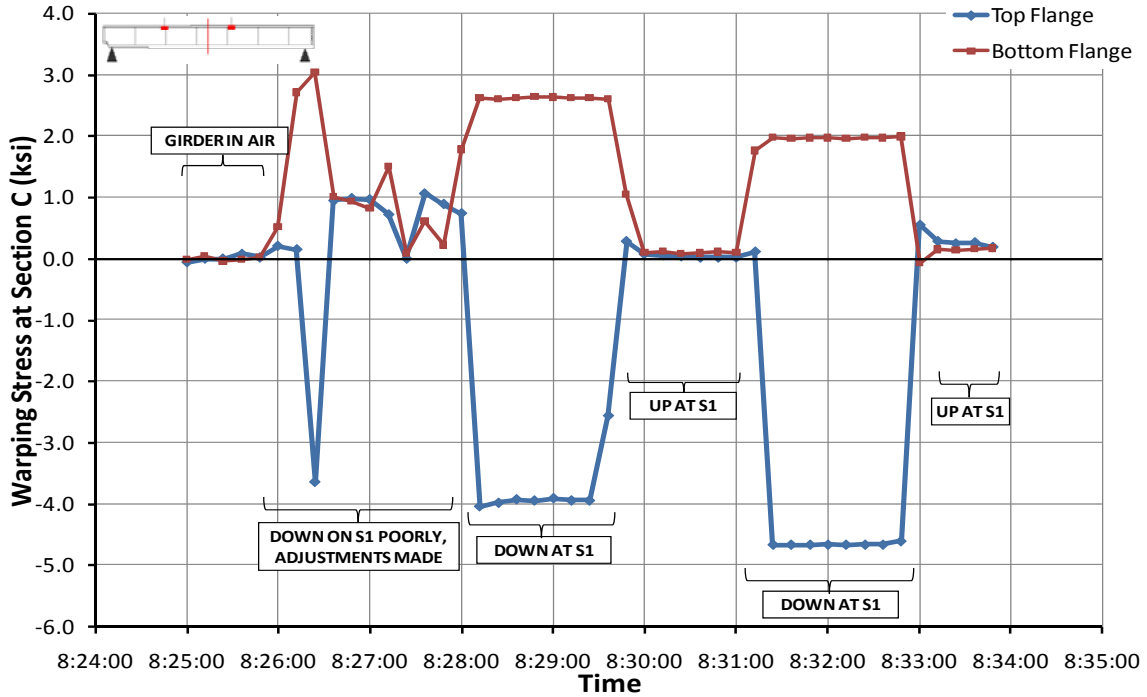
Figure 3.42 16C4 Warping Stress Change at Section C for Support Location S1
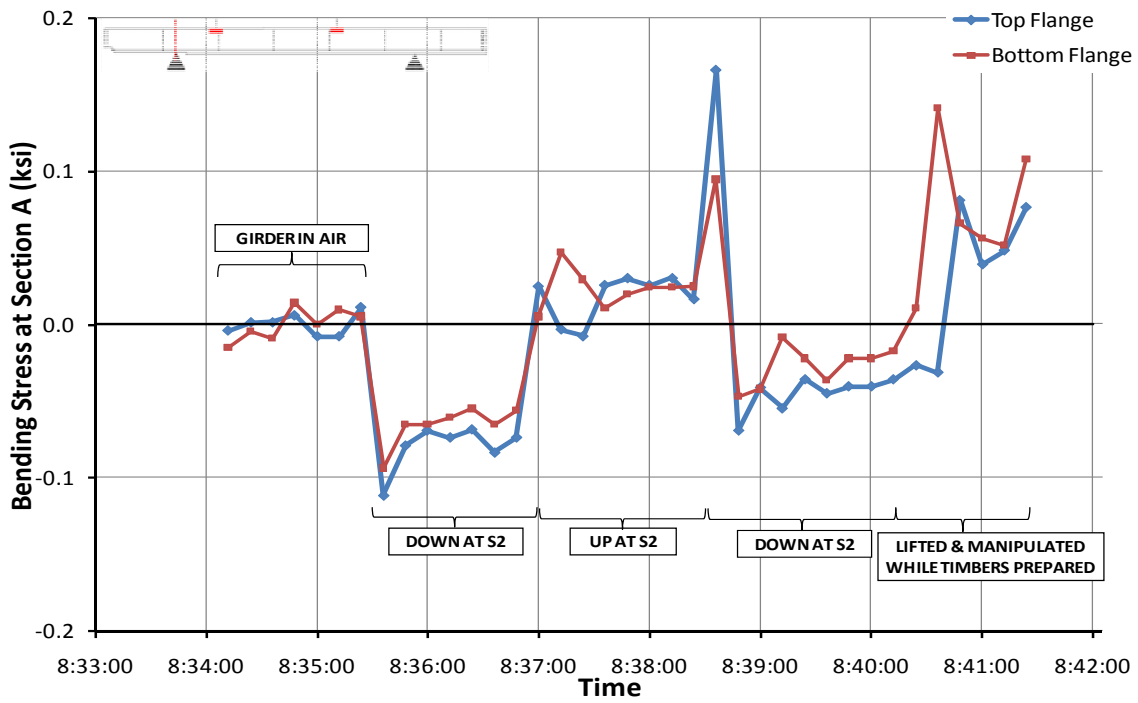
Figure 3.43 16C4 Bending Stress Change at Section A for Support Location S2
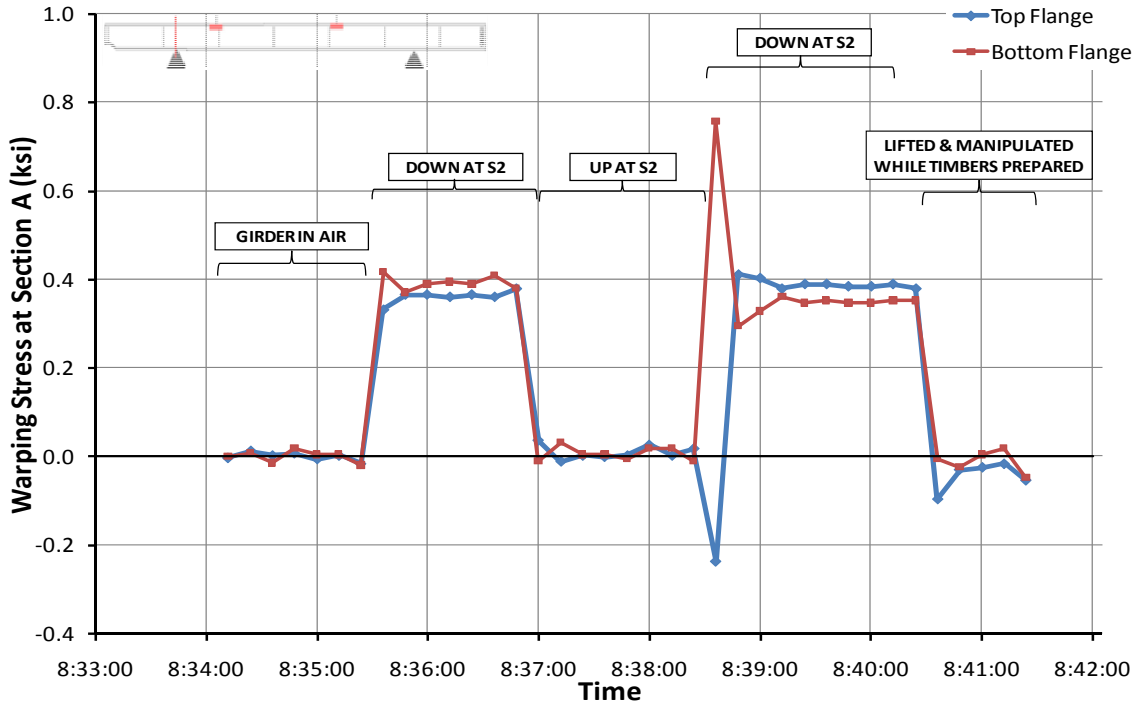
Figure 3.44 16C4 Warping Stress Change at Section A for Support Location S2

66
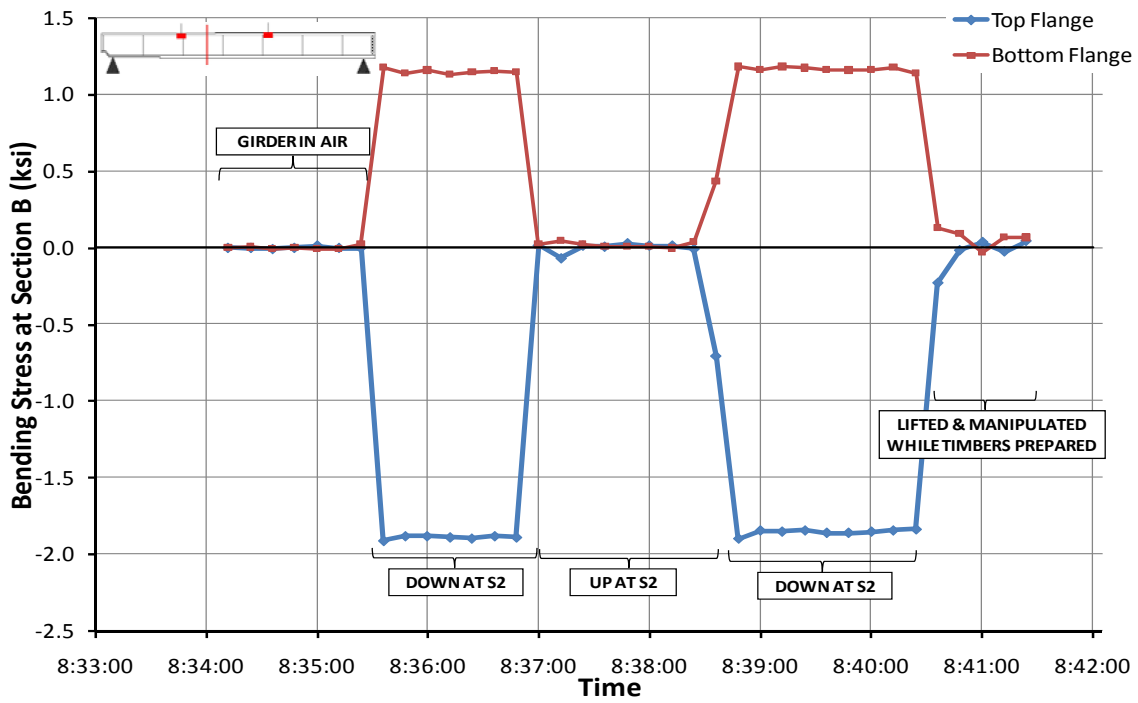
Figure 3.45 16C4 Bending Stress Change at Section B for Support Location S2
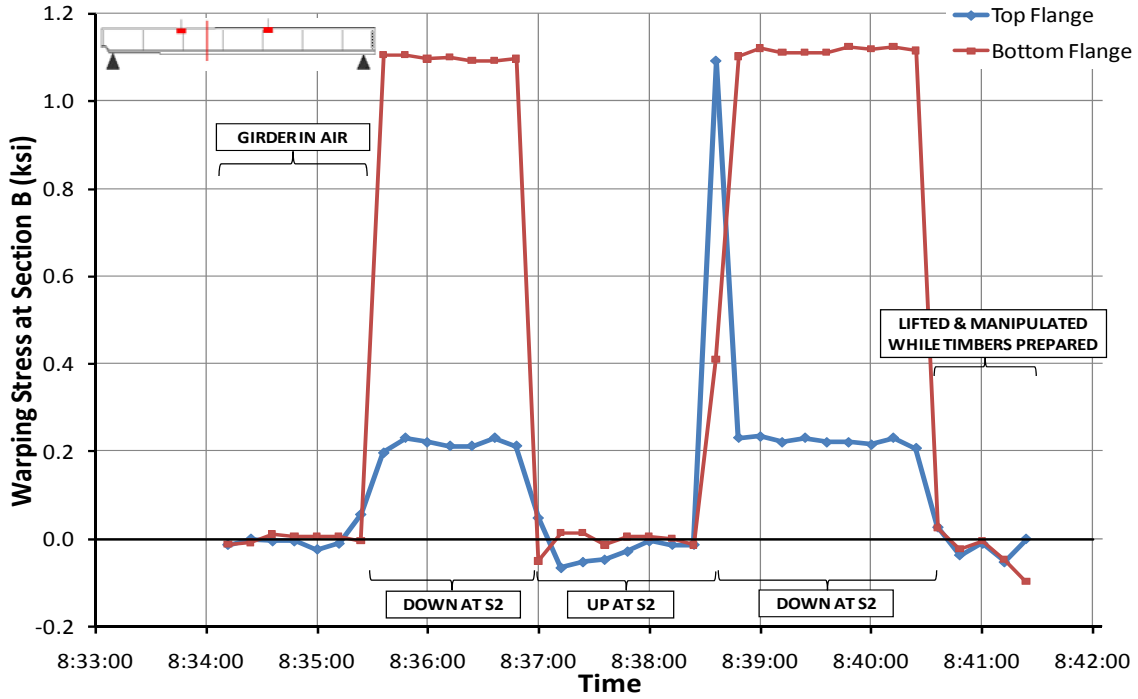
Figure 3.46 16C4 Warping Stress Change at Section B for Support Location S2

67
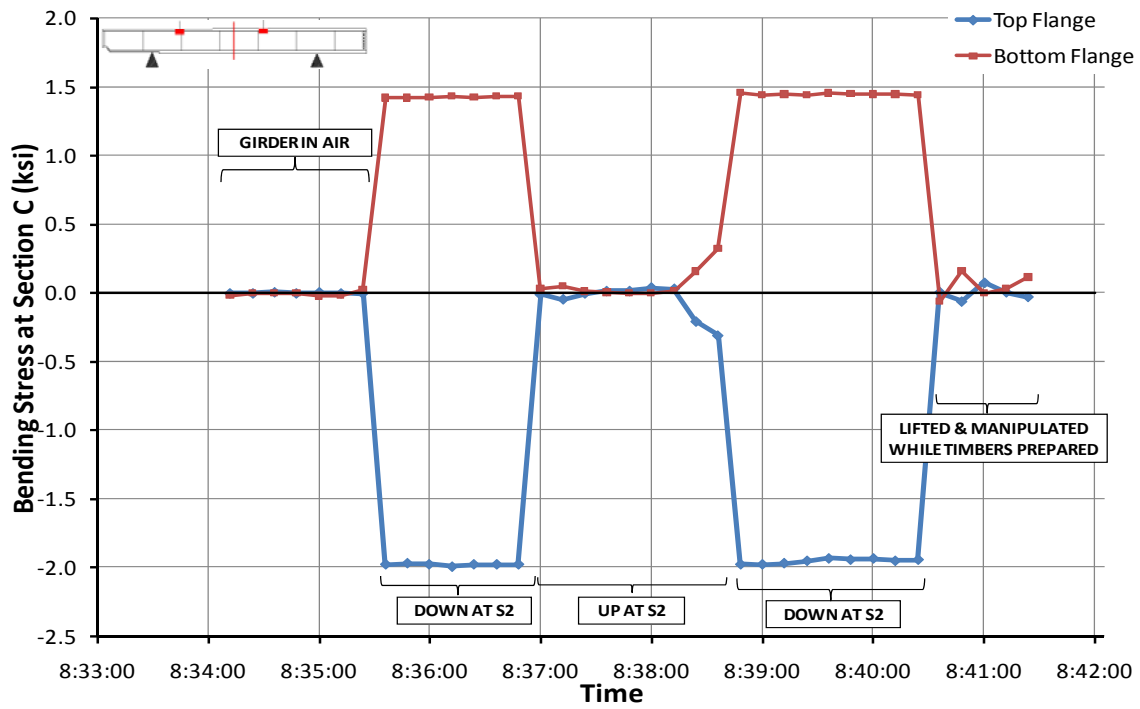
Figure 3.47 16C4 Bending Stress Change at Section C for Support Location S2
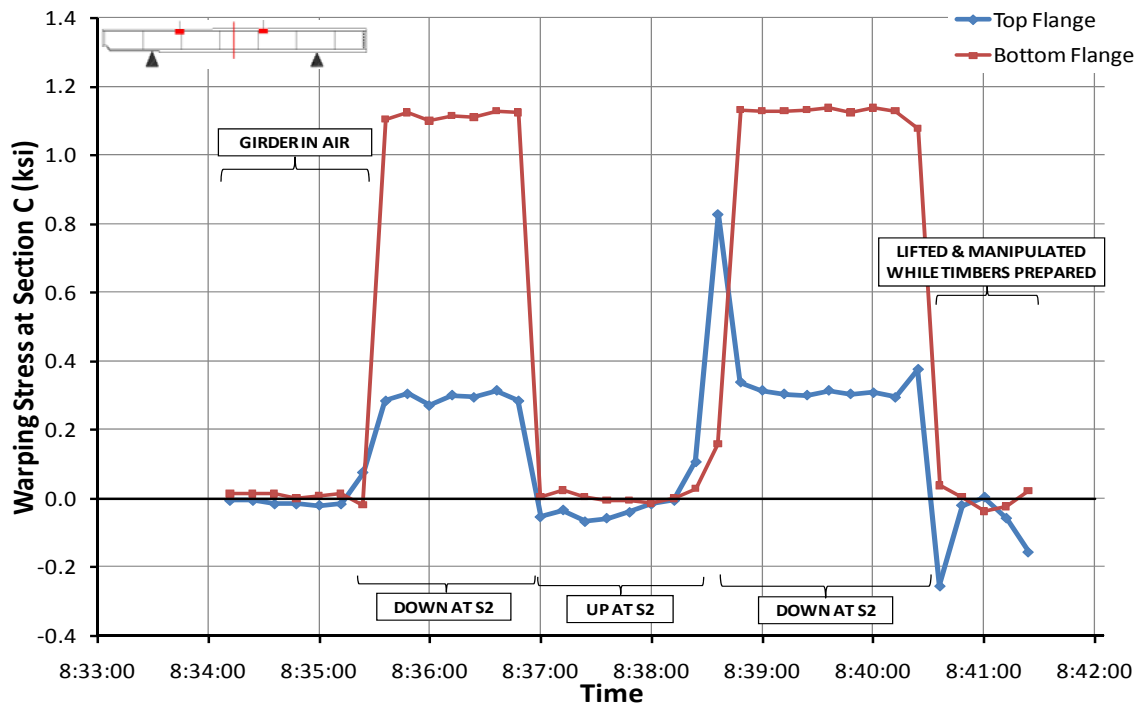
Figure 3.48 16C4 Warping Stress Change at Section C for Support Location S2

68

3.7.2 Summary of 16C4 Results

3.7.2.1 Rotations

Location	16C4 Rotation Change During Event (Degrees)	
	Down on S1	Down on S2
Tilt Sensor 1	3.3	2.9
Tilt Sensor 2	6.0	2.9
Tilt Sensor 3	6.5	2.9
Tilt Sensor 4	5.7	2.7
Tilt Sensor 5	3.1	2.7

Table 3.3 16C4 Rotation Change Summary

Table 3.3 summarizes the rotation changes observed at each tilt sensor location when 16C4 was placed on S1 and S2. The values are given in degrees and are all of the same sign because the girder exhibited a rigid body rotation due to the girder's curvature in all cases presented in this study. This aspect of curved I-girder lifting is discussed more thoroughly in Chapter 4.

For the rotation changes at S1 shown in Figure 3.35, the values were taken as those observed during the second placement of the girder on S1. This was due to the significant differences during the first placement suggesting that even when the girder was repositioned at 8:26, the rotations remained affected. The second placement was therefore a better value to present in the results above.

When the girder was placed on S2, the rotation changes at all tilt sensors are approximately the same. This indicates that the observed rotations were attributed entirely to rigid body rotation of the girder. When the girder was placed down on S1, a maximum rotation change of 6.5 degrees occurred at Tilt Sensor 3, at the midspan of the girder.

3.7.2.2   Stresses

Location	Stress	Flange	16C4 Stress Change During Specified Event (ksi)	
			Down on S1	Down on S2
Section A	Bending	Top	-1.9	0.0
		Bottom	+2.4	0.0
	Warping	Top	-3.2	+0.4
		Bottom	+4.0	+0.4
Section B	Bending	Top	-3.7	-1.9
		Bottom	+2.3	+1.2
	Warping	Top	-3.1	+0.2
		Bottom	+6.2	+1.1
Section C	Bending	Top	-3.4	-2.0
		Bottom	+2.6	+1.4
	Warping	Top	-4.7	+0.3
		Bottom	+2.6	+1.1

*Table gives larger stress change if repeatability does not exist

Table 3.4 16C4 Stress Change Summary

Table 3.4 summarizes the stress change values at the instrumented sections of 16C4 when it was placed on S1 and S2. The stress changes associated with placement on S1 are larger than those for S2. As mentioned earlier, this is caused by more dramatic differences between the moment diagram of S1 and the moment diagram of the girder while lifted. Conversely, the moment diagram of S2 is relatively similar to the lifted diagram, as evidenced by the lower changes in stress in Table 3.4.

Section A is the only cross section of 16C4 that is doubly symmetric; however, the magnitudes of the stress values at the top and bottom flange are slightly different by approximately 0.5 ksi. Section B and C are singly symmetric, with the centroid below midheight since the bottom flange is larger than the top flange. The results confirm this, with larger magnitude bending stresses present at the top flange. The largest bending stress change observed was at Section B's top flange when the girder was placed on S1, which induced a change of -3.7 ksi.

The relative sign of the warping stress change was different for S2. Unlike the opposite signs exhibited by the flanges for S1, the top and bottom flange warping stress

change had the same sign when the girder was placed on S2. Both classic theory and the results from the SH 130/US 71 erection show that the warping stresses are typically of opposite direction (sign) in the top and bottom flange of a given cross section. However, a finite element analysis on the girders during lifting also showed this same behavior, attributing it to a weak axis bending. When the girder undergoes the observed rigid body rotation relative to its position on S2, a component of the self weight induces bending about the weak axis, which acts against the warping stresses present in one of the flanges (the top in this case) and with those in the bottom flange. The result is the appearance of warping stresses acting in the same direction in both flanges, although it is actually the result of weak axis bending overshadowing the warping stresses in one flange and yielding a small positive value in the case of 16C4. The maximum warping stress change was +6.2 ksi at the bottom flange of Section B when the girder was placed on S1.

3.7.3   14C2 Results
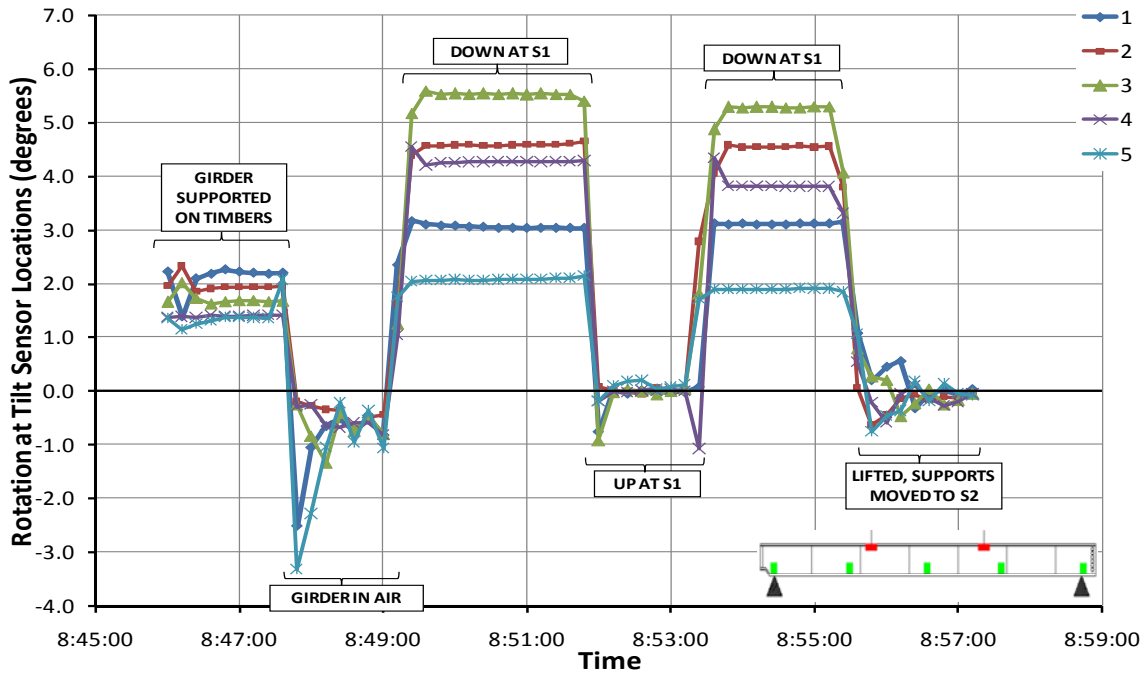
Figure 3.49 14C2 Rotation Changes for Support Location S1
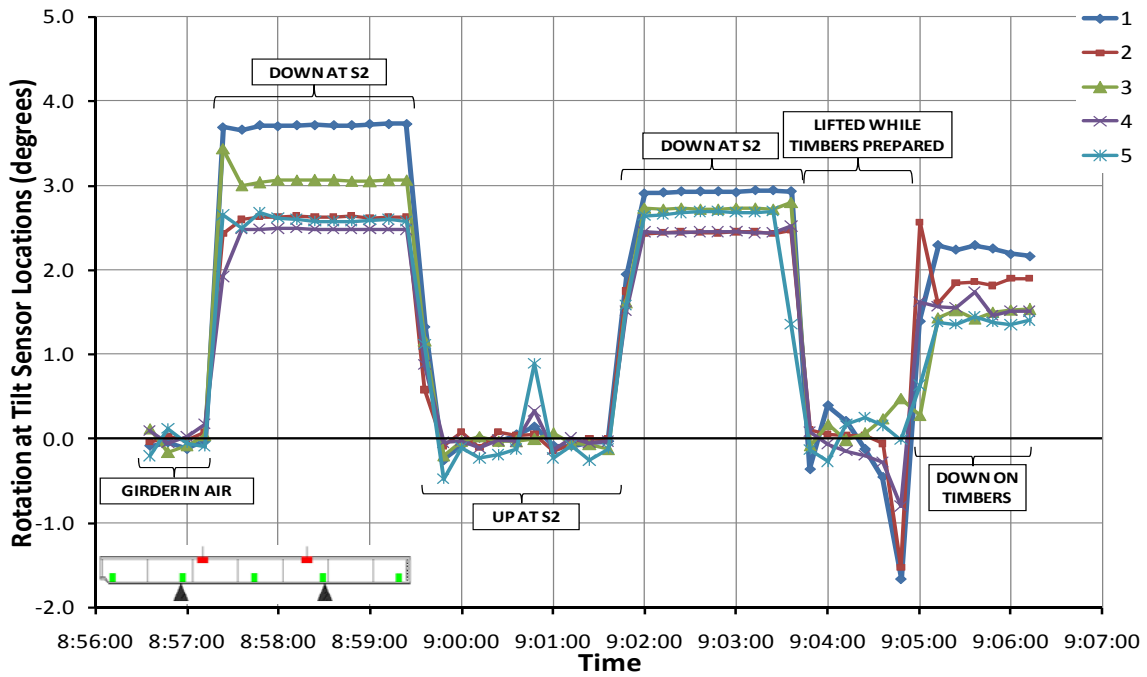
Figure 3.50 14C2 Rotation Changes for Support Location S2

72
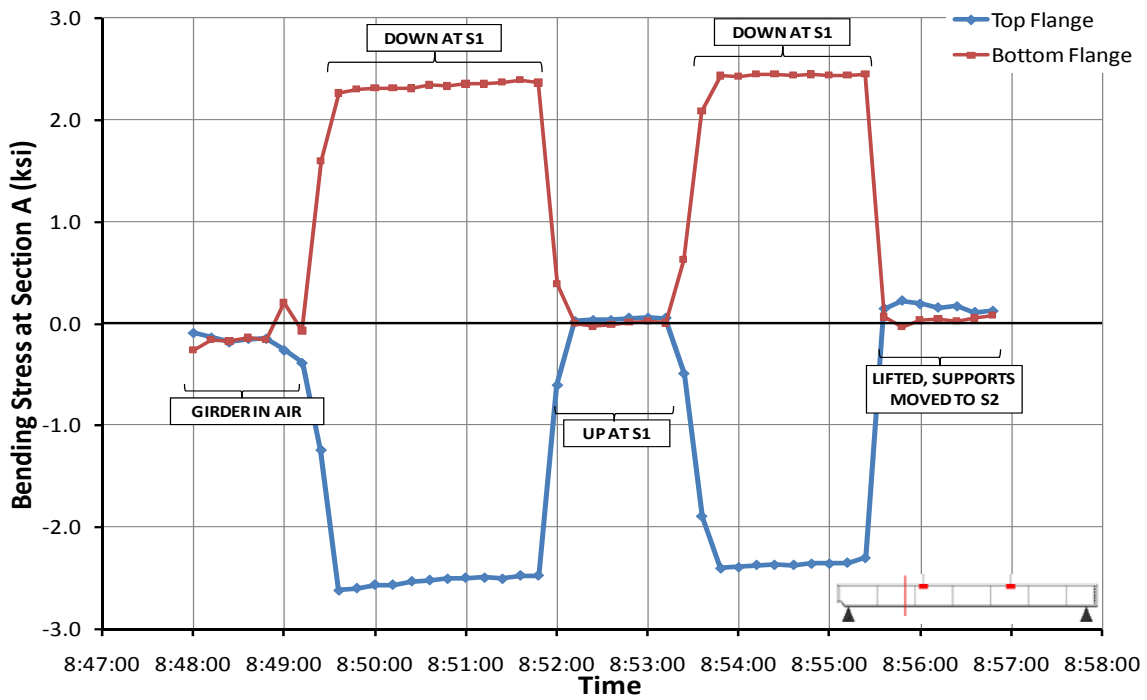
Figure 3.51 14C2 Bending Stress Change at Section A for Support Location S1
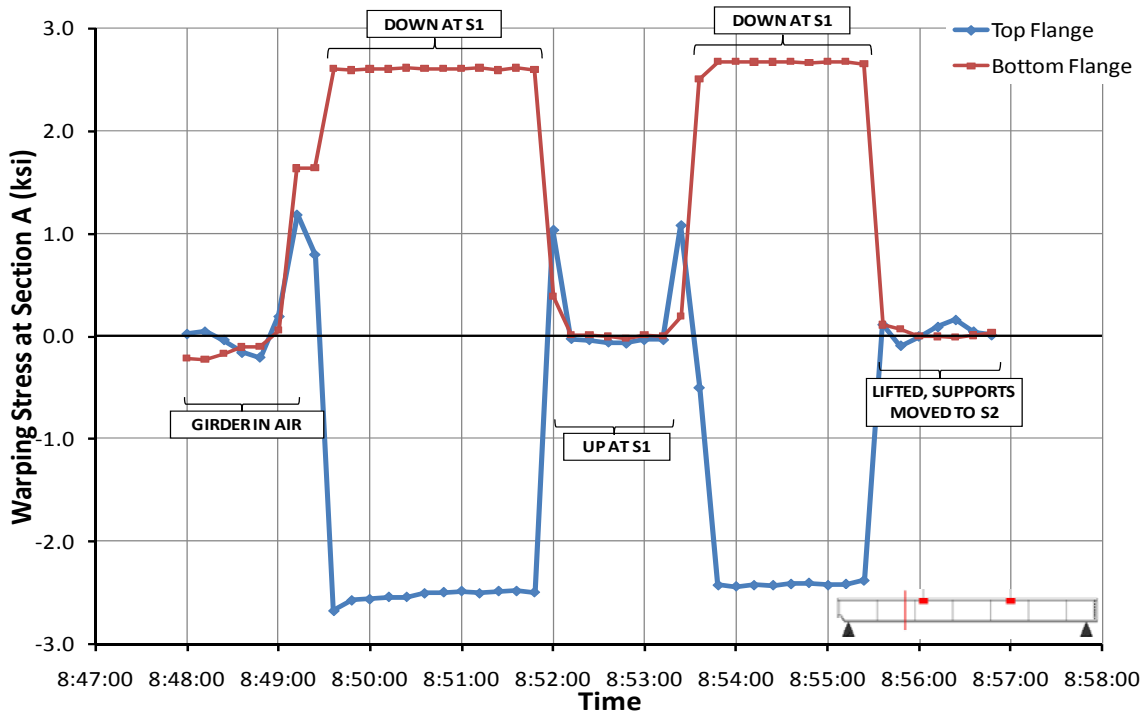
Figure 3.52 14C2 Warping Stress Change at Section A for Support Location S1

73
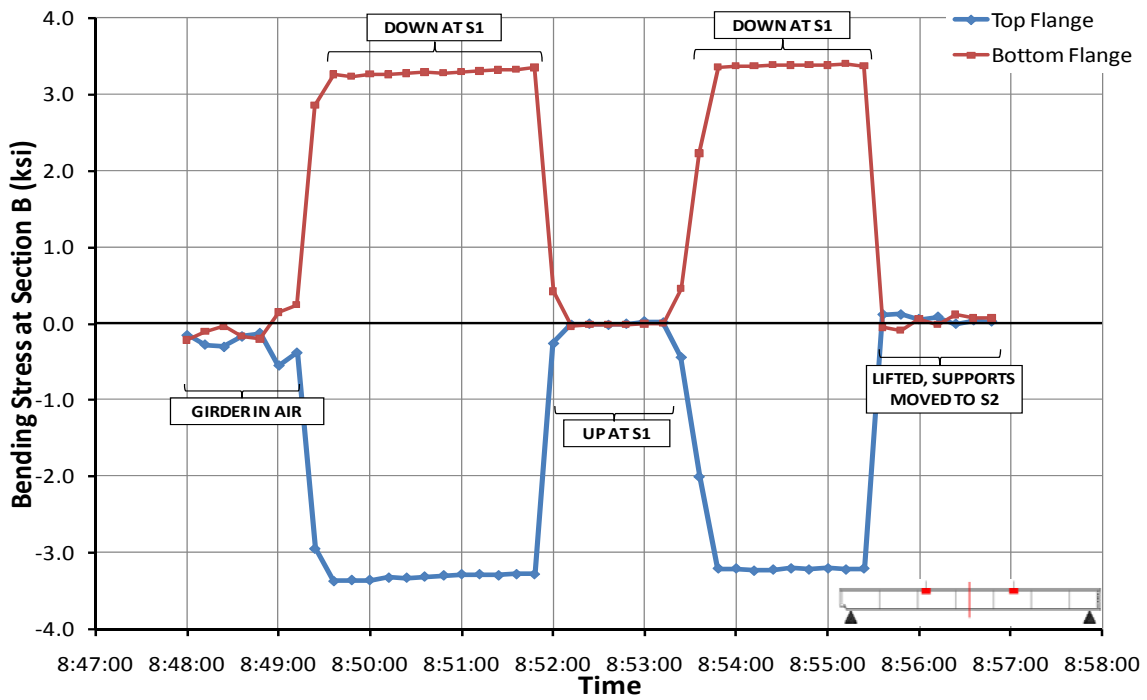
Figure 3.53 14C2 Bending Stress Change at Section B for Support Location S1
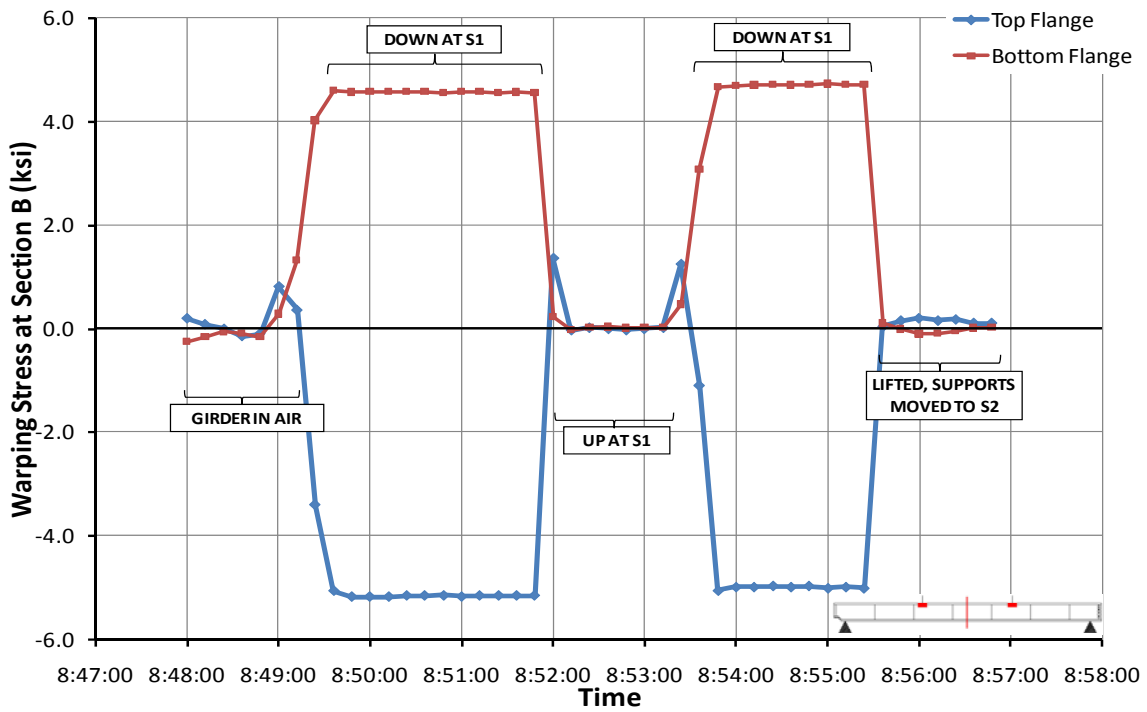
Figure 3.54 14C2 Warping Stress Change at Section B for Support Location S1

74
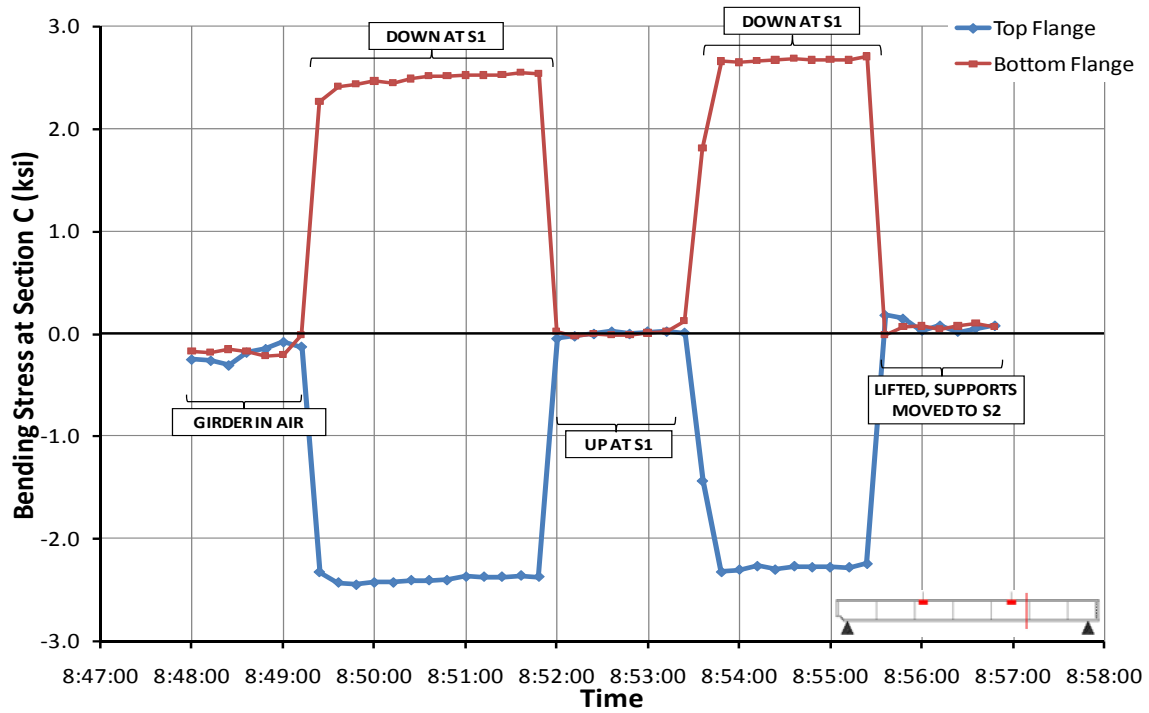
Figure 3.55 14C2 Bending Stress Change at Section C for Support Location S1
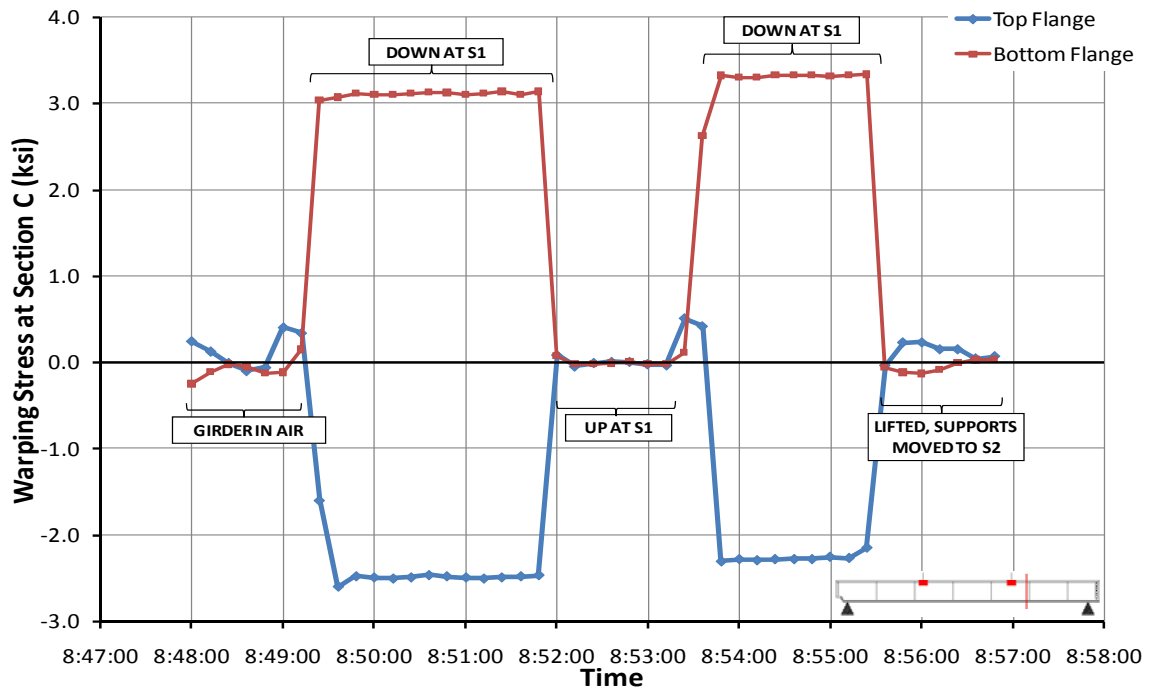
Figure 3.56 14C2 Warping Stress Change at Section C for Support Location S1

75
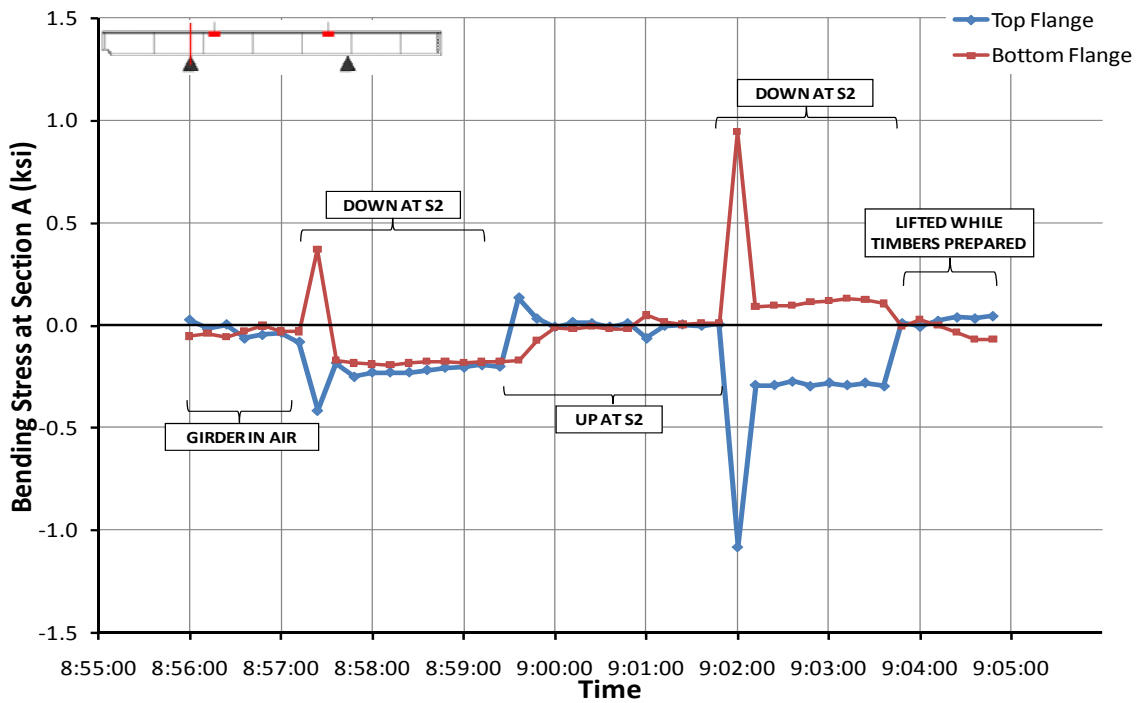
Figure 3.57 14C2 Bending Stress Change at Section A for Support Location S2
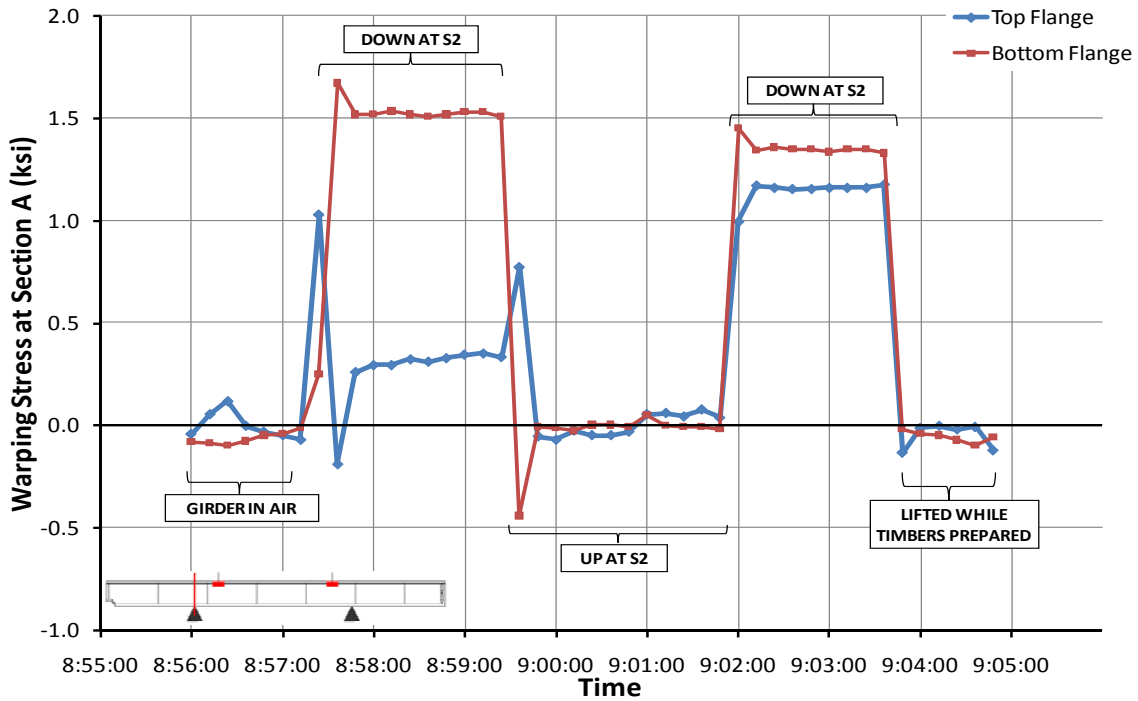
Figure 3.58 14C2 Warping Stress Change at Section A for Support Location S2

76
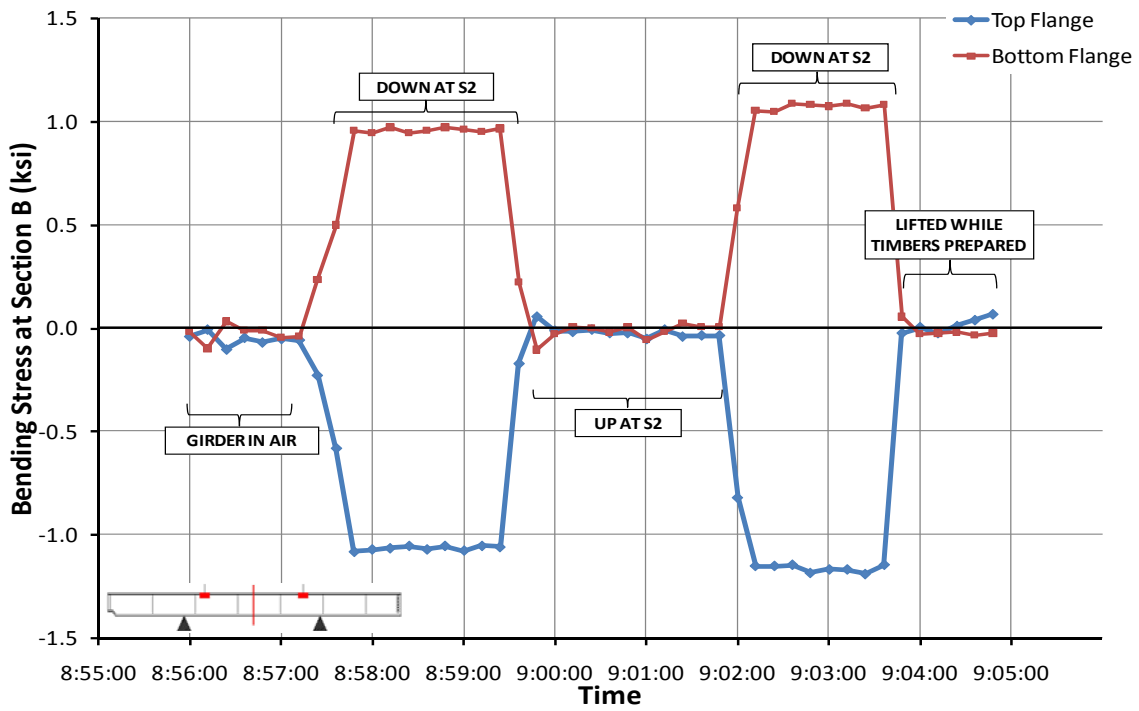
Figure 3.59 14C2 Bending Stress Change at Section B for Support Location S2
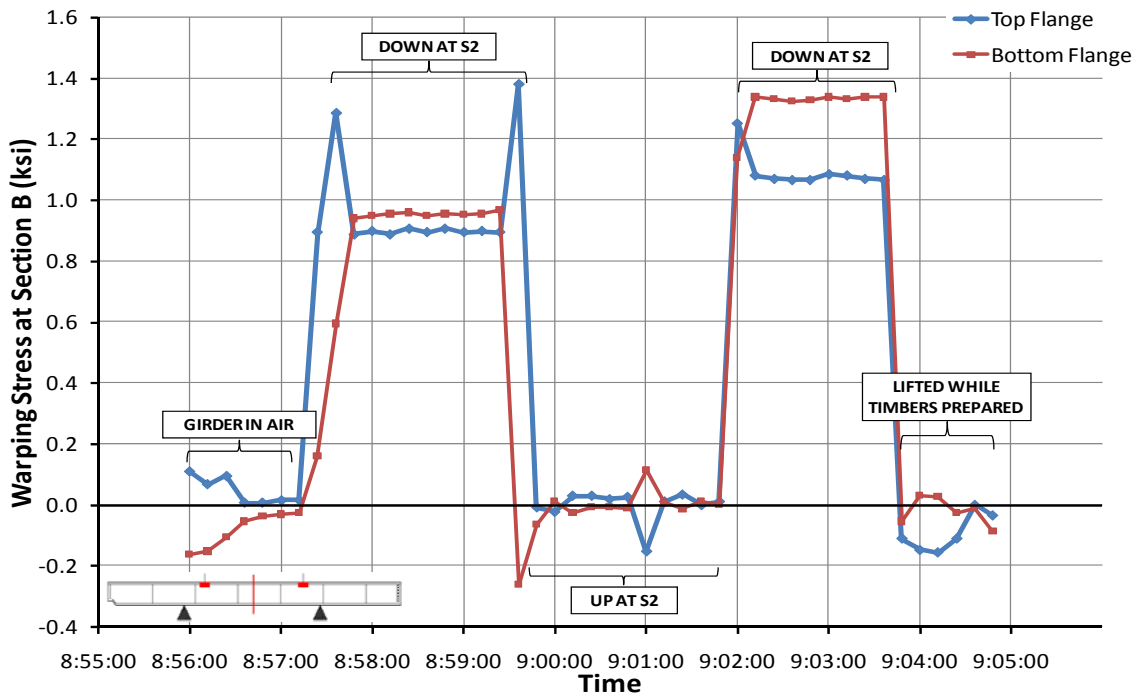
Figure 3.60 14C2 Warping Stress Change at Section B for Support Location S2

77
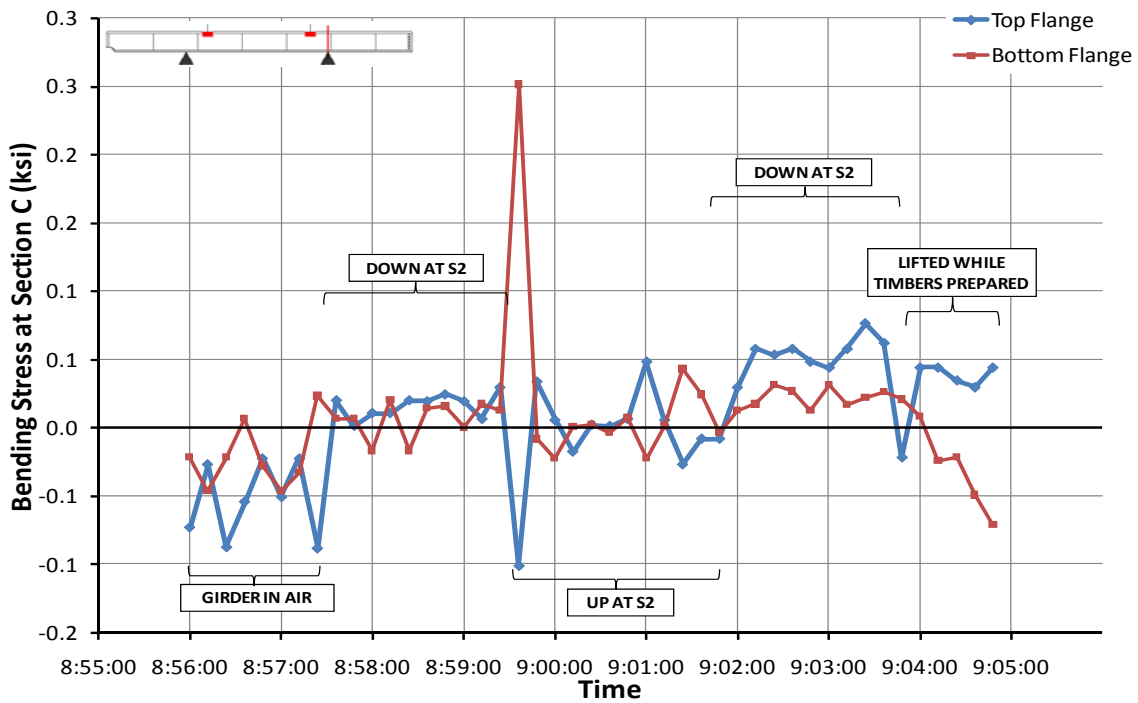
Figure 3.61 14C2 Bending Stress Change at Section C for Support Location S2
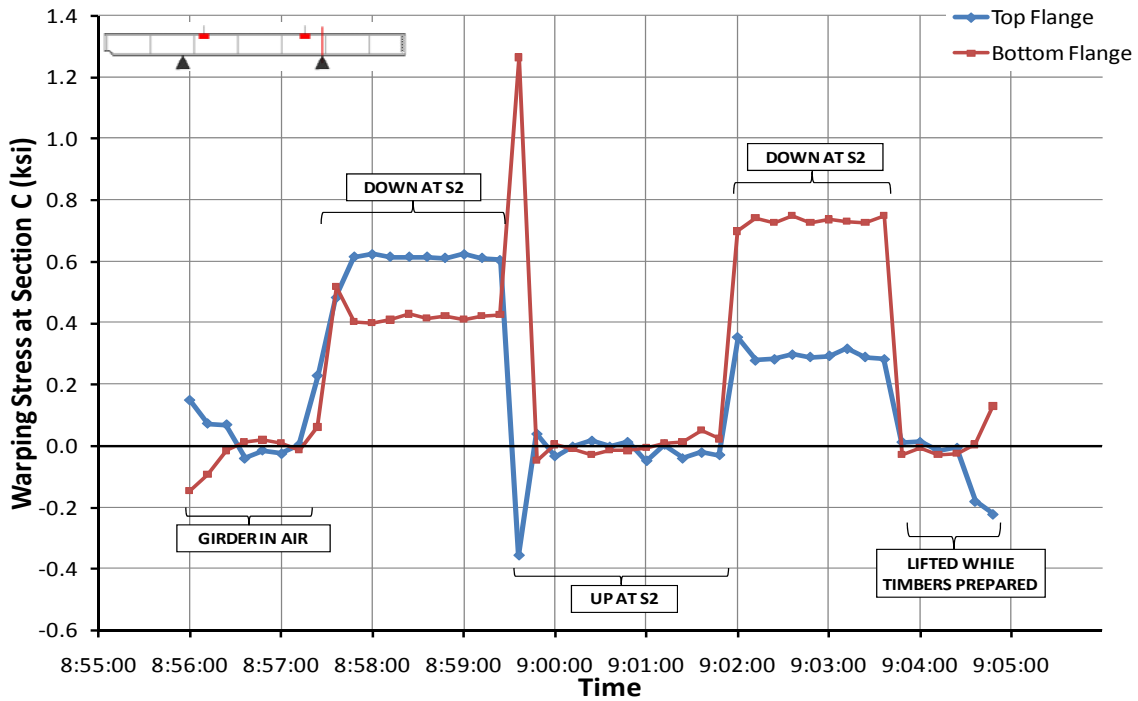
Figure 3.62 14C2 Warping Stress Change at Section C for Support Location S2

78

3.7.4 Summary of 14C2 Results

3.7.4.1 *Rotations*

Location	14C2 Rotation Change During Event (Degrees)	
	Down on S1	Down on S2
Tilt Sensor 1	3.1	3.7
Tilt Sensor 2	4.6	2.6
Tilt Sensor 3	5.4	3.1
Tilt Sensor 4	4.0	2.5
Tilt Sensor 5	2.0	2.6

Table 3.5 14C2 Rotation Change Summary

Table 3.5 summarizes the rotation changes observed at each tilt sensor location when 14C2 was placed on S1 and S2. The sign convention follows the same convention as was used for 16C4.

For the rotation changes at S2 shown in Figure 3.50, the values were taken as those observed during the first placement of the girder on S2. During the second placement on S2, the girder made slight contact with the ground at the dapped end due to the camber, which may have caused less rotation at Tilt Sensor 1 than would have normally occured. This contact was not observed in the stress change results and can be considered to have negligible impact on the tests; however, the first placement was tabulated to account for this in the presentation of the rotation results.

The maximum twist that 14C2 underwent when placed on S1 was 5.4 degrees at midspan (Tilt Sensor 3). For S2, the maximum rotation was 3.7 degrees occurring at the dapped end (Tilt Sensor 1).

3.7.4.2   Stresses

Location	Stress	Flange	14C2 Stress Change During Specified Event (ksi)	
			Down on S1	Down on S2
Section A	Bending	Top	-2.5	0.0
		Bottom	+2.5	0.0
	Warping	Top	-2.5	+1.2
		Bottom	+2.6	+1.5
Section B	Bending	Top	-3.3	-1.1
		Bottom	+3.3	+1.1
	Warping	Top	-5.1	+1.1
		Bottom	+4.7	+1.3
Section C	Bending	Top	-2.5	0.0
		Bottom	+2.5	0.0
	Warping	Top	-2.5	+0.6
		Bottom	+3.3	+0.7

*Table gives larger stress change if repeatability does not exist

Table 3.6 14C2 Stress Change Summary

Table 3.6 shows the stress change values at the instrumented sections of 14C2 when it was placed on S1 and S2. The stress changes associated with placement on S1 are larger than those for S2 for the same reasons as mentioned earlier for 16C4.

All of the cross sections of 14C2 are doubly symmetric. The magnitudes of bending stress changes during placement on both S1 and S2 reflect this, with absolute values being the same at the top and bottom flange for all sections. In addition, Section A and C were located at the approximate quarter points, placing them at the same location as the S2 supports. Since the lift locations were very near the gage and support locations, no bending stress change was observed at Section A and C. However, small warping stresses were still observed. The maximum bending stress change for 14C2 was recorded at Section B's top and bottom flange when placed on S1, with values of -3.3 ksi and +3.3 ksi, respectively.

The same weak axis bending phenomenon occurred for the S2 stress changes in 14C2 as was noted for 16C4. As shown in the table, all warping stresses for S2 are positive, which is attributed to the weak axis bending introduced by the rotating of the

girder. The maximum warping stress change was -5.1 ksi at the top flange of Section B when the girder was placed on S1.

3.8 HIRSCHFELD LIFT TESTS CONCLUSIONS

The Hirschfeld lift tests provided rotation and stress data for calibrating the finite element model. By using a simple test setup with two statically determinate supports, the data obtained from the tests can be appropriately compared with analytical models for validation purposes. In addition to the data, conclusions can be taken from the lift tests.

Rigid body rotation is an important issue when lifting curved I-girders. Depending on how the girder is lifted, the rigid body rotations can create significant serviceability problems. Difficulty in placement and fit up would follow during girder erection. Also, the situation seen with the warping stress changes at S2 (same signs in both flanges) can present itself, which is a difficult stress state to predict for designers and erectors.

As in the earlier study, warping stresses during lifting continue to be equal if not greater than bending stresses in curved I-girders. Using this data to develop analytical tools to perform parametric studies will further illustrate the possible stability issues with curved I-girders.

3.9 SUMMARY

The details and data from erection of two girders of Span 14 of the SH 130/US 71 direct connector were presented in this chapter. The data showed that significant warping stresses were induced, particularly during the cross frame installation and fit up.

The setup and data from the Hirschfeld lift tests were outlined. The data that was collected and analyzed consisted of bending and warping stresses, as well as girder rotations. The results showed that rigid body rotations of the girders while lifted can cause stress distributions in the girder flanges that are significantly different than predicted from the theory of warping torsion. Not only is serviceability and the ability to maneuver the girder affected by this rotation, but the data shows that stresses induced by

weak axis bending can also be caused by rotations during lifting. The next chapter focuses on the issue of curved I-girder rotation during lifting.

CHAPTER 4

Curved I-Girder Rotation During Lifting

4.1 INTRODUCTION

The complicated issues inherent in curved I-girder behavior stem from the geometry of the girder. The curved geometry creates numerous challenges for engineers and contractors including but not limited to transportation, staging, lifting, and prediction of stresses. Many of these issues are caused by the potential for excessive girder rotations during lifting due to the curved geometry. Excessive rotations make the girders unwieldy and difficult to position and assemble. To understand these geometric effects, it is helpful to employ the principles of statics, with comparisons to experimental and analytical data. This section explains the static analysis of a curved I-girder to determine the effect of the center of gravity location on the behavior during lifting. The process by which a finite element model constructed in ANSYS was validated by static results and the rotation data collected from the Hirschfeld lift tests is also presented.

4.2 STATICS

4.2.1 Straight vs. Curved Girders

The center of gravity (C.G.) of a straight, prismatic, doubly symmetric I-girder is located at the midspan of the girder, in the center of the web at mid-depth. Since the center of gravity lies on the girder center line, any two lift points along the girder length will create a line of support that runs through the C.G. Since there is no eccentricity between the line of support and the center of gravity, no rotation about the longitudinal axis of the girder is expected to occur when the girder is lifted into the air, regardless of the positioning of the lift points.

Once horizontal curvature is introduced, the location of the center of gravity shifts away from the girder center line, which now has the properties of an arc. The center of gravity for a straight and curved girder with uniform, symmetric cross section along its length are depicted in the plan views shown in Figure 4.1.
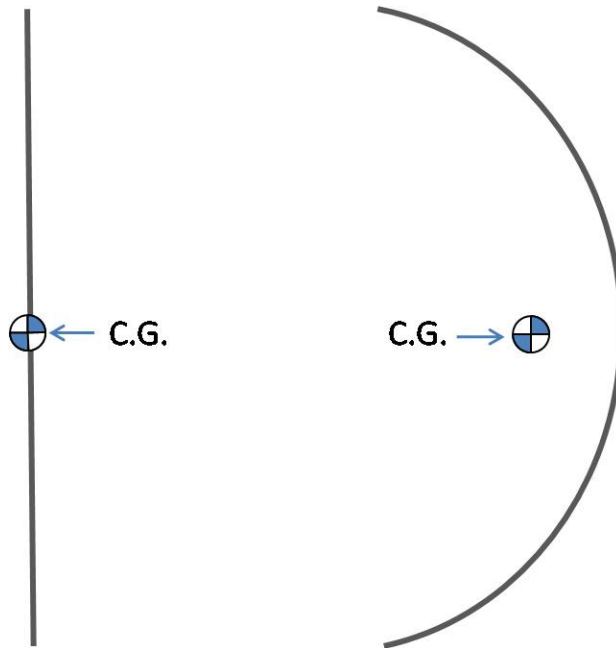
Figure 4.1 Center of Gravity for Straight and Curved Girder

The location of the C.G. for a curved, prismatic girder is given by Equation 4.1, which is the C.G. of an arc of length L. The equation gives the location as a distance from the center of the circle comprised of the arc to the arc C.G. A numeric example using 14C2 (Radius = 1215.06 ft, Length = 124 ft) from the Hirschfeld lift tests is provided.
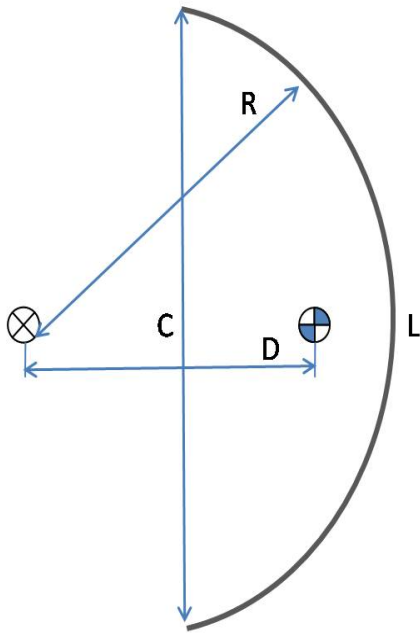
$$D = R * \frac{C}{L} \qquad\qquad \textit{Equation 4.1}$$

$$R = Radius\ of\ Curvature\ (ft)$$

$$C = Chord\ Length\ (ft) = 2R \sin\left[\frac{180° * L}{2\pi R}\right]$$

$$L = Girder\ Length\ (ft)$$

$$C = 2(1215.06) \sin\frac{180° * 124}{2\pi(1215.06)} = 123.95\ ft$$

$$D = R * \frac{C}{L} = 1215.06 * \frac{123.95}{124} = 1214.53\ ft$$

Once the C.G. location is determined using Equation 4.1, additional geometric properties of circles and arc lengths can be used to find the C.G.'s location with reference to any point on or around the girder. A numeric example is given in Section 4.2.3 that shows the calculation of the eccentricity between the center of gravity and the line of the support. This eccentricity is the determining factor in the prediction of curved I-girder rotation during lifting.

4.2.2 Line of Support

During curved girder lifting, it is common for the lift points to be selected as close to the quarter points of the girder as the available spreader bar will allow. By lifting at these locations, approximately half of the girder weight (two .25L cantilevers on either side of lift points) will lie on one side of the line of support provided by the lift points. The other half (.5L span between the lift points) lies on the other side of the line of support, in hopes of providing balance and limiting large rotations during the lift.

85

The reasoning presented above is applicable only to curved girders with uniform, symmetric cross section (C.G. at mid-depth) and assumes the center of gravity is located such that the line of support created by lift points located at .25L and .75L will pass through it. If the line of support action does not pass through the center of gravity, the girder will rotate once it is lifted so that the center of gravity is in line with the lift points to satisfy moment equilibrium. This situation is illustrated in Figure 4.2. This rotation will occur about an axis of rotation above the girder, usually at a point on the lifting mechanism that allows rotation. The magnitude and direction of the rotation is determined by the eccentricity (e) between the girder C.G. and the line of support formed by the lift points. Determining these characteristics is shown and discussed in the following section.
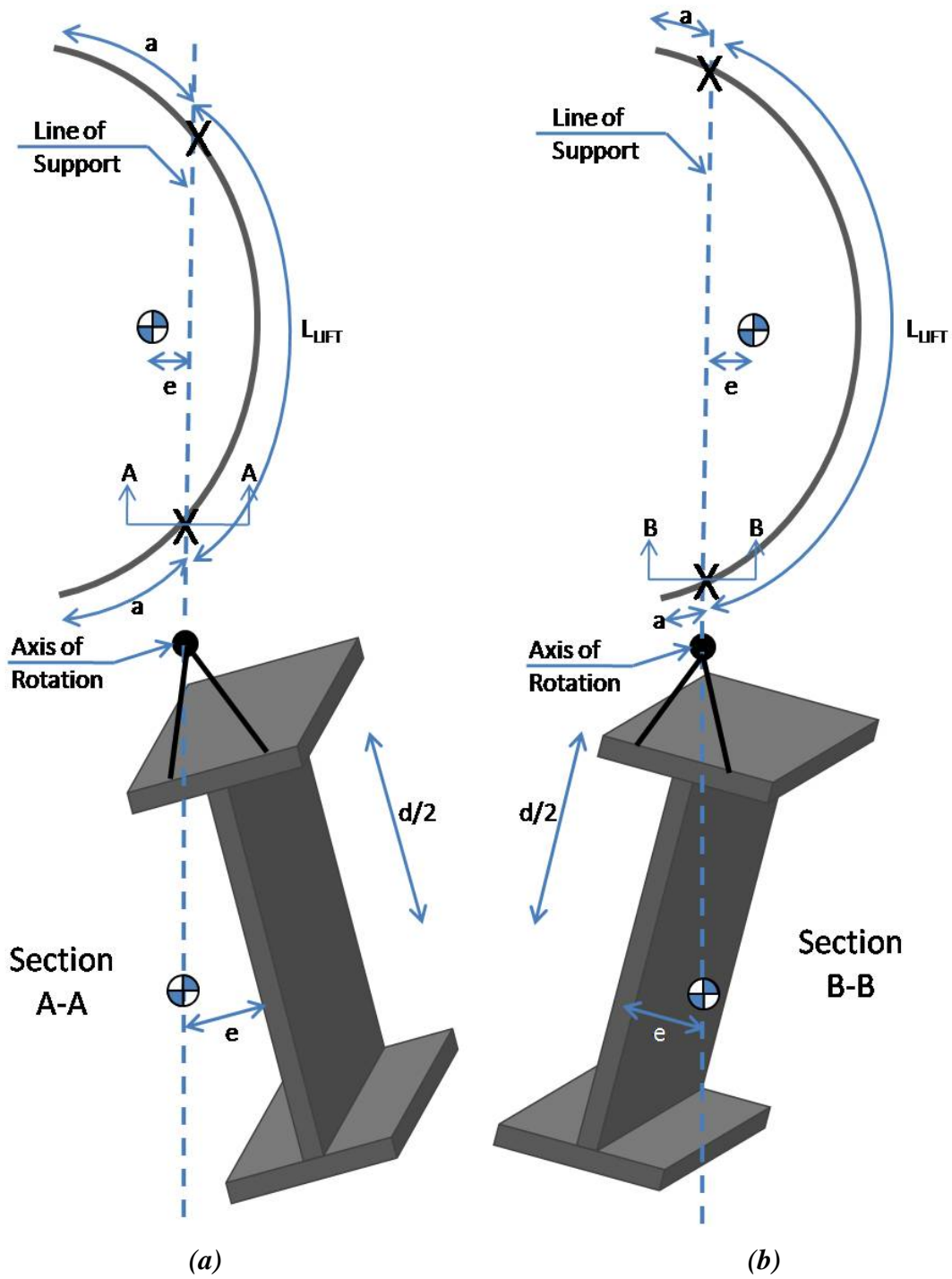
Figure 4.2 Effect of C.G./Line of Support Eccentricity: (a) Girder Rotates Outward;

(b) Girder Rotates Inward

4.2.3 Static Analysis of 14C2

To illustrate this phenomenon further, it is helpful to continue the example above to find the value, e, from which an additional calculation can be made to resolve the associated girder rotation, θ. The lift points of 14C2 were located approximately at 1/3 span locations. These locations were based on the length of the MIJACK's lift apparatus ($L_{LIFT} = 40.333\ ft$) and the girder length ($L = 124\ ft$). The height from the girder to the axis of rotation (H) is taken to be 30". This parameter and its effect on rotation will be discussed in Section 4.2.4.2. The lift clamp apparatus is shown with the assumed axis of rotation in Figure 4.3, with the 30" dimension noted.

Figure 4.3 Lift Apparatus and Axis of Rotation Location

4.2.3.1 Sample Static Rotation Calculation

The numeric example presented below details the process of determining the eccentricity between the center of gravity and the line of the support (e) (Equation 4.2) and the girder rotation (θ) (Equation 4.3) when the location of the C.G. (D), span between lift point locations (L_{LIFT}), axis of rotation height (H), and the cross section's web height (h_w) and top flange thickness (t_f) are known.

$$e = R - D - \left(R \sin\left[\frac{180° * L_{LIFT}}{2\pi R}\right] * \tan\left[\frac{180° * L_{LIFT}}{4\pi R}\right]\right) \qquad \textit{Equation 4.2}$$

$$R = Radius\ of\ Curvature\ (ft)$$
$$D = C.G.Location\ (ft)given\ by\ Equation\ 4.1$$
$$L_{LIFT} = Span\ Between\ Lift\ Points\ (ft)$$

$$\theta = \tan^{-1}\left[\frac{e}{\left(H + t_f + .5h_w\right)}\right] \qquad \textit{Equation 4.3}$$

$$H = Height\ of\ Axis\ of\ Rotation\ Above\ Girder\ (in)$$
$$e = Eccentricity\ of\ C.G.from\ Line\ of\ Support\ (in)$$

$$e = 1215.06 - 1214.53 - \left(1215.06 \sin\left[\frac{180° * 40.33}{2\pi(1215.06)}\right] * \tan\left[\frac{180° * 40.33}{4\pi(1215.06)}\right]\right)$$

$$e = .3627\ ft = 4.35\ in$$

$$\theta = \tan^{-1}\left[\frac{4.35}{(30 + 1.25 + .5 * 84)}\right] = 3.4\ degrees$$

As given by Equation 4.2 and Equation 4.3 above, the eccentricity of 14C2's C.G. from the line of support provided by the 40'-4" MIJACK lift apparatus was calculated to be 4.35". The C.G. of the girder must therefore translate 4.35" in order for the center of gravity to coincide with the line of action of the lift points.

Figure 4.4 14C2 Statics Example   *Figure 4.5 14C2 Rotation*

shows the geometry employed in Equation 4.3 to calculate the 3.4 degrees of rotation that the girder undergoes to shift the center of gravity 4.35". Figure 4.5 shows 14C2 during the lift tests rotating approximately 3.65 degrees at the dapped end, as measured from the tilt sensors.
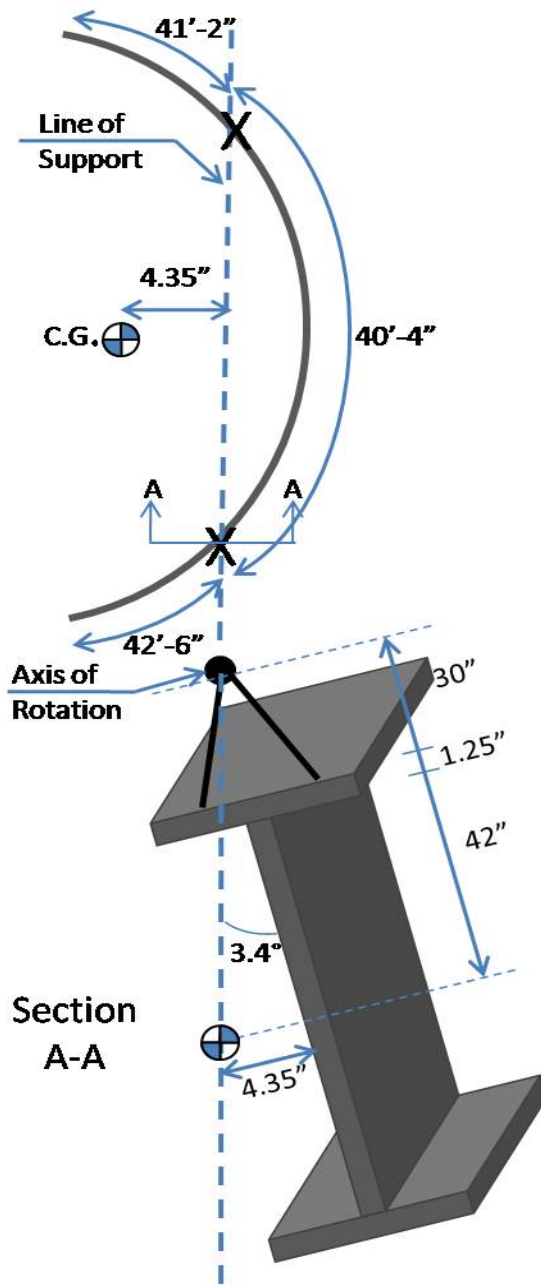
Figure 4.4 14C2 Statics Example

Figure 4.5 14C2 Rotation

4.2.3.2   Sign Convention

The eccentricity (e) calculated in Equation 4.2 can be either a positive or negative value. A positive value corresponds to the situation illustrated in Figure 4.2a, with a

91

resulting outward girder rotation with respect to curvature (positive θ from Equation 4.3). A negative value relates to the configuration shown in Figure 4.2b, where the resulting rotation is negative (inward). Therefore, the rotation sign convention is the following: positive rotation corresponds with outward girder rotation with respect to the curvature. Negative rotation corresponds with inward girder rotation with respect to the curvature.

4.2.3.3 General Comments

A small approximation is made in assuming the 4.35" is the perpendicular distance from the girder web to the C.G., when it is actually to the rotated section's web (horizontal distance in figure). Since rotations are relatively small, the difference is considered to be negligible.

In addition, any dimensions given with respect to the curvature of the girder can be interchanged with linear dimensions. For example, in figures presented earlier, L_{LIFT} is referenced with respect to curvature; however, the length of the lift apparatus or spreader bar (linear dimension) can be used as well. Even at relatively small radii, the difference in these values is negligible.

The equations and process presented above assumes the lift locations are approximately centered on the girder length. In other words, roughly the same distance exists between each lift point and its respective girder end (the girder dimension a in Figure 4.2).

4.2.4 Sensitivity

The example presented above details the calculations and reasoning involved in the static analysis of a prismatic, doubly symmetric curved I-girder. However, plate girders are often not symmetric, as designers tend to adopt smaller top flanges to optimize the section and take advantage of composite action once the deck is poured. The influence of this unsymmetric geometry on the static analysis of the curved girder is

92

discussed in this section. In addition, assumptions and variables in both the lifting geometry and modeling of the girder can have an impact on results.

4.2.4.1 Effect of Symmetry

If the bottom flange is larger than the top flange, the centroid of the section shifts downward. As the center of gravity moves farther down the section, the rotation required to align the C.G. of the girder and chord line between the lift points decreases.
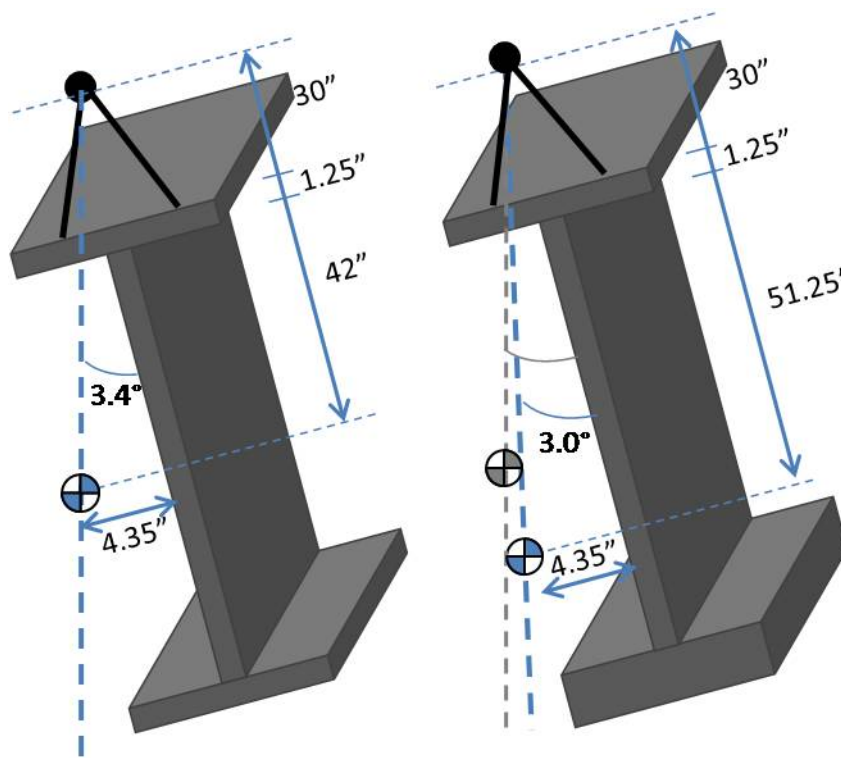
Figure 4.6 Effect of Lower CG

Figure 4.6 depicts the effect of a lower girder C.G. using girder 14C2 presented earlier. The bottom flange thickness has been increased from 1.25" to 2.5", causing the C.G. of the section to move from mid-depth (42" down web) to 51.25" down the web. The static analysis would predict a decrease in expected rotation from 3.4 degrees to 3.0 degrees. This value is obtained from substituting 51.25" rather than $.5h_w$ in Equation 4.3. It follows that if the top flange was increased to 2.5" with the bottom flange

93

remaining at 1.25", the rotation would increase to 3.8 degrees. However, a singly symmetric I-shape with larger top flange is not practical due to its inefficient composite behavior.

A finite element analysis confirms the effect of symmetry and the associated C.G. shift on rotation during lifting. Increasing the bottom flange thickness from 1.25" to 2.5" alters the predicted rotation from 3.74 degrees to 3.31 degrees.

Though notable, the difference in rotation predicted by statics (supported with finite element results) between a doubly and singly symmetric girder is relatively small. A difference of half of a degree, considering the large difference in flange sizes (bottom flange twice the size of top), is an acceptably small deviation to warrant the use of the doubly symmetric solution as an effective, conservative approximation of expected curved I-girder rotation during lifting for a singly symmetric, prismatic girder.

4.2.4.2   *Effect of Location of Axis of Rotation*

The location of the curved girder's axis of rotation is a parameter that has a profound effect on rotation of the lifted girder. The height of the axis of rotation (H) affects the rotation predicted by statics as indicated by the geometry and Equation 4.3.

Figure 4.7 shows the change in geometry that occurs when the height of the axis of rotation is varied from 30" to 48" for 14C2. The rotations associated with these values are given by Equation 4.3. Figure 4.8 shows the girder rotation of 14C2 associated with a range of H values. The amount of girder rotation decreases as the value of H is increased. An H value of zero, which correlates to the axis rotation occurring at the top flange, produces the largest rotation of 5.75 degrees. The selection of the height of the axis of rotation of 30" is discussed in the following section.

94
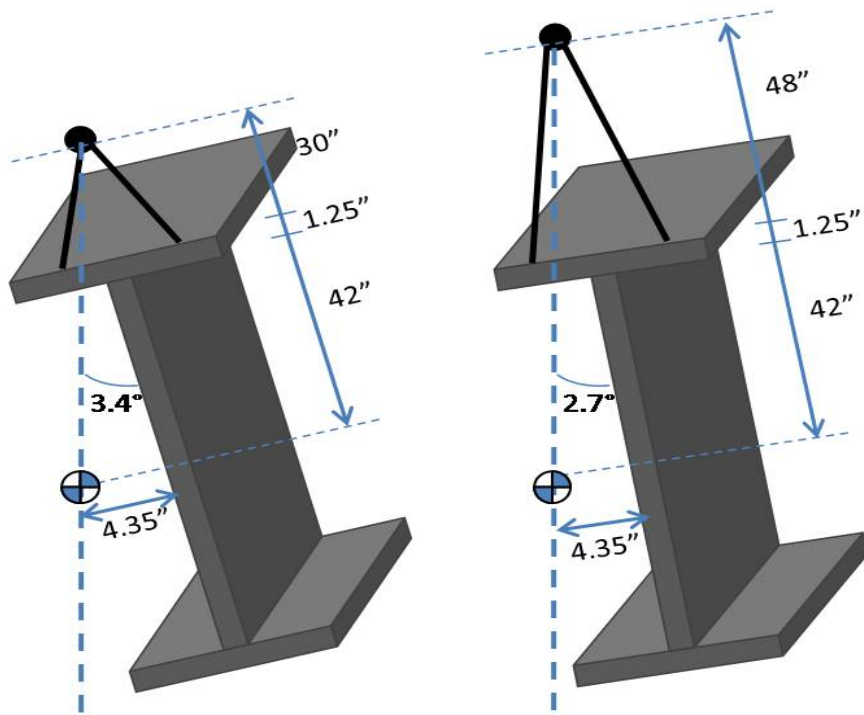
Figure 4.7 Effect of H on Girder Rotation
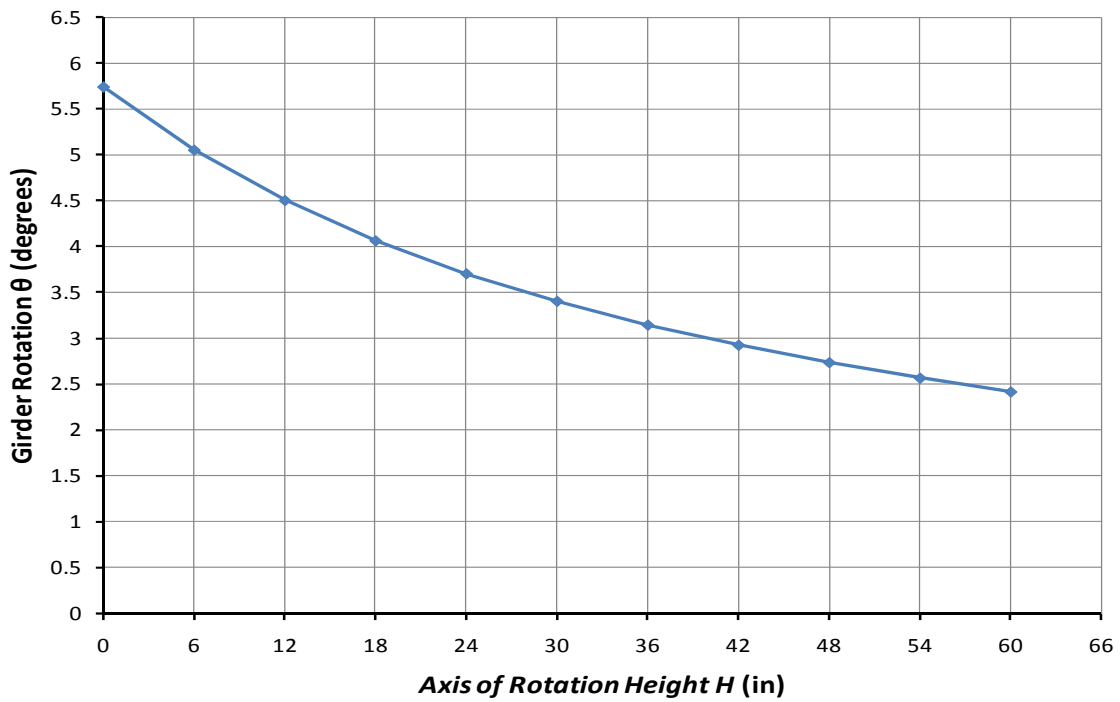
Figure 4.8 H vs. θ for 14C2

4.3   FINITE ELEMENT MODEL VALIDATION

4.3.1   Model Description

The finite element software used in the parametric study is the general purpose program ANSYS 11.0 (ANSYS 2007). The user-defined parametric language allows variables to be assigned to parameters, allowing for a wide variety of systems to be easily modeled with a single input file. The model of the curved I-girder during lifting utilizes 8-node shell elements for the girder cross sectional elements such as the flanges, webs, and stiffeners.

To accurately model the lifting apparatus of the MI-JACK utilized at Hirschfeld, truss elements were used. These elements were connected to the girder flange near the clamp lift points and pinned at the clevis as detailed in Figure 4.9. The pin was free to rotate and served as the axis of rotation. The necessary parameter needed to calibrate the model is the height of this axis of rotation from the top of the girder (H).
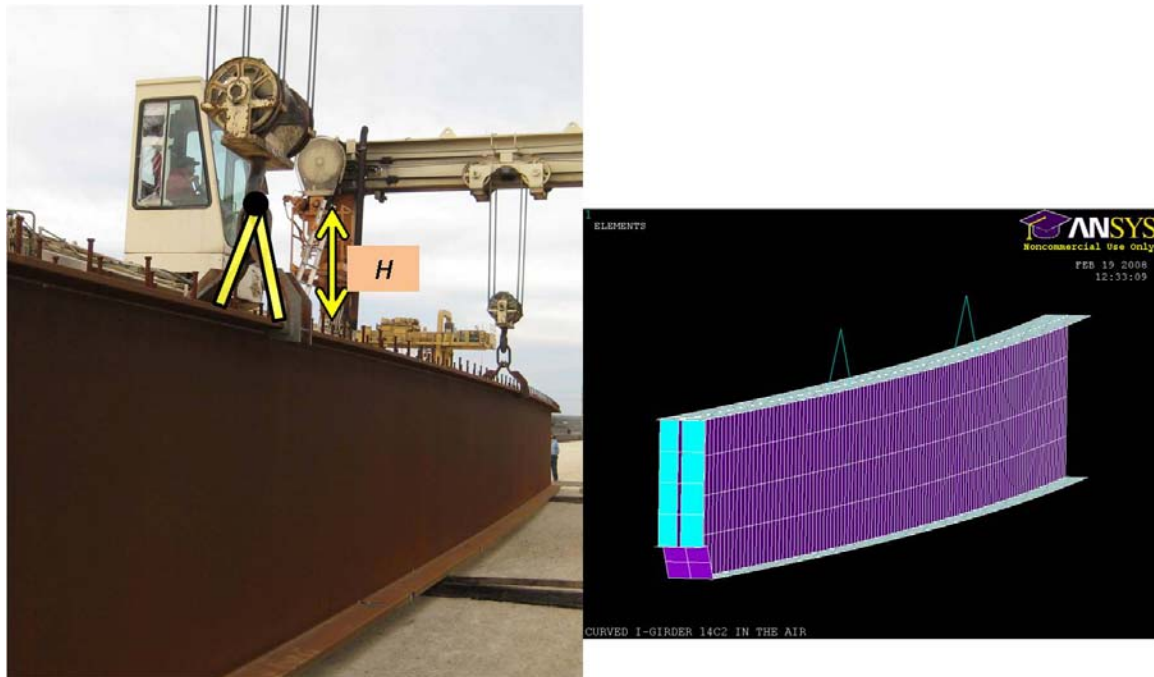
Figure 4.9 Modeling of the Lifting Apparatus

4.3.2   Selection of H

The rotation data from the Hirschfeld lift tests was utilized to determine the proper value of H to be used in the finite element model. The parameter H was selected by comparing the rotation exhibited by 14C2 when lifted with results outputted from the ANSYS model. Values calculated from statics discussed in the preceding section were also compared.

From the rotation data for 14C2, an in air rotation of 3.65 degrees was resolved. This value was calculated by adding the measured absolute rotation at each end of the girder while initially resting on timbers before the test to each ends' respective change in rotation once the girder was lifted off the timbers. Figure 4.10 shows the targeted rotation value of 3.65 degrees on a graph of rotations from the ANSYS model and from static calculations, with variable H. The predictions from ANSYS and statics follow the same trend of decreasing girder rotation with increasing axis of rotation height.
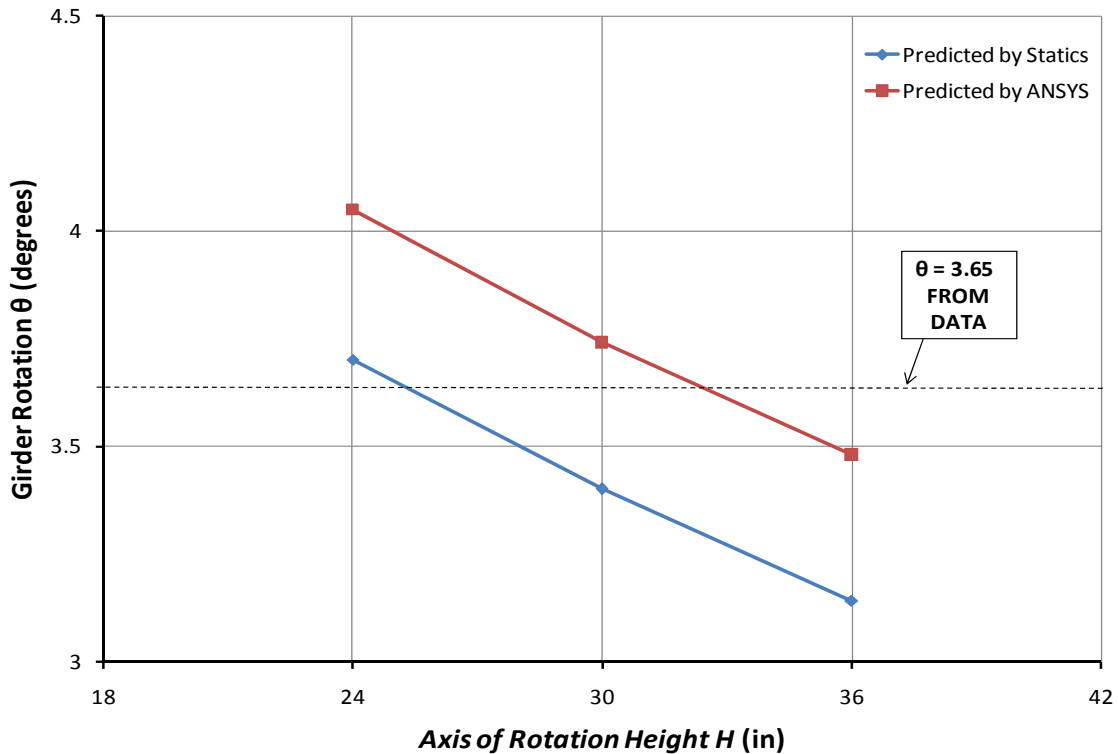
Figure 4.10 Rotation Predictions Compared w/ Field Rotation

An *H* of 30" was selected for the ANSYS model, since it showed the best correlation to both statics and the rotation value obtained from the field tests. The rotation outputted from the ANSYS model of 16C4's lift using an *H* of 30" showed good correlation with statics and rotation data, giving further confirmation that the finite element model was calibrated appropriately.

In addition, the height was scaled using photographs from the test, providing more evidence that 30" was an appropriate height for the axis of rotation, which coincided with the clevis of the lift clamp mechanism. Also, the stress changes monitored during the field test of 14C2 correlate relatively well with stress changes predicted from ANSYS using an *H* of 30". Table 4.1 summarizes this comparison for support location S1, which provides further evidence that an *H* of 30" was suitable for the validation of the finite element model.

Location	Stress	Flange	14C2 Stress Change for S1 (ksi)	
			Field Data	ANSYS (H=30")
Section A	Bending	Top	-2.5	-2.1
		Bottom	+2.5	+2.6
	Warping	Top	-2.5	-4.0
		Bottom	+2.6	+3.2
Section B	Bending	Top	-3.3	-3.3
		Bottom	+3.3	+3.2
	Warping	Top	-5.1	-8.1
		Bottom	+4.7	+5.0
Section C	Bending	Top	-2.5	-2.2
		Bottom	+2.5	+2.2
	Warping	Top	-2.5	-4.6
		Bottom	+3.3	+3.5

Table 4.1 Stress Change Comparison for 14C2 w/ H = 30"

4.4 SUMMARY

This chapter provides a solution for predicting the rigid body rotation of a curved I-girder during lifting based on fundamental static principles. Results from this solution show reasonably good correlation with field rotations and values predicted by the finite element model. It was shown that the height of the axis of rotation of the girder is a crucial parameter in predicting the rotation during lifting. The length of the lifting apparatus relative to the total girder length i.e. the lift point locations also affects the C.G. eccentricity and thus the girder rotation. These results were based on a prismatic girder.

The validation of the finite element model constructed in ANSYS was discussed. The height of the axis of rotation (H) was set at 30" to perform the parametric study presented in Chapter 6. However, with regard to recommendations for engineers, the choice of H should be carefully considered. As shown by the differences between the MIJACK lift apparatus employed during the Hirschfeld lift tests (Figure 4.11 left) and the spreader bar lift clamp used during the direct connector erection (Figure 4.11 right), it can be difficult to ascertain the appropriate height of the axis of rotation.
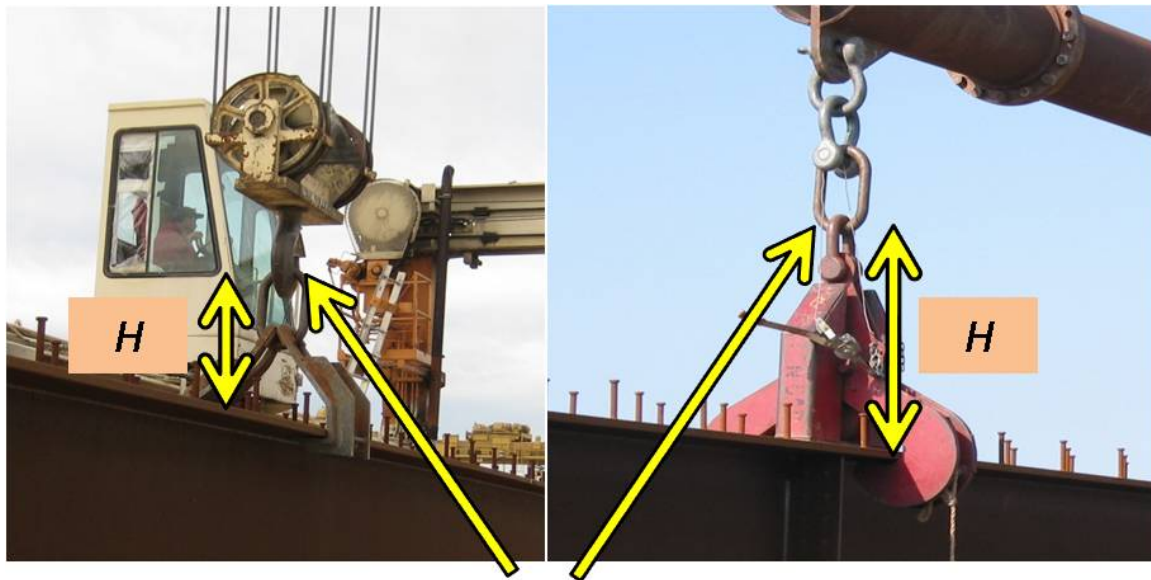
Figure 4.11 Approximating the Axis of Rotation Location (H)

In theory, this should be a location on the lift apparatus where no moment is transferred and a pivoting motion is relatively uninhibited. Since there is a significant amount of uncertainty as to what type of lift apparatus will be used for a specific lift or where the axis of rotation is located on the apparatus, it is advisable to make a conservative, smaller assumption for H. From the process outlined above and as predicted by the finite element model, using a smaller H directly translates into larger calculated rotations which would be an appropriate, conservative approximation of curved I-girder rotation during lifting.

The finite element model in ANSYS was validated with rotation and stress data from the Hirschfeld lift tests. The next chapter discusses the use of the model to perform a parametric study of lateral-torsional buckling of curved I-girders during lifting. Results of the study are used to improve the understanding of curved I-girder stability during lifting.

CHAPTER 5

Parametric Study of the Lateral-Torsional Buckling of Curved I-Girders During Lifting

5.1 INTRODUCTION

The results of the parametric study conducted using the finite element program, ANSYS, is discussed in this chapter. Eigenvalue buckling analyses were performed on curved I-girders during lifting. The effect of various parameters on the eigenvalue was determined. Trends and results from these observations are discussed. The formulation of the expression for C_L to account for lifting effects on girder stability is presented and discussed. The process by which this factor is used to check girder stability during lifting is also detailed.

5.2 STUDY DESCRIPTION

5.2.1 Eigenvalue

The eigenvalue (λ) represents the scale factor that should be multiplied to the applied load to yield the critical buckling load. The applied load in all cases of this study is the self weight of the girder. This relationship is shown in Equation 5.1 below.

$$w_{cr} = \lambda * w_{SW} \qquad \textit{Equation 5.1}$$
$$w_{cr} = Critical\ Buckling\ Load\ (k/ft)$$
$$\lambda = Eigenvalue$$
$$w_{SW} = Girder\ Self\ Weight\ (k/ft)$$

The critical buckling load was converted to a critical buckling moment (M_{cr}) by calculating the moment in the girder using the self weight multiplied by the eigenvalue (λM_{max}). This process was described by equations given in Chapter 1 shown below.

$$M_{cr} = \lambda M_{max} \qquad\qquad \textbf{\textit{Equation 1.6}}$$

$$\lambda = Eigenvalue\ Obtained\ From\ Buckling\ Analysis$$

$$M_{max} = Maximum\ Moment\ From\ Static\ Analysis$$

$$M_{max} = \frac{wa^2}{2} \geq \left| \frac{w(L_{LIFT})^2}{8} - \frac{wa^2}{2} \right| \qquad\qquad \textbf{\textit{Equation 1.7}}$$

$$w = Factored\ Girder\ Self\ Weight\ (k/ft)$$

$$a = Cantilever\ Length\ (ft)$$

$$L_{LIFT} = Span\ Between\ Lift\ Points\ (ft)$$

5.2.2 Parameter Descriptions

The parameters selected for the parametric study were the radius of curvature (R), the flange width to girder depth ratio (b/d), the span to depth ratio (L/d), and lift point location (a/L).

5.2.2.1 Radius of Curvature, Flange Width to Depth Ratio, and Span to Depth Ratio

The radius of curvature of a curved girder refers to the radius of the arc (girder) that comprises a circle. The horizontal geometry of a roadway typically utilizes arc lengths and tangent lines to describe their profile. Radius of curvatures used in this study ranged from 250 ft to straight. Most curved girders in Texas are used for highway interchanges and have a radius of curvature greater than 800'.
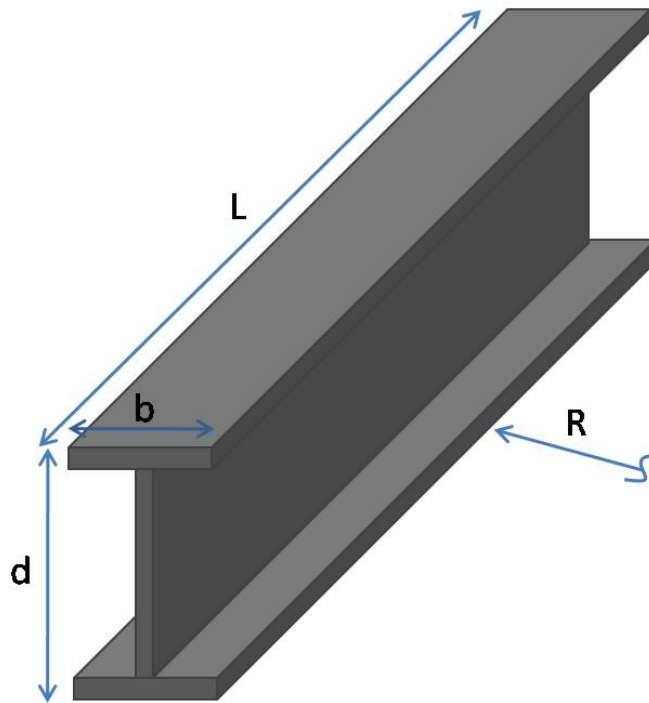
Figure 5.1 Girder Parameter Definition

Figure 5.1 shows each of the dimensions that were varied in the parametrical study. The minimum suggested flange width to depth ratio is given in the TXDOT Preferred Practices for Steel Bridge Design, Fabrication, and Erection is $d/3$ (TXDOT 2007). This limit is intended to prevent designers from specifying small flanges in an attempt to take advantage of composite action once the bridge's concrete deck is poured. If the flange widths are decreased, the girder's stability is reduced. AASHTO has a less stringent limit of $d/6$ given by Equation 6.10.2.2-2 of the AASHTO LRFD Bridge Specification (AASHTO 2007). The b/d ratios used in this study were 1/3, 1/4, and 1/6. For all cases when this ratio was varied, both the top and bottom flange were altered to maintain a doubly symmetric section.

As the span to depth ratio is increased, it is expected that the eigenvalue will decrease due to the increasing slenderness of the girder. Span to depth ratios of 10, 15, 20, and 25 were used in the study. The girder cross section was prismatic over the full length.

5.2.2.2 Lift Point Locations

The lift point locations are given as a ratio of the overhang or cantilever length (taken as the distance from the lift points to the edge of the girder) (a) to the total length of the girder (L). Figure 5.2 visualizes these dimensions. The cantilever length (a) was kept constant through the cases studied; however, the effect of having an unsymmetric cantilever length (unequal a's) was examined for one geometry.
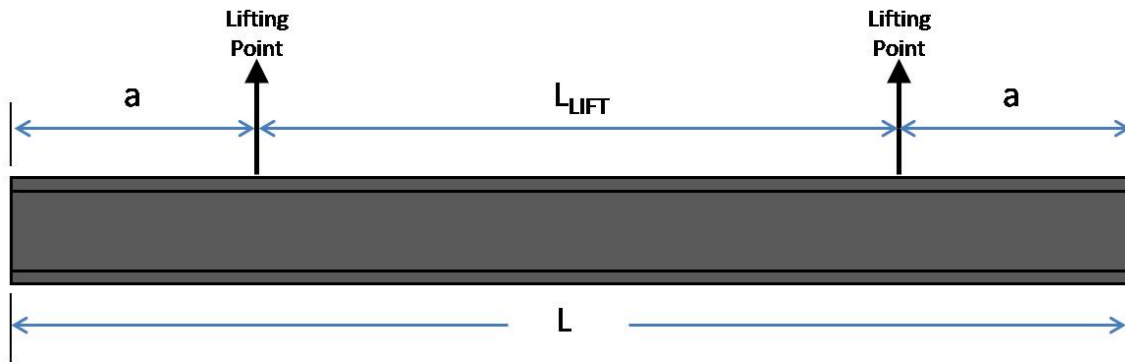
Figure 5.2 Lift Point Location Variable Definition

5.2.2.3 Constants

Certain cross section properties were kept constant throughout the study, in an effort to isolate the effect of the parameters mentioned above. The depth of the cross section (d) was kept constant at 72", which consisted of a web height (h_w) of 69" and flange thicknesses (t_f) of 1.5" each. The web thickness (t_w) was .75". The web slenderness was 92 and was selected ensure web buckling did not occur. The cross section was kept symmetric and prismatic for all cases. Stiffeners were located on both sides of the girder web with a spacing of 15' for all girder lengths. Stiffeners were also located at each end of the girder. As described in Chapter 5, each lift point location was modeled with two truss elements pinned together at the top and attached to the top flange at a distance of $b/4$ from the flange edges. Results demonstrating the effect of the height of these truss elements (H) on the eigenvalue are presented later.

5.3 NON-ROTATED VS. ROTATED GEOMETRY

This section presents a comparison of the eigenvalues from a linear buckling analysis on geometric configurations that are referred to as: 1) the non-rotated and 2) the rotated girder. In the non-rotated model, a static analysis was performed on the girder assuming no rotation (vertical web) followed by the buckling analysis returning the eigenvalue for a self weight applied load. The rotated girder model performed a geometrically nonlinear static analysis, which takes into account the rigid body rotation that occurs when the girder is lifted due to the effect of the center of gravity eccentricity to the line of action of the lifting points. The eigenvalue buckling analysis was then run on the rotated, updated geometry of the girder.

The tables below present the comparison between the eigenvalue given by the non-rotated geometry and the eigenvalue given by the rotated geometry. The percent difference is also given. The girder self weight is the reference load used in all cases. The comparisons are made for a b/d of .25, a L/d of 15, and R of 250', 500', 1000', and straight. Additional analyses were performed for b/d of .167, L/d of 15, and R of 500'.

R = 250 ft, b/d = .25, L/d = 15			
a/L	λ		% Difference
	Non-Rotated Geometry	Rotated Geometry	
0.1	9.08	9.08	0.00
0.15	19.88	21.06	5.60
0.2	56.71	57.55	1.46
0.225	115.61	115.41	-0.17
0.25	127.89	124.10	-3.05
0.275	91.42	85.96	-6.35
0.3	61.80	58.87	-4.98
0.35	37.46	37.45	-0.03
0.4	22.86	24.25	5.73

Table 5.1 Eigenvalue for Non-Rotated vs. Rotated Geometry $R = 250\ ft$

R = 500 ft, b/d = .25, L/d = 15			
a/L	λ		% Difference
	Non-Rotated Geometry	Rotated Geometry	
0.1	9.53	10.01	4.76
0.15	19.69	19.91	1.10
0.2	55.62	55.74	0.21
0.225	111.71	111.75	0.04
0.25	125.60	125.54	-0.05
0.275	83.21	82.92	-0.36
0.3	56.09	55.99	-0.19
0.35	35.29	35.49	0.55
0.4	22.12	22.48	1.60

Table 5.2 Eigenvalue for Non-Rotated vs. Rotated Geometry $R = 500\,ft$

R = 1000 ft, b/d = .25, L/d = 15			
a/L	λ		% Difference
	Non-Rotated Geometry	Rotated Geometry	
0.1	9.55	9.66	1.14
0.15	19.61	19.67	0.31
0.2	55.51	55.57	0.11
0.225	110.95	110.98	0.03
0.25	124.72	124.79	0.06
0.275	81.72	81.77	0.06
0.3	55.24	55.27	0.05
0.35	34.98	35.02	0.11
0.4	21.99	22.05	0.27

Table 5.3 Eigenvalue for Non-Rotated vs. Rotated Geometry $R = 1000\,ft$

R = Straight, b/d = .25, L/d = 15			
a/L	λ		% Difference
	Non-Rotated Geometry	Rotated Geometry	
0.1	9.55	9.57	0.19
0.15	19.59	19.60	0.07
0.2	55.49	55.50	0.02
0.225	110.74	110.75	0.01
0.25	124.45	124.46	0.01
0.275	81.38	81.39	0.01
0.3	55.06	55.07	0.01
0.35	34.92	34.92	-0.02
0.4	21.96	21.96	-0.03

Table 5.4 Eigenvalue for Non-Rotated vs. Rotated Geometry Straight

R = 500 ft, b/d = .167, L/d = 15			
a/L	λ		% Difference
	Non-Rotated	Rotated Geometry	
0.1	4.27	4.57	6.60
0.15	8.80	8.95	1.62
0.2	25.63	25.74	0.43
0.225	60.56	60.70	0.23
0.25	68.43	68.75	0.47
0.275	35.99	35.75	-0.69
0.3	23.20	23.12	-0.37
0.35	13.84	13.89	0.32
0.4	8.84	8.95	1.28

Table 5.5 Eigenvalue for Non-Rotated vs. Rotated Geometry $b/d =.167$

The tables above show that the non-rotated and rotated eigenvalues are in reasonable agreement in all cases. Other analyses with different span to depth ratios and flange width to thickness ratios were also conducted, with the same results. In all cases where differences exceed 5%, the non-rotated eigenvalue was less and therefore conservative. For the remainder of the parametric studies, the non-rotated eigenvalue is used.

5.4 PARAMETRIC STUDY RESULTS

5.4.1 Effect of Radius of Curvature on Eigenvalue Buckling

Figure 5.3 provides a graph of the eigenvalues as a function of radius of curvature while the other parameters remained constant. The flange width to depth ratio was constant at 0.25 (flange width of 18" and depth of 72"). The span to depth ratio was 15 for the 90' girder. The lift locations were placed with an a/L of 0.25.
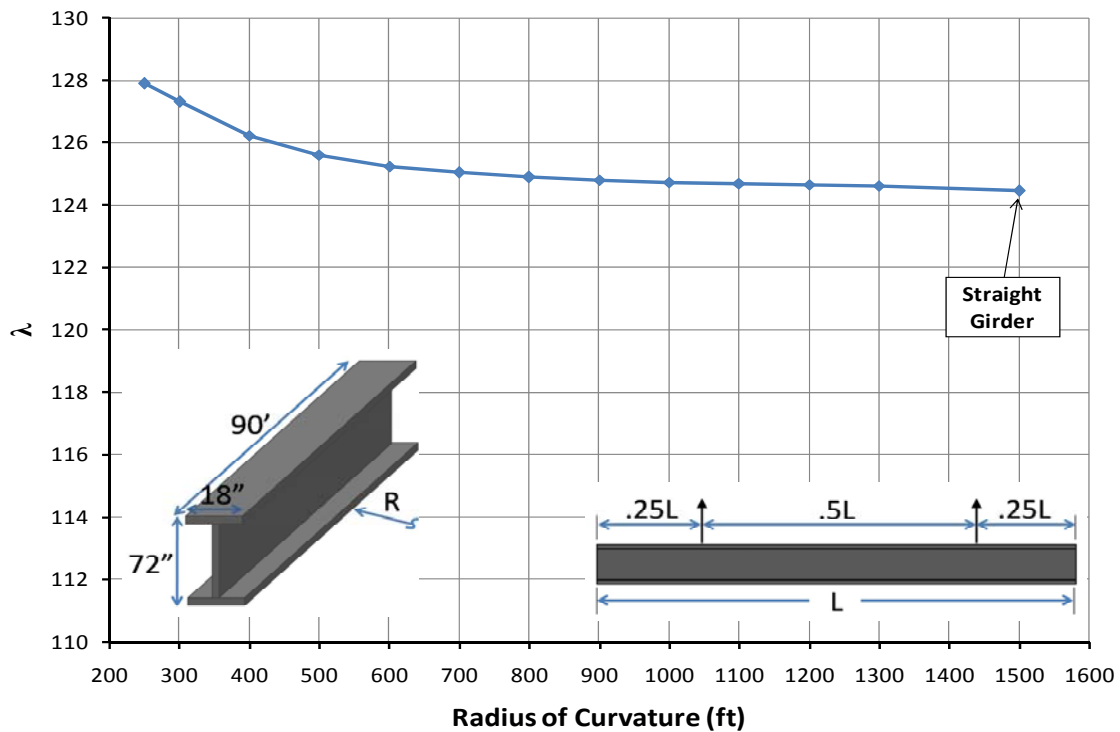
Figure 5.3 Effect of Radius of Curvature on Eigenvalue

108

As seen in the figure, varying the radius of curvature has little effect on the eigenvalue. A small increase is observed with decreasing radius. However, the differences are small: λ of 127.89 for radius of 250' versus a λ of 124.45 for a straight girder (infinite R). Since this change is less than 3%, this parameter was considered to have no effect for the remaining studies. The radius of curvature for all other tests was set at 500'.

5.4.2 Effect of Flange Width to Depth Ratio on Eigenvalue Buckling

Figure 5.4 shows the result of varying the flange width to depth ratio while keeping other parameters constant. The radius of curvature was set at 500'. The span to depth ratio was 15 for a 90' girder. The lift locations were placed with an a/L of 0.25. As mentioned earlier, the examined b/d ratios represent the TXDOT preferred practice manual's minimum flange width limit and the AASHTO minimum flange width limit, with one intermediate value.
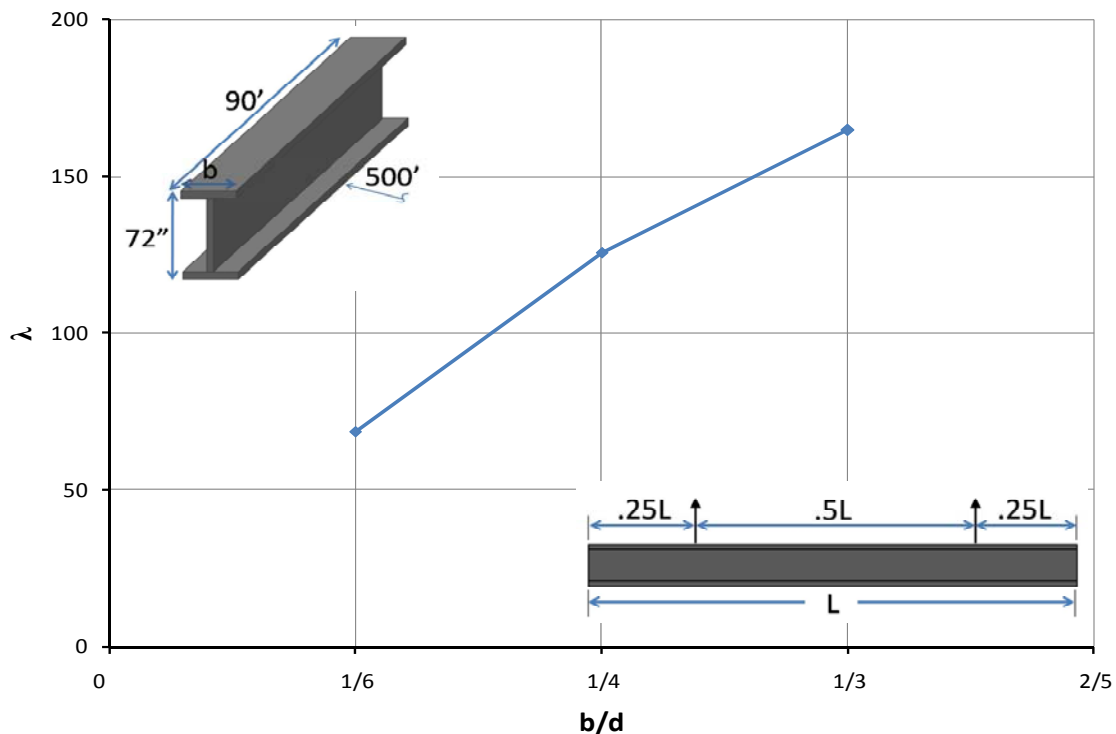
Figure 5.4 Effect of Flange Width to Depth Ratio on Eigenvalue

109

As the flange width to depth ratio increases, the eigenvalue of the lifted girder section increases for a given a/L, radius, and span to depth ratio. This is an expected result, since the warping stiffness of the section increases as the flange width increases. The warping stiffness for a girder section is proportional to I_y. Equation 1.1 shows this relationship.

5.4.3   Effect of Span to Depth Ratio on Eigenvalue Buckling

Figure 5.5 shows the result of varying the span to depth ratio while keeping other parameters constant. The radius of curvature was set at 500'. The flange width to depth ratio was .25, giving an 18" flange width. Again, the lift locations were placed with an a/L of .25. The L/d ratios of 10, 15, 20, 25 correspond to girder lengths of 60', 90', 120', and 150', respectively, for the constant 72" girder depth.
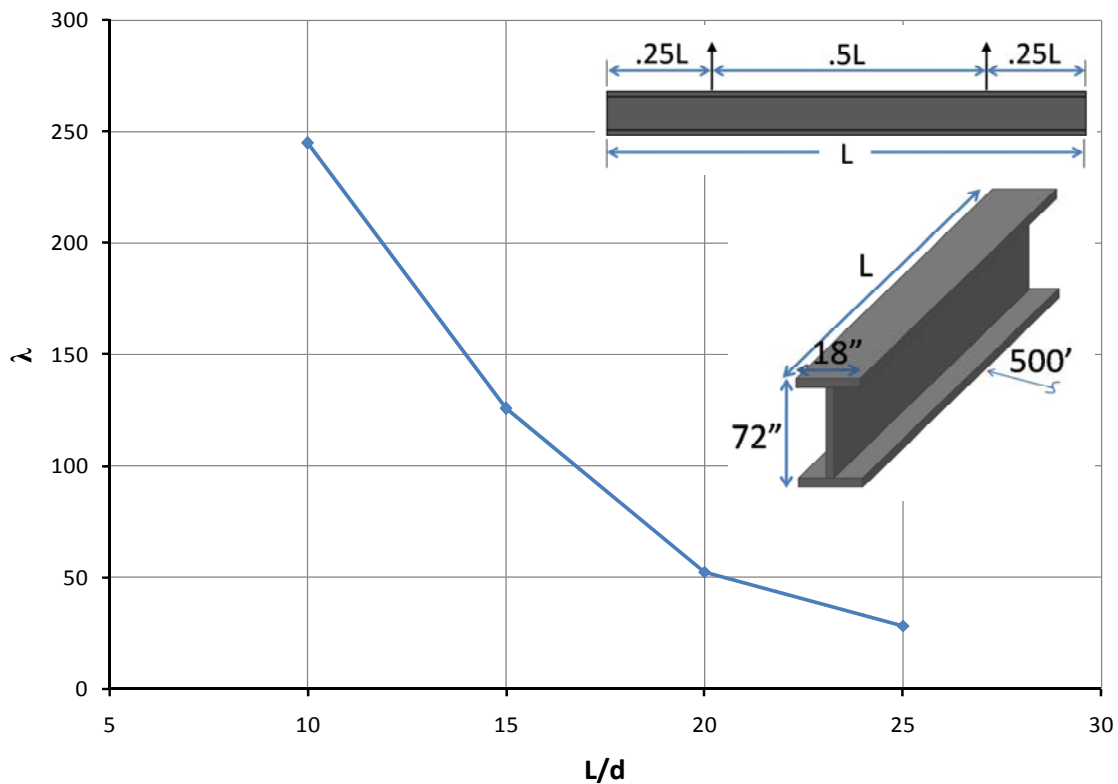
Figure 5.5 Effect of Span to Depth Ratio on Eigenvalue

Figure 5.5 shows that the eigenvalue buckling capacity during girder lifting decreases as the span to depth ratio increases (for a given a/L, radius, and span to depth ratio). The decrease appears to be exponential, which correlates well with linear buckling theory. As the girder length increases and the section becomes more slender, the unbraced length of the section increases, decreasing the lateral-torsional buckling capacity. The decrease is shown by Equation 1.1 for M_o, where the buckling moment capacity is inversely proportional to unbraced length (L_b).

5.4.4 Effect of Lift Location on Eigenvalue Buckling

The following figures present the effect of varying a/L on the eigenvalue. Each figure shows this effect for the other parameters as well.
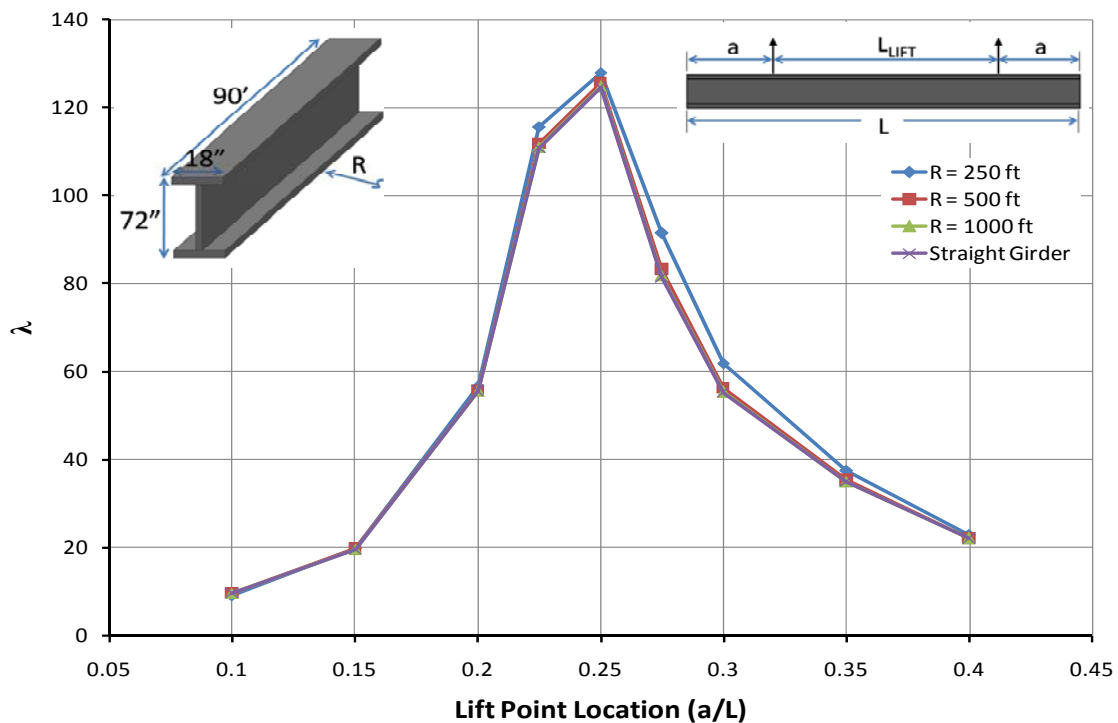
Figure 5.6 Effect of Lift Location and Radius of Curvature on Eigenvalue

111
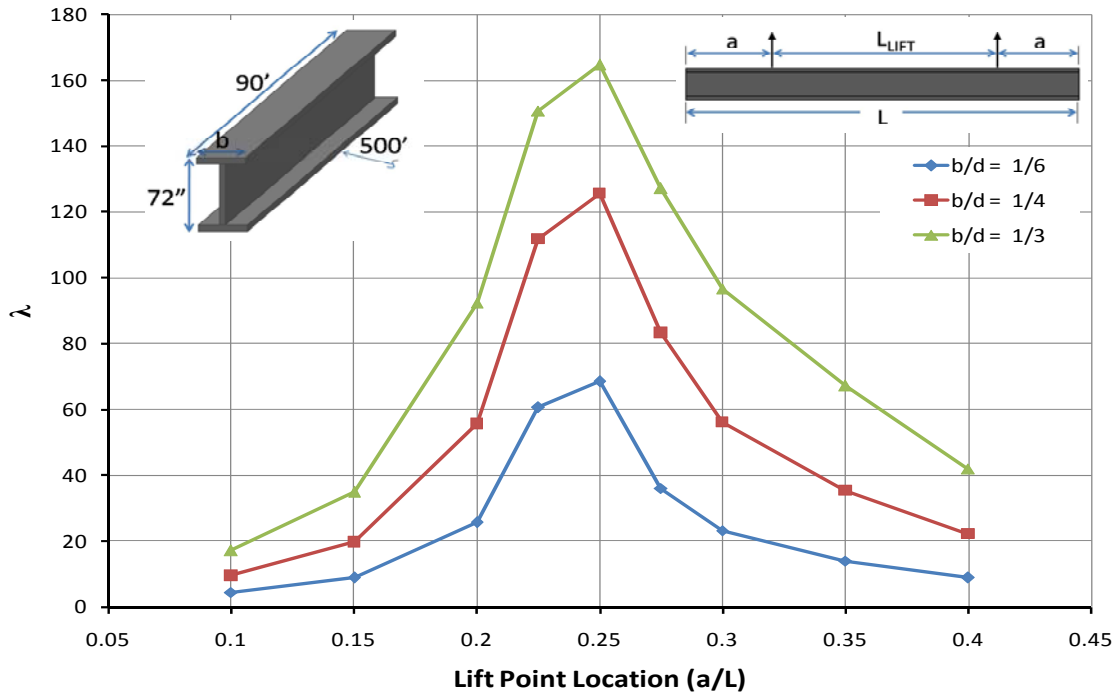
Figure 5.7 Effect of Lift Location and b/d on Eigenvalue
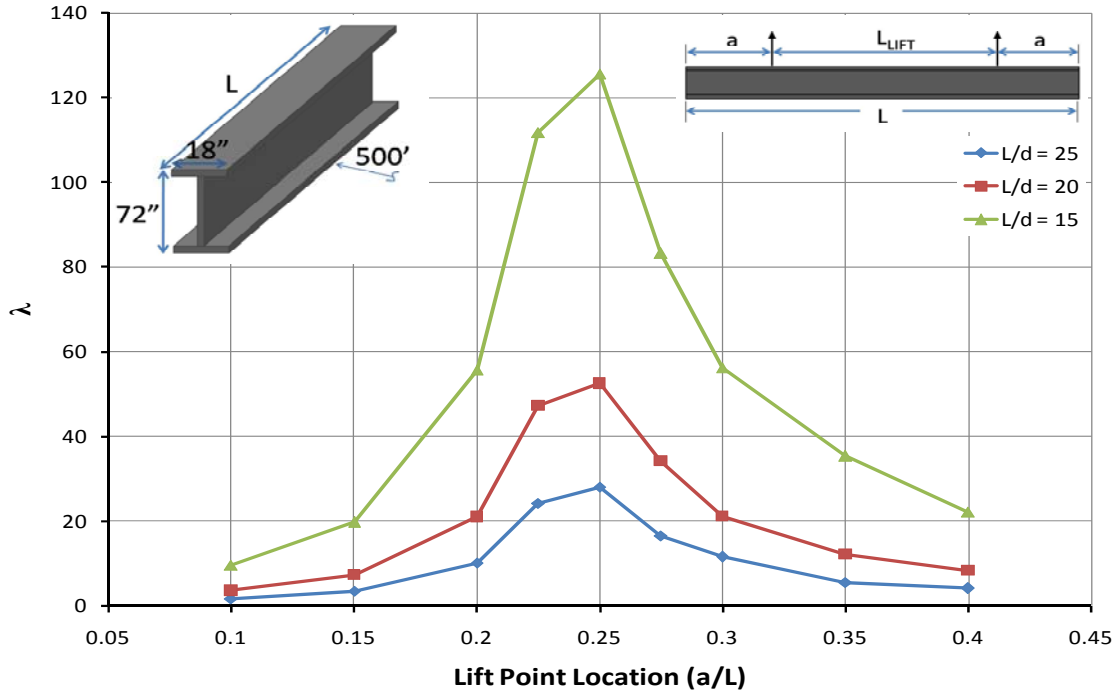
Figure 5.8 Effect of Lift Location and L/d on Eigenvalue

112

As shown in all figures, the maximum eigenvalues are achieved at an a/L of 0.25. The eigenvalue decreases quickly when the lift location deviates from this configuration. The smallest eigenvalues occurred at the extremes of the lifting points that were considered, at values of a/L of .1 and .4. The effect of changing a/L is similar in all of the plots. Refer to Appendix E to see these values in tabular form.

The buckled shapes are shown for a/L values of 0.1 through .4 in Figure 5.9. The location of the lifting attachments are represented by yellow lines. For an a/L of 0.1, the girder buckles with the top flange in single curvature. This is due to the top flange being primarily in compression along most of the segment length when the lift locations are near the ends. As a/L increases, the torsional displacements become more prominent. When the eigenvalue reaches the maximum value at an a/L of 0.25, there is very little twist at the lift points; however the predominant deformation along the rest of the girder length is a pure twist. When the lift point locations are greater than a/L of 0.35, the buckling deformation is dominated by the overhang section with the largest lateral deformations on the bottom flange due to the compression from the cantilever-like support conditions.
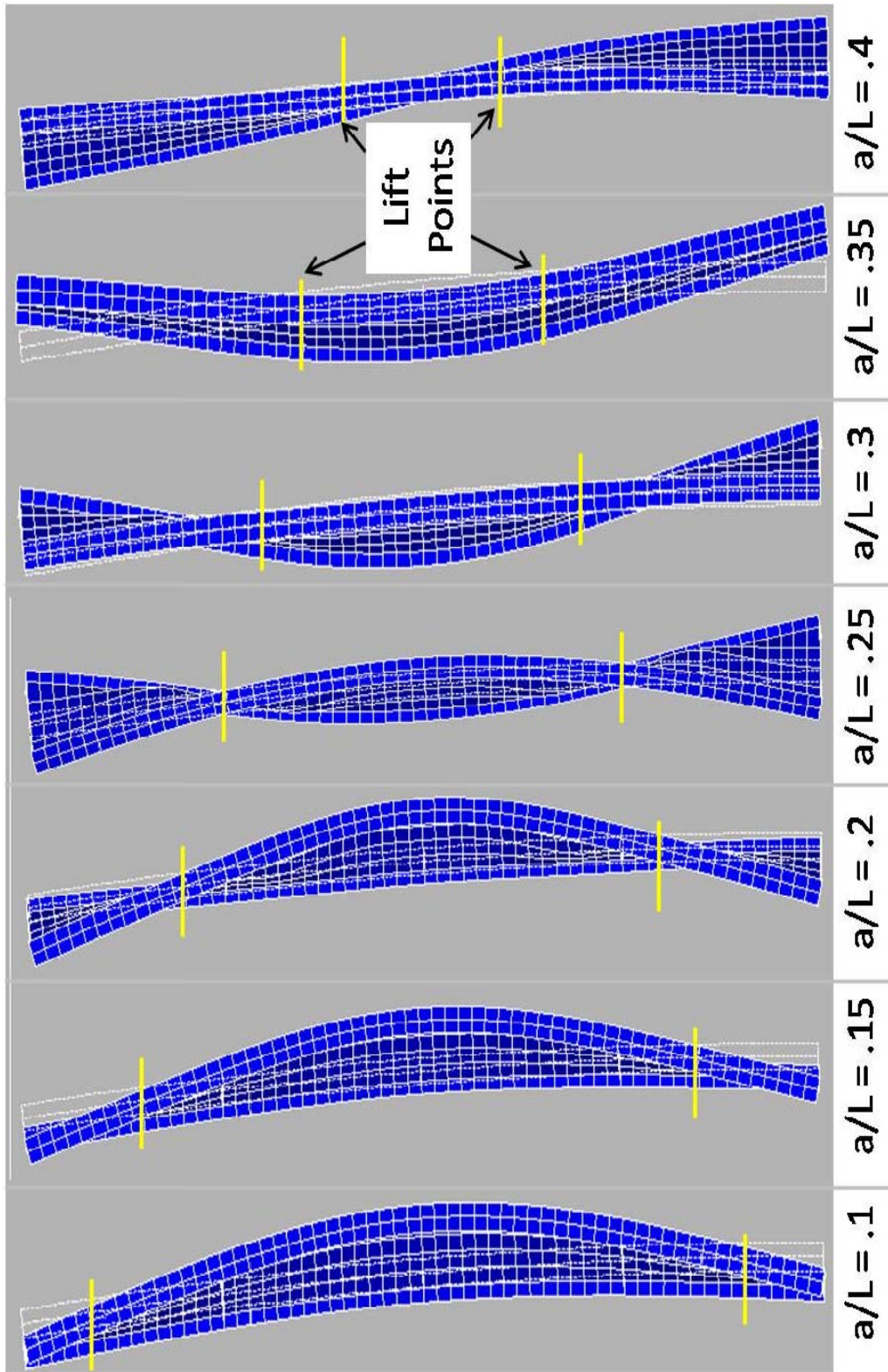
Figure 5.9 Curved Girder Buckled Shapes for L/d = 10, b/d = .25, R = 500 ft

114

Figure 5.10 compares the eigenvalue for the lift case where the lift points are not located symmetrically along the girder length. The comparison is given between the symmetric case (overhang length of a) and where one overhang length is shorter ($0.8a$). This represents an extreme case. As shown in the figure, the eigenvalue for the symmetric lift case is greater if a/L is less than 0.25. When a/L is greater than 0.25, the unsymmetric lift case eigenvalue is greater than the symmetric lift case. This case would be similar to the situation that occurs when the girder section is non-prismatic due to the flange transitions in continuous girders.
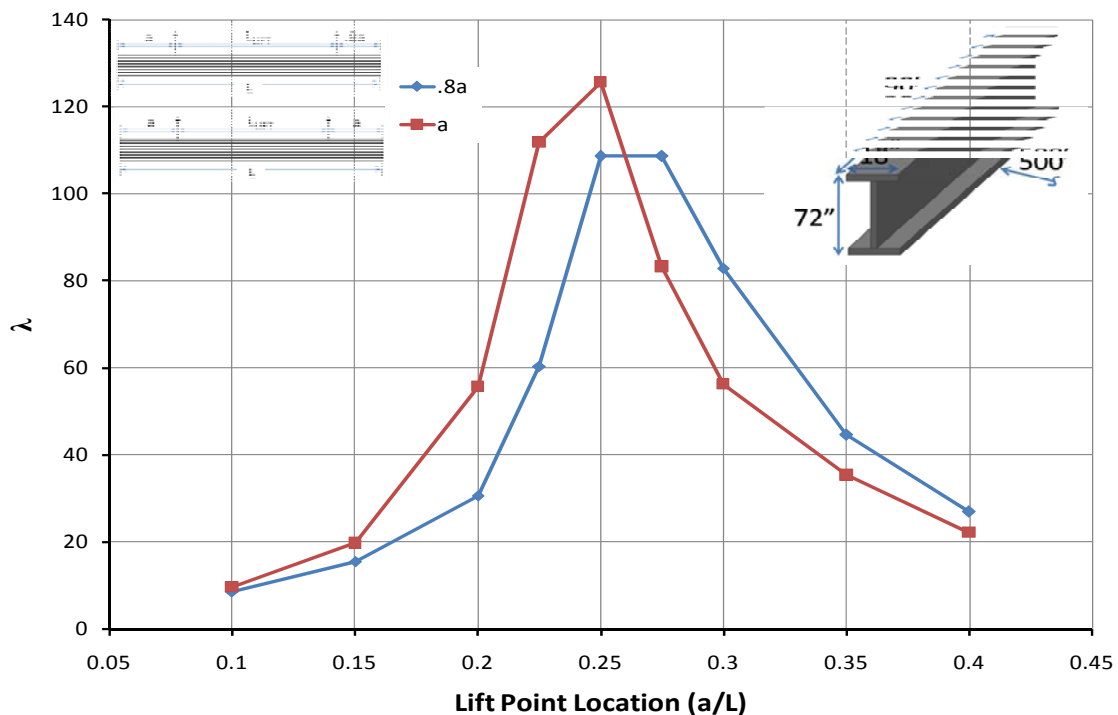
Figure 5.10 Effect of Unsymmetric Lift Locations on Eigenvalue

5.5   EFFECT OF AXIS OF ROTATION HEIGHT (H)

The location of the curved girder's axis of rotation is a parameter that was shown in Chapter 5 to have a significant impact on the rigid body rotation of the lifted girder. The effect of this parameter on the eigenvalue was also investigated. Figure 5.11 shows

the relationship of λ normalized by λ for an axis height of 30" as a function of H for a given lift point configuration (a/L).
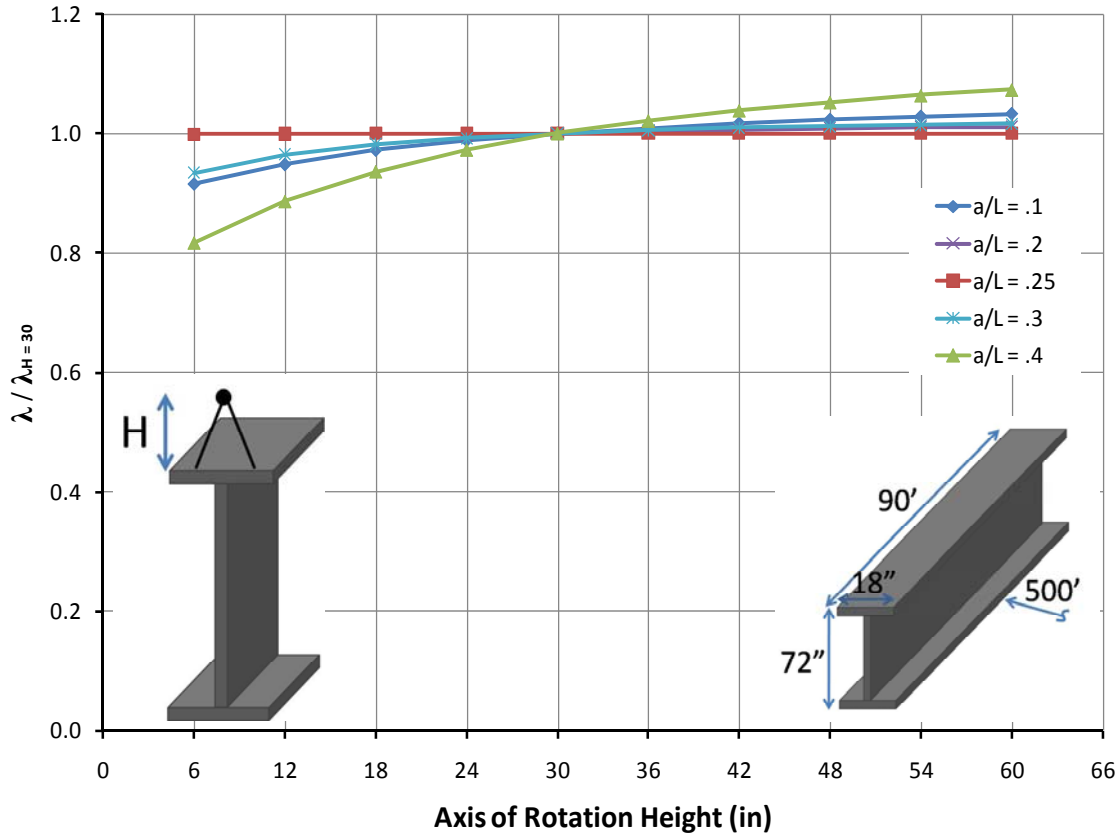
Figure 5.11 λ vs. H for Given a/L

The trend observed in Figure 5.11 is that as H increases, the eigenvalue also increases. Recall from Chapter 5 that as H increased, the girder rotation (θ) during lifting decreased. These two trends are similar since a smaller girder rotation would be consistent with a larger buckling capacity. Another important trend to note is the change in magnitude of the eigenvalue. For a/L of 0.2, 0.25, and 0.3, the difference is relatively small. In contrast, for the more extreme cases of 0.1 and 0.4, the difference is more significant. This is due in part to the smaller magnitude of the eigenvalue at the extreme case. As stated in Chapter 5 regarding the validation of the finite element model, an H of

30" was used for finite element analyses based upon comparisons of the measurements from field data and the finite element analysis results.

5.6   ACCOUNTING FOR THE EFFECT OF LIFTING ON CURVED I-GIRDER STABILITY

The purpose of the presented parametric study was to determine the effect of parameters on the stability of curved I-girders during lifting. The following section discusses the adjustment factor for girder lifting, C_L, and its use in checking the stability of a curved I-girder during lifting.

5.6.1   Expression for C_L

As stated in Chapter 1, once the eigenvalue is obtained from the results presented in this chapter, Equation 1.5 can be used to observe trends in C_L, the proposed adjustment factor to account for the effects of lifting on curved I-girders. The C_L value from the FEA studies was found for a given lifting geometry by comparing the eigenvalue buckling capacity for the lifting geometry with Equation 1.1. The C_L factor is the ratio of the maximum moment along the girder length with the buckling capacity for uniform moment given by Equation 1.1. The expressions used to evaluate C_L are given in the following equations and figures. Refer to Appendix E for detailed tables showing the calculated values.

$$C_L = \frac{M_{cr}}{M_o} \qquad \qquad \textbf{\textit{Equation 1.5}}$$

$$M_{cr} = Critical\ Buckling\ Moment\ Determined\ Analytically$$

$$M_o = Buckling\ Moment\ from\ Equation\ 1.1$$

$$M_o = \frac{\pi}{L_b}\sqrt{EI_yGJ + E^2I_yC_w\left(\frac{\pi^2}{L_b^2}\right)} \qquad \qquad \textbf{\textit{Equation 1.1}}$$

$$L_b = Unbraced\ Length\ of\ Girder\ (in) = L_{LIFT} \geq a$$

$$E = Modulus\ of\ Elasticity\ (ksi)$$

$$I_y = Weak\ Axis\ Moment\ of\ Inertia\ (in^4)$$

$$G = Shear\ Modulus\ (ksi)$$

$$J = Torsional\ Constant\ (in^4) = \sum \frac{bt^3}{3}$$

$$C_w = Warping\ Constant\ (in^6) = \frac{I_yh^2}{4}$$

$$M_{cr} = \lambda M_{max} \qquad \qquad \textbf{\textit{Equation 1.6}}$$

$$\lambda = Eigenvalue\ Obtained\ From\ Buckling\ Analysis$$

$$M_{max} = Maximum\ Moment\ From\ Static\ Analysis$$

$$M_{max} = \frac{wa^2}{2} \geq \left|\frac{w(L_{LIFT})^2}{8} - \frac{wa^2}{2}\right| \qquad \qquad \textbf{\textit{Equation 1.7}}$$

$$w = Girder\ Self\ Weight\ (k/ft)$$

$$a = Cantilever\ Length\ (ft)$$

$$L_{LIFT} = Span\ Between\ Lift\ Points\ (ft)$$
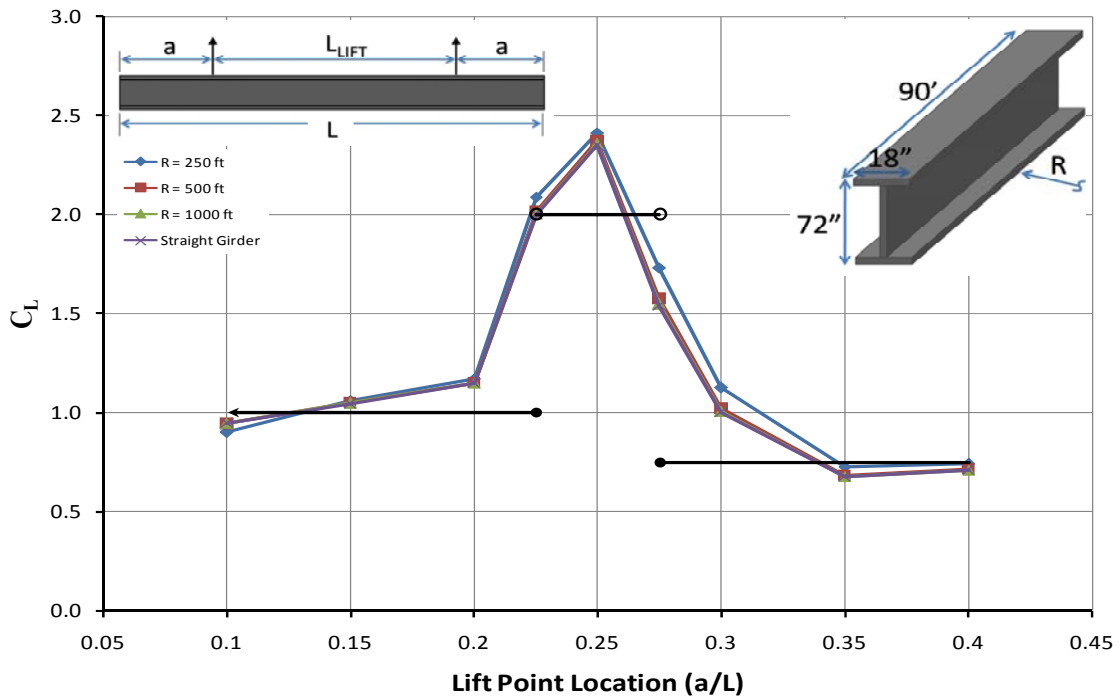
Figure 5.12 C_L vs. a/L for Given Radius of Curvatures
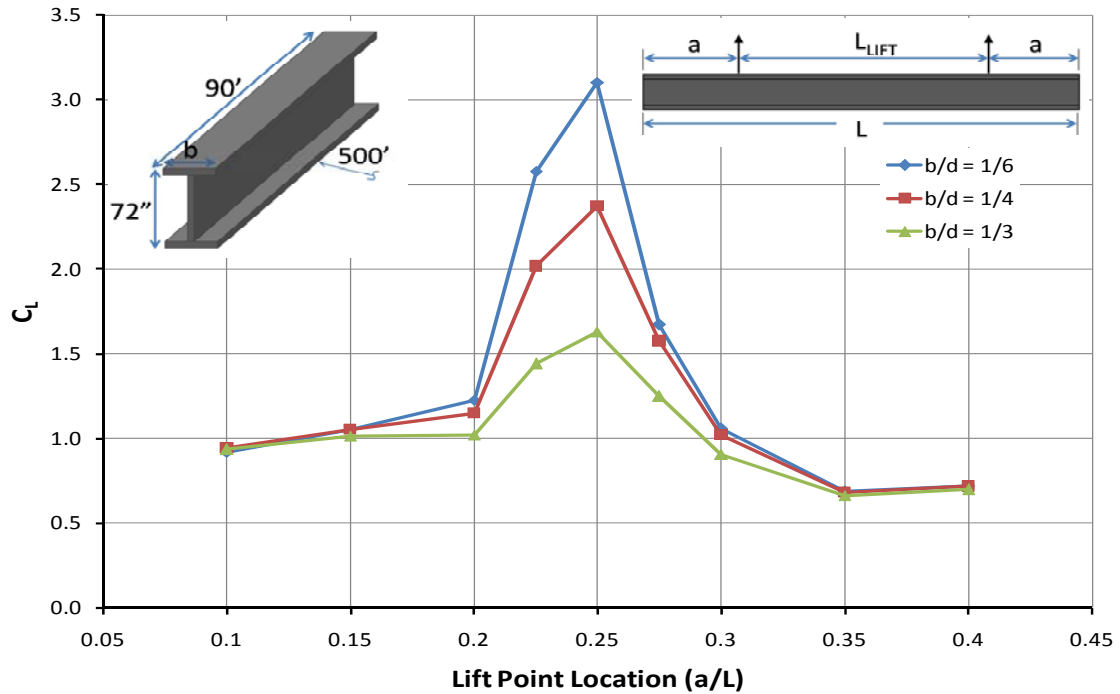
Figure 5.13 C_L vs. a/L for Given Flange Width to Depth Ratio

119
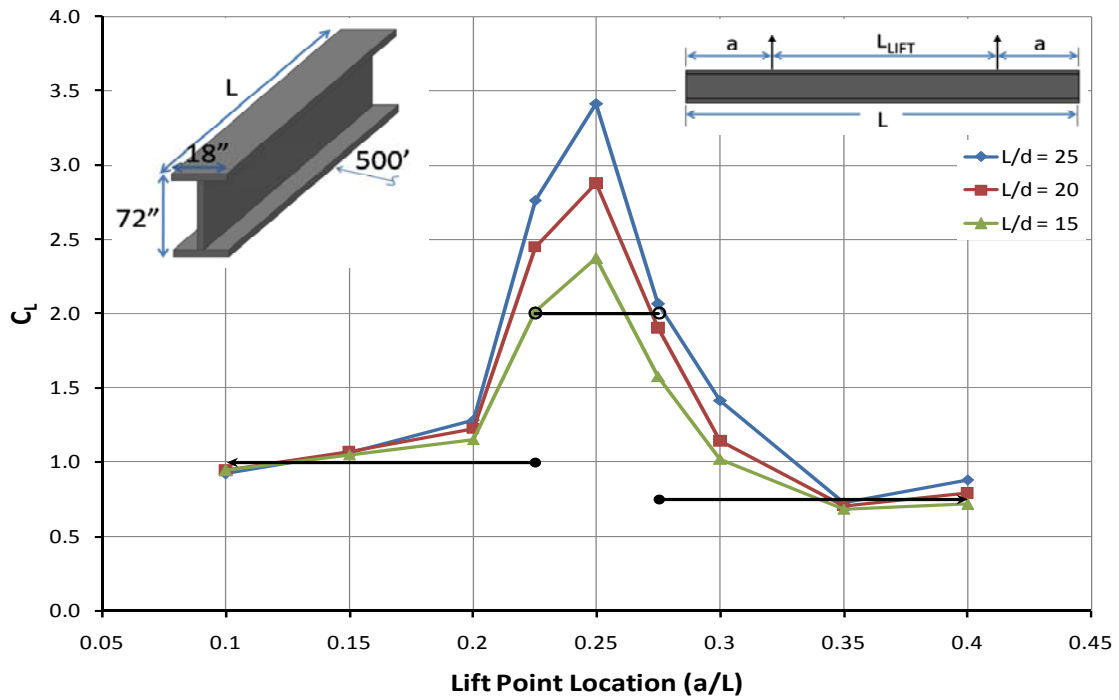
Figure 5.14 C_L vs. a/L for Given Span to Depth Ratio
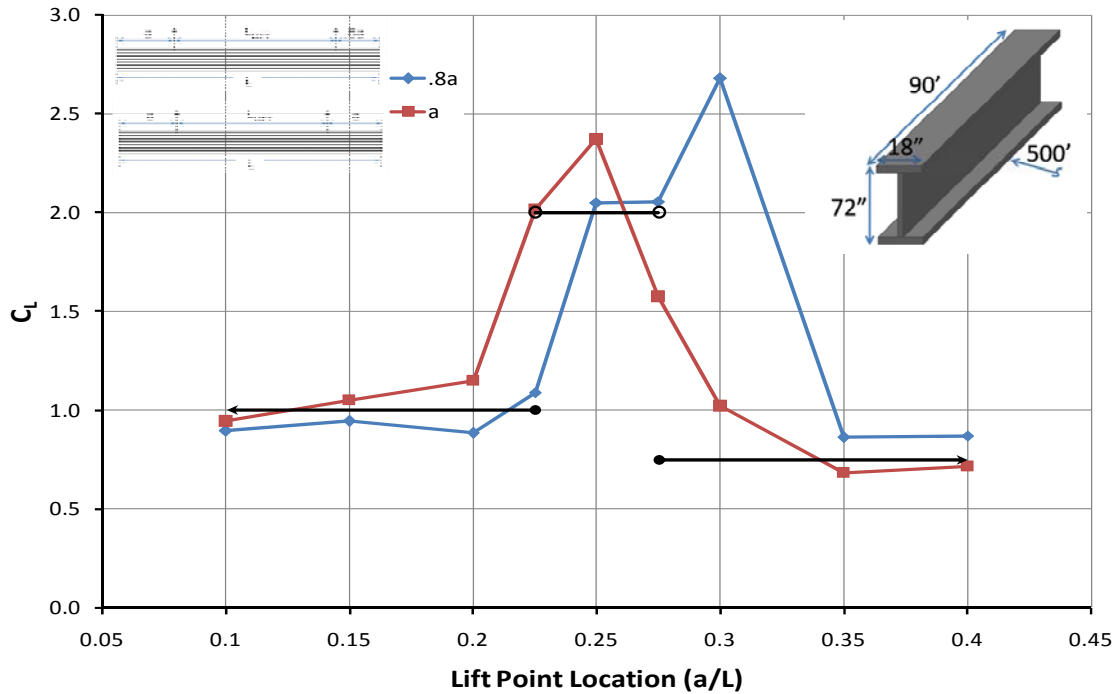
Figure 5.15 C_L vs. a/L for Unsymmetric Lift Points

120

From the trends presented in the figures, the expression for C_L was formulated and given in Equation 5.2 below. This expression is shown in Figure 5.12, Figure 5.14, and Figure 5.15 as a black trend line.

$$C_L = 1.0 \quad for \quad \frac{a}{L} \leq 0.225$$

$$C_L = 0.5 * \frac{d}{b} \leq 2.5 \quad for \quad 0.225 < \frac{a}{L} < 0.275 \qquad \textbf{\textit{Equation 5.2}}$$

$$C_L = 0.75 \quad for \quad \frac{a}{L} \geq 0.275$$

5.6.2 Critical Buckling Moment of a Curved I-Girder During Lifting

Using C_L from Equation 5.2, the Timoshenko critical buckling moment, M_o, can be adjusted to yield the critical buckling moment for the girder during lifting. If $M_{max} < M_{cr}$, the girder is stable. Equation 5.3 shows this check.

$$M_{max} < \phi M_{cr} = \phi\, C_L * \frac{\pi}{L_b} \sqrt{EI_y GJ + E^2 I_y C_w \left(\frac{\pi^2}{L_b^2}\right)} \qquad \textbf{\textit{Equation 5.3}}$$

$M_{max} = Factored\ Maximum\ Moment\ From\ Static\ Analysis$

$M_{cr} = Critical\ Buckling\ Moment$

$\phi = Reduction\ Factor = 0.9$

$C_L = Lift\ Adjustment\ Factor$

$L_b = Unbraced\ Length = L_{LIFT} \geq a$

$E = Modulus\ of\ Elasticity\ (ksi)$

$I_y = Weak\ Axis\ Moment\ of\ Inertia\ (in^4)$

$G = Shear\ Modulus\ (ksi)$

$J = Torsional\ Constant\ (in^4) = \sum \frac{bt^3}{3}$

$C_w = Warping\ Constant\ (in^6) = \frac{I_y h^2}{4}$

5.6.3 Checking the Stability of 14C2

To demonstrate how C_L can be used to check lifting stability of a curved girder, the example of girder 14C2 from the Hirschfeld lift tests is used. Figure 5.16 shows the girder dimensions and relevant section properties of 14C2. Details on the girder cross section dimensions were provided in Figure 2.16 and Section 2.4.1. The load factor applied to w_{sw} is taken as 1.25 (AASHTO 2007 Table 3.4.1-2). The reduction factor, ϕ, is taken as .9.
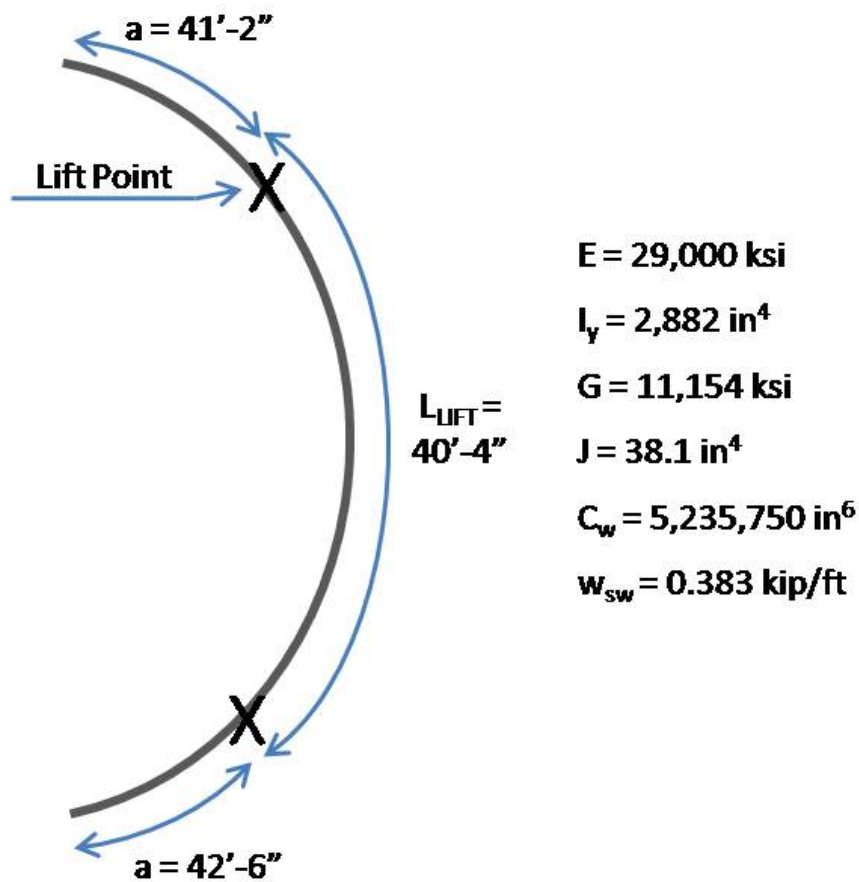
Figure 5.16 14C2 Lift Dimensions and Section Properties

122

$$\frac{a}{L} = \frac{42.5\ ft}{124\ ft} = .34$$

$$\frac{a}{L} \geq .275 \ \ so \ \ C_L = 0.75$$

$$L_{LIFT} < a \ \ so \ L_b = a = 42.5\ ft$$

$$M_{cr} = \phi\,C_L * \frac{\pi}{L_b} \sqrt{EI_y GJ + E^2 I_y C_w \left(\frac{\pi^2}{L_b^2}\right)}$$

$$EI_y GJ = (29{,}000)(2{,}882)(11{,}154)(38.1) = 3.552 * 10^{13}$$

$$E^2 I_y C_w \left(\frac{\pi^2}{L_b^2}\right) = (29{,}000)^2(2{,}882)(5{,}235{,}750)\left(\frac{\pi^2}{(42.5 * 12)^2}\right) = 4.815 * 10^{14}$$

$$M_{cr} = (0.9)(0.75) * \frac{\pi}{(42.5 * 12)} \sqrt{(3.552 * 10^{13}) + (4.815 * 10^{14})}$$

$$\boxed{M_{cr} = 88{,}896\ kip * in = 7{,}408\ kip * ft}$$

$$M_{max} = \frac{wa^2}{2} \geq \left|\frac{w(L_{LIFT})^2}{8} - \frac{wa^2}{2}\right|$$

$$w = 1.25 w_{sw} = 1.25(.383) = .479\ kip/ft$$

$$\frac{wa^2}{2} = \frac{(.479)(42.5)^2}{2} = 432.6\ kip * ft$$

$$\left|\frac{w(L_{LIFT})^2}{8} - \frac{wa^2}{2}\right| = \left|\frac{(.479)(40.33)^2}{8} - \frac{(.479)(42.5)^2}{2}\right| = 335.2\ kip * ft$$

$$\frac{wa^2}{2} \geq \left|\frac{w(L_{LIFT})^2}{8} - \frac{wa^2}{2}\right| \ \ so \ \ \boxed{M_{max} = 433\ kip * ft}$$

$$\boxed{M_{max} < M_{cr} \ \ STABILITY\ DURING\ LIFTING\ OK}$$

This calculation demonstrates the stability check for 14C2, showing that the girder is in no danger of lateral-torsional buckling when lifted as shown. However, less favorable girder cross section dimensions and properties or less appropriate lift locations could potentially lead to structural instability.

5.7 SUMMARY

This chapter presented results of an elastic buckling analysis of a curved I-girder during lifting. A parametric study of the lateral-torsional buckling of curved I-girders during lifting was performed. A comparison of using the non-rotated versus rotated geometry to output the eigenvalue was given. It was found appropriate to use the non-rotated geometry to conduct the eigenvalue buckling analysis.

The radius of curvature was found to have a negligible effect on the eigenvalue. A radius of curvature of 500' was used for the majority of the studies. As the flange width to depth ratio increased, the eigenvalue also increased. In contrast, as the span to depth ratio increased, the eigenvalue decreased.

The effect of the locations of lifting the girder was also explored. The largest eigenvalues were observed when the girder was lifted with an a/L of .25. Minimum values were seen at an a/L of .1 and .4. A discussion of the buckled shapes for given a/L's is provided. In addition, the effect of lifting the girder with unsymmetric lift points is examined.

The axis of rotation height (H) was found in Chapter 5 to greatly influence the curved girder rotation during lifting. The effect of axis of rotation height on the eigenvalue was studied. As the height increased, the eigenvalue of the lifted girder also increased. An axis of rotation height of 30" was used in all studies.

The expression for C_L, the adjustment factor for curved I-girder lifting, was determined. C_L was based on the results from the parametric study of a prismatic, curved I-girder. In addition, the use of this factor to calculate the critical buckling moment is described, and an example is provided showing the necessary stability check. For additional examples of this check, refer to Appendix A.

CHAPTER 6

Conclusions

6.1   INTRODUCTION

This chapter summarizes the findings presented in this thesis and provides conclusions and recommendations for the safe lifting of horizontally curved steel I-girders. Two distinct issues must be considered when checking the lifting safety of curved I-girders:

- Controlling the rigid body rotation associated with how the girder is lifted
- Structural stability of the curved girder

The following sections provide conclusions and recommendations for accommodating these two concerns of lifting curved I-girders. These conclusions were based on field tests and verified analytical models discussed within this thesis. The recommendations are based on a prismatic, symmetric curved girder.

6.2   CURVED I-GIRDER ROTATION DURING LIFTING

Chapter 5 should be referenced for in depth discussion of the rotation caused by lifting curved I-girders. This rotation arises as a result of the eccentricity between the line of support created by the lift points and the center of gravity of the curved girder section. The following parameters have an impact on the amount of rotation a curved girder is expected to exhibit when lifted:

- Radius of curvature and girder span length
- Lift point locations along span
- Location of the center of gravity of the cross section
- Height of the axis of rotation determined by lifting apparatus

125

The eccentricity (e) between the girder C.G. and the line of support formed by the lift points is a function of the radius of curvature, girder span length, and the lift point locations. The magnitude of the rigid body rotation expected during girder lift is affected by the eccentricity, cross section properties, and the height of the axis of rotation on the lifting apparatus above the girder. Equation 4.1, Equation 4.2, and Equation 4.3 provide these relationships.

$$D = R * \frac{C}{L}$$ **Equation 4.1**

$D = Center\ of\ Gravity\ Location\ (ft)$

$R = Radius\ of\ Curvature\ (ft)$

$C = Chord\ Length\ (ft) = 2R\sin\left[\frac{180° * L}{2\pi R}\right]$

$L = Girder\ Length\ (ft)$

$$e = R - D - \left(R\sin\left[\frac{180° * L_{LIFT}}{2\pi R}\right] * \tan\left[\frac{180° * L_{LIFT}}{4\pi R}\right]\right)$$ **Equation 4.2**

$R = Radius\ of\ Curvature\ (ft)$

$D = C.G.Location\ (ft)given\ by\ Equation\ 5.1$

$L_{LIFT} = Span\ Between\ Lift\ Points\ (ft)$

$$\theta = \tan^{-1}\left[\frac{e}{(H + t_f + .5h_w)}\right]$$ **Equation 4.3**

$H = Height\ of\ Axis\ of\ Rotation\ Above\ Girder\ (in)$

$e = Eccentricity\ of\ C.G.from\ Line\ of\ Support\ (in)$

The following conclusions can be made regarding rotation of curved girders during lifting:

- The point about which the girder rotates when lifted (axis of rotation) is located above the girder and is a function of the lifting apparatus
- Increasing the height of the axis of rotation (H) decreases the calculated girder rotation
- A singly symmetric girder with a larger bottom flange than top flange exhibits slightly less rotation than a doubly symmetric girder. It is therefore appropriately conservative to calculate the rotation based upon a doubly symmetric girder.

The following recommendations should be considered to limit rotation of curved I-girders during lifting:

- Minimize the eccentricity (e) between the girder C.G. and the line of support created by the lift points
    - Select an appropriate spreader bar or lift apparatus length (L_{LIFT}) based on given girder length and radius of curvature
    - Locate the lift points such that they are centered along girder length (equal overhangs) and attempt to place their line of support near the girder center of gravity
- Use a lift apparatus with a large axis of rotation height (H)
    - Approximate the location on the lift apparatus where no moment is transferred and a pivoting motion is relatively uninhibited to take as the axis of rotation location and associated height
    - When it is uncertain where the axis of rotation of a lift apparatus is located, it is conservative to use a smaller H to calculate rotations using the process set forth in Chapter 5

6.3 STABILITY OF CURVED I-GIRDERS DURING LIFTING

Chapter 6 presented the parametric elastic buckling study. In this study, the effect of various parameters on the eigenvalue buckling of a curved girder was observed. The purpose of the study was to determine the expression for the C_L factor, which could be applied to the Timoshenko critical buckling moment to calculate the lateral-torsional buckling capacity of the curved girder during lifting. Chapter 1 presents the background on structural stability and the use of an adjustment factor to account for girder lifting.

The following conclusions were made regarding the eigenvalue of a curved girder section when specific parameters were varied:

- Radius of curvature has negligible effect on the eigenvalue
- As the span to depth ratio increases, the eigenvalue decreases
- As the flange width to depth ratio increases, the eigenvalue increases
- As the height of the axis of rotation increases, the eigenvalue generally increases by a negligible amount for the range of practical heights
- With regard to lift point location (Figure 6.1), the eigenvalue is maximized at an a/L of 0.25. The eigenvalue is minimized at small and large a/L, like 0.1 or 0.4.
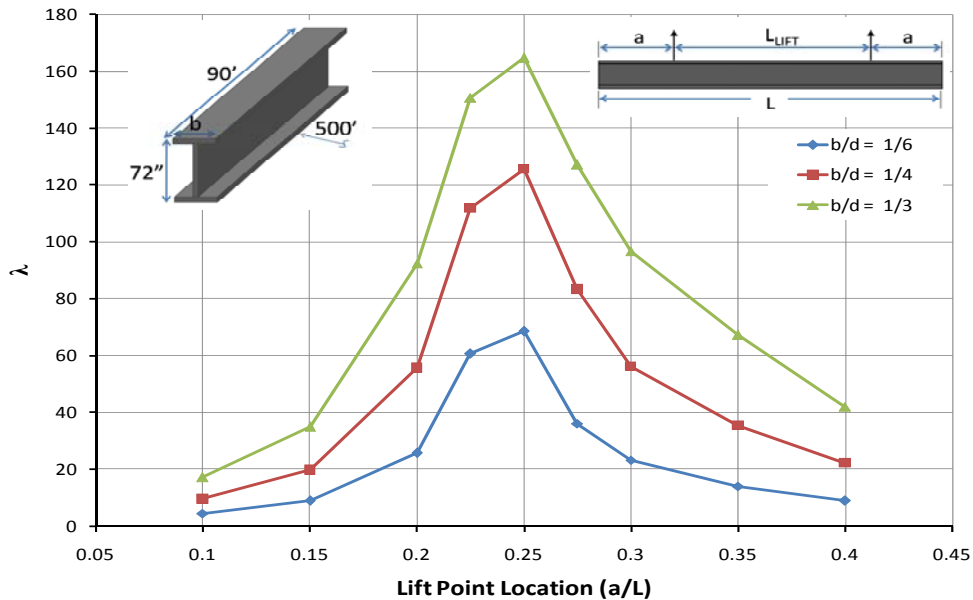
Figure 6.1 Lift Point Location Variable Definition

128

From the results of the parametric study, an expression for C_L for girder lifting was devised. The following equations (Equation 5.2 and 5.3) present this expression, as well as the stability check needed to ensure that a curved I-girder is not susceptible to lateral-torsional buckling during lifting.

$$C_L = 1.0 \quad for \quad \frac{a}{L} \leq 0.2$$

$$C_L = 0.5 * \frac{d}{b} \quad for \quad 0.2 < \frac{a}{L} < 0.3 \qquad \textit{Equation 5.2}$$

$$C_L = 0.75 \quad for \quad \frac{a}{L} \geq 0.3$$

$$M_{max} < \phi\, M_{cr} = \phi\, C_L * \frac{\pi}{L_b} \sqrt{EI_y GJ + E^2 I_y C_w \left(\frac{\pi^2}{L_b{}^2}\right)} \qquad \textit{Equation 5.3}$$

$$M_{max} = Factored\ Maximum\ Moment\ From\ Static\ Analysis$$

$$M_{cr} = Critical\ Buckling\ Moment$$

$$\phi = Reduction\ Factor = 0.9$$

$$C_L = Lift\ Adjustment\ Factor$$

$$L_b = Unbraced\ Length = L_{LIFT} \geq a$$

$$E = Modulus\ of\ Elasticity\ (ksi)$$

$$I_y = Weak\ Axis\ Moment\ of\ Inertia\ (in^4)$$

$$G = Shear\ Modulus\ (ksi)$$

$$J = Torsional\ Constant\ (in^4) = \sum \frac{bt^3}{3}$$

$$C_w = Warping\ Constant\ (in^6) = \frac{I_y h^2}{4}$$

6.4 **SUMMARY OF THE BEHAVIOR OF CURVED I-GIRDERS DURING LIFTING**

The location of the lift points has been shown to be a defining factor of how curved I-girders behave during the lifting process. This parameter profoundly impacts the rotation and girder stability during lifting. The stability of a curved I-girder is maximized by lifting at the quarter points ($a/L = 0.25$). This guideline is typically adequate to control the rigid body rotation of the girder in the air; however, lifting closer to the fifth points ($a/L = 0.21$) of the girder minimizes rotations expected during the lift. Specific cases should always be checked using the procedures detailed in this thesis or other appropriate numerical analysis techniques to optimize both the rotations and girder stability during lifting.

This chapter concludes this thesis and describes the guidelines and recommendations for the safe lifting of horizontally curved I-girders. Equations are presented to account for two key issues: controlling girder rotations and ensuring that the girder will be stable during lifting. Refer to the associated chapters for more detailed information on either of these issues.

In lieu of codified guidelines from AASHTO or other specifications, this thesis provides information on the behavior of horizontally curved steel I-girders during the lifting process.

APPENDIX A
Design Examples

A.1 INTRODUCTION

This appendix provides design examples that illustrate the use of the equations and guidelines presented in this thesis to predict the behavior of curved I-girders during lifting. The process shown in Chapter 4 is utilized to determine optimal lift points and expected rotations during lifting. The use of C_L to check the curved girder stability during lifting is also shown.

A.2 EXAMPLE PROBLEMS

Two example problems are given to demonstrate the functionality of this thesis's guidelines. Example #1 finds the optimal lift point locations (a) and lifting apparatus length (L_{LIFT}) to minimize the expected rigid body rotation of a curved I-girder during lifting. The lateral-torsional buckling capacity of this lifting configuration is then checked using C_L and the suggested equations. Example #2 uses the guidelines to calculate expected rotations and check the stability during lifting when less than favorable lifting conditions are enforced, as may be the case in practice.

131

Example # 1: Determining Optimal Lift Points and Checking the Stability of 14C2

Given:

$$h_w := 84 \cdot in \qquad b_f := 24 \cdot in \qquad L := 124 \, ft$$

$$t_w := .625 \cdot in \qquad t_f := 1.25 \cdot in \qquad R := 1215 \, ft$$

$$d := h_w + 2 \cdot t_f = 86.5 \, in \qquad h := h_w + t_f = 85.25 \, in$$

$$w := 1.25 \cdot (2 \cdot b_f \cdot t_f + h_w \cdot t_w) \cdot 490 pcf = 0.48 \frac{kip}{ft}$$

Determine the location of the girder's center of gravity

Equation 5.1:
$$C := 2 \cdot R \cdot \sin\left[\frac{(180 deg \cdot L)}{(2 \cdot \pi \cdot R)}\right] = 123.95 \, ft$$

$$D := R \cdot \frac{C}{L} = 1214.47 \, ft$$

$$D' := D - .5 \cdot \sqrt{4 \cdot R^2 - C^2} \qquad\qquad \textbf{\textit{Equation A.1}}$$

$$D' = 1.05 \, ft \quad \longrightarrow \quad \text{Distance from chord C to center of gravity}$$

Determine support location (a) to create line of action running though C.G.

$$a := \frac{C}{2} - \sqrt{R^2 - \left(D' + .5 \cdot \sqrt{4 \cdot R^2 - C^2}\right)^2} \qquad\qquad \textbf{\textit{Equation A.2}}$$

$$a = 26.18 \, ft \qquad L_{LIFT} := L - 2 \cdot a = 71.63 \, ft \qquad \frac{a}{L} = 0.21$$

Lift points should be placed at a distance **a** from each end of the girder. A spreader bar of length **L_LIFT** should be used.

This configuration minimizes the rotation of the girder during lifting and therefore optimizes the lift point locations for girder rotation. The girder stability should now be checked, as shown below.

Calculate the lift adjustment factor, C_L, for the girder with an a/L of .21

$$C_L = 1.0 \qquad \text{for} \qquad \frac{a}{L} \le 0.225$$

Equation 6.2:
$$C_L = 0.5 \cdot \frac{d}{b} \le 2.5 \qquad \text{for} \qquad 0.225 < \frac{a}{L} < 0.275$$

$$C_L = 0.75 \qquad \text{for} \qquad \frac{a}{L} \ge 0.275$$

$$C_L := \text{if}\left(\frac{a}{L} \le .225, 1.0, \text{if}\left(\frac{a}{L} \ge .275, .75, \text{if}\left(0.5 \cdot \frac{d}{b_f} \le 2.5, .5 \cdot \frac{d}{b_f}, 2.5\right)\right)\right) = 1$$

$$\frac{a}{L} = 0.21 \qquad C_L = 1 \longrightarrow \text{Lift Adjustment Factor}$$

Calculate the the critical buckling moment, M_{cr}

Equation 6.3:
$$M_{max} < \phi M_{cr} = \phi \cdot C_L \cdot \frac{\pi}{L_b} \cdot \sqrt{E \cdot I_y \cdot G \cdot J + E^2 \cdot I_y \cdot C_w \cdot \left(\frac{\pi^2}{L_b^2}\right)}$$

L_b equals the greater of $\quad$ a $\quad$ OR $\quad L_{LIFT}$

Unbraced Length $\left\{\begin{array}{l} L_b := \text{if}\left(L_{LIFT} \ge a, L_{LIFT}, a\right) \\[6pt] L_b = 71.63\,\text{ft} \end{array}\right.$

$$\phi := .9 \qquad C_L = 1 \qquad E := 29000\,\text{ksi} \qquad G := 11200\,\text{ksi}$$

$$I_y := 2 \cdot \left(\frac{t_f \cdot b_f^3}{12}\right) + \frac{h_w \cdot t_w^3}{12} = 2881.71\,\text{in}^4$$

$$C_w := \frac{I_y \cdot h^2}{4} = 5235750.04\,\text{in}^6 \qquad J := 2 \cdot \left(\frac{b_f \cdot t_f^3}{3}\right) + \frac{h_w \cdot t_w^3}{3} = 38.09\,\text{in}^4$$

133

$$\phi M_{cr} := \phi \cdot C_L \cdot \frac{\pi}{L_b} \cdot \sqrt{E \cdot I_y \cdot G \cdot J + E^2 \cdot I_y \cdot C_w \cdot \left(\frac{\pi^2}{L_b^2} \right)} = 3925.89 \, \text{kip} \cdot \text{ft}$$

Calculate the maximum moment in the girder, M_{max}

Equation 1.7: M_{max} equals the greater of

$$\frac{w \cdot a^2}{2}$$

OR

$$\left| \frac{w \cdot L_{LIFT}^2}{8} - \frac{w \cdot a^2}{2} \right|$$

$$M_{max} := \text{if}\left(\frac{w \cdot a^2}{2} \geq \left| \frac{w \cdot L_{LIFT}^2}{8} - \frac{w \cdot a^2}{2} \right|, \frac{w \cdot a^2}{2}, \left| \frac{w \cdot L_{LIFT}^2}{8} - \frac{w \cdot a^2}{2} \right| \right)$$

$$M_{max} = 164.03 \, \text{kip} \cdot \text{ft}$$

Check the stability of the girder

$$M_{max} < \phi M_{cr}$$

$$\text{CHECK} := \text{if}\left(M_{max} < \phi M_{cr}, \text{"stable"}, \text{"unstable"} \right) = \text{"stable"}$$

CHECK = "stable"

Example # 2: Determining the Rotation and Stability of a Curved I-Girder with Unfavorable Lift Points

$h_w := 60 \cdot in$ $b_f := 9 \cdot in$ $L := 125 \cdot ft$

$t_w := .5 \cdot in$ $t_f := .5 \cdot in$ $R := 1200 \cdot ft$

$d := h_w + 2 \cdot t_f = 61 \cdot in$ $h := h_w + t_f = 60.5 \cdot in$

Given: $w := 1.25 \cdot \left(2 \cdot b_f \cdot t_f + h_w \cdot t_w \right) \cdot 490 pcf = 0.17 \dfrac{kip}{ft}$

$L_{LIFT} := 40 \cdot ft$ $H := 24 \cdot in$

$a := \dfrac{\left(L - L_{LIFT} \right)}{2} = 42.5 \cdot ft$ $\dfrac{a}{L} = 0.34$

$\Big\}$ Lifting constraints imposed by lift apparatus availability

Determine the eccentricity (e) between the girder's center of gravity and the line of action created by the lift points

Equation 5.1: $C := 2 \cdot R \cdot \sin \left[\dfrac{(180 deg \cdot L)}{(2 \cdot \pi \cdot R)} \right] = 124.94 \, ft$

$D := R \cdot \dfrac{C}{L} = 1199.46 ft$

Equation 5.2: $e := R - D - \left(R \cdot \sin \left(\dfrac{180 deg \cdot L_{LIFT}}{2 \cdot \pi \cdot R} \right) \cdot \tan \left(\dfrac{180 deg \cdot L_{LIFT}}{4 \cdot \pi \cdot R} \right) \right)$

$e = 4.51 \cdot in$

Determine the rotation (θ) of the girder when lifted

Equation 5.3 $\theta := atan \left[\dfrac{e}{\left(H + t_f + .5 \cdot h_w \right)} \right]$

$\theta = 4.73 \cdot deg$

135

Calculate the lift adjustment factor, C_L, for the girder with an a/L of .21

$$C_L = 1.0 \qquad \text{for} \qquad \frac{a}{L} \leq 0.225$$

Equation 6.2:
$$C_L = 0.5 \cdot \frac{d}{b} \leq 2.5 \qquad \text{for} \qquad 0.225 < \frac{a}{L} < 0.275$$

$$C_L = 0.75 \qquad \text{for} \qquad \frac{a}{L} \geq 0.275$$

$$C_L := \text{if}\left(\frac{a}{L} \leq .225, 1.0, \text{if}\left(\frac{a}{L} \geq .275, .75, \text{if}\left(0.5 \cdot \frac{d}{b_f} \leq 2.5, .5 \cdot \frac{d}{b_f}, 2.5\right)\right)\right) = 0.75$$

$$\frac{a}{L} = 0.34 \qquad \boxed{C_L = 0.75} \longrightarrow \text{Lift Adjustment Factor}$$

Calculate the the critical buckling moment, M_{cr}

Equation 6.3:
$$M_{max} < \phi M_{cr} = \phi \cdot C_L \cdot \frac{\pi}{L_b} \cdot \sqrt{E \cdot I_y \cdot G \cdot J + E^2 \cdot I_y \cdot C_w \cdot \left(\frac{\pi^2}{L_b^2}\right)}$$

Unbraced Length
$$\left\{
\begin{array}{l}
L_b \quad \text{equals the greater of} \quad \begin{array}{l} a \\ \text{OR} \\ L_{LIFT} \end{array} \\[12pt]
L_b := \text{if}\left(L_{LIFT} \geq a, L_{LIFT}, a\right) \\[8pt]
L_b = 42.5 \, \text{ft}
\end{array}
\right.$$

$$\phi := .9 \qquad C_L = 0.75 \qquad E := 29000 \, \text{ksi} \qquad G := 11200 \, \text{ksi}$$

$$I_y := 2 \cdot \left(\frac{t_f \cdot b_f^3}{12}\right) + \frac{h_w \cdot t_w^3}{12} = 61.38 \, \text{in}^4 \qquad J := 2 \cdot \left(\frac{b_f \cdot t_f^3}{3}\right) + \frac{h_w \cdot t_w^3}{3} = 3.25 \, \text{in}^4$$

$$C_w := \frac{I_y \cdot h^2}{4} = 56161.96 \, \text{in}^6 \qquad \phi M_{cr} := \phi \cdot C_L \cdot \frac{\pi}{L_b} \cdot \sqrt{E \cdot I_y \cdot G \cdot J + E^2 \cdot I_y \cdot C_w \cdot \left(\frac{\pi^2}{L_b^2}\right)} = 144.86 \, \text{kip} \cdot \text{ft}$$

136

Calculate the maximum moment in the girder, M_{max}

Equation 1.7: M_{max} equals the greater of $\dfrac{w \cdot a^2}{2}$ OR $\left| \dfrac{w \cdot L_{LIFT}^2}{8} - \dfrac{w \cdot a^2}{2} \right|$

$$M_{max} := if\left(\frac{w \cdot a^2}{2} \geq \left| \frac{w \cdot L_{LIFT}^2}{8} - \frac{w \cdot a^2}{2} \right|, \frac{w \cdot a^2}{2}, \left| \frac{w \cdot L_{LIFT}^2}{8} - \frac{w \cdot a^2}{2} \right| \right)$$

$$M_{max} = 149.82\, kip \cdot ft$$

Check the stability of the girder

$$M_{max} < \phi M_{cr}$$

$$CHECK := if\left(M_{max} < \phi M_{cr}, \text{"stable"} , \text{"unstable"} \right) = \text{"unstable"}$$

CHECK = "unstable"

A.3 SUMMARY

Example #1 and Example #2 demonstrate the use of the guidelines set forth in this thesis. Figure A.1 shows Table 17-26 from the AISC *LRFD* specification (*Load* 13th 2005). This table gives the properties of a circle. Many of these properties were used to derive the equations presented and used throughout this thesis.
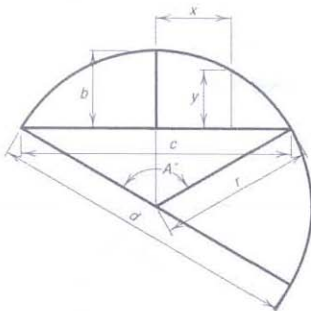
Table 17–26
Properties of the Circle

Circumference $= 6.28378$ $r = 3.14159d$
Diameter $= 0.31831$ circumference
Area $= 3.14159 r^2$

Arc $a = \dfrac{\pi r A^\circ}{180^\circ} = 0.017453 r A^\circ$

Angle $A^\circ = \dfrac{180^\circ a}{\pi r} = 57.29578 \dfrac{a}{r}$

Angle $A^\circ = 2 \sin^{-1}(c/2r)$

Angle $A^\circ = 4 \tan^{-1}(2b/c)$

Radius $r = \dfrac{4b^2 + c^2}{8b}$

Chord $c = 2\sqrt{2br - b^2} = 2r \sin \dfrac{A}{2}$

Rise $b = r - \dfrac{1}{2}\sqrt{4r^2 - c^2} = \dfrac{c}{2}\tan \dfrac{A}{4}$

$\quad = 2r \sin^2 \dfrac{A}{4} = r + y - \sqrt{r^2 - x^2}$

$y = b - r + \sqrt{r^2 - x^2}$

$x = \sqrt{r^2 - (r + y - b)^2}$

Diameter of circle of equal periphery as square	$= 1.27324$ side of square
Side of square of equal periphery as circle	$= 0.78540$ diameter of circle
Diameter of circle circumscribed about square	$= 1.41421$ side of square
Side of square inscribed in circle	$= 0.70711$ diameter of circle

Figure A.1 Arc Properties

APPENDIX B
Literature Review of Curved I-Girders

B.1 INTRODUCTION

The following appendix provides a summary of former studies performed on various aspects of curved I-girder behavior. Landmark, large scale research efforts are discussed, as well as work completed in specific areas of curved girder research. Lastly, the need for field studies of curved I-girder behavior during erection is highlighted, with emphasis on the lifting stage of construction.

The first investigation into curved beams dates back to 1840s with the work done by Barre De Saint Venant. Numerous other studies and work has been done since then, however, widespread interest and organized research efforts into curved steel bridges in the United States did not begin until 1969.

B.2 LANDMARK ORGANIZED RESEARCH EFFORTS

B.2.1 Consortium of University Research Teams (CURT)

In 1969, the United States Federal Highway Administration (FHWA) formed the Consortium of University Research Teams (CURT) to conduct the first major research into analysis and behavior of horizontally curved bridges. The members of CURT included Carnegie Mellon University, the University of Pennsylvania, the University of Rhode Island, and Syracuse University.

The research conducted by the CURT project focused on scale model laboratory tests, supplemented with theoretical work and analytical studies. Scale tests on I-girders explored the behavior of a single girder, as well as girder pairs (Moser and Culver 1970; Mozer et al. 1971, 1973). Tests utilizing representative curved bridge systems examined girder interaction with bracing members and adjacent girder lines (Brennan 1970, 1971, 1974), providing data to validate the first analytical techniques developed for curved bridges. Some of this analytical and theoretical work aimed at developing methods for

139

predicting behaviors such as overall strength of doubly symmetric curved I girders in bending (McManus 1971), and local buckling behavior of curved girder flanges (Nasir 1970). Exploring further into the stability of curved I-girders, the local buckling of the compression flange of curved I-girders was investigated in both the elastic and inelastic range (Culver and Frampton 1970; Culver and Nasir 1971).

The research efforts by the CURT project resulted in the development of allowable stress design (ASD) specifications in 1975. Load factor design (LFD) criteria were developed from ASD and CURT research in a project funded by the American Iron and Steel Institute (AISI). The American Association of State Highway Transportation Officials (AASHTO) adopted and combined ASD and LFD into the first edition of the Guide Specifications for Horizontally Curved Highway Bridges in 1980 (AASHTO 1980).

B.2.2 Curved Steel Bridge Research Project (CSBRP)

The 1980 Guide Specs governed the analysis and design of curved bridges until the early 1990s, when Structural Stability Research Council (SSRC) on Horizontally Curved Girders published a report detailing problems with the 1980 Guide Specs and recommended areas in need of additional research (SSRC 1991). As a result of this report, numerous research projects were undertaken to expand the understanding of curved girder behavior and analysis.

The first and most influential project was the Curved Steel Bridge Research Project (CSBRP) initiated in 1992 by the FHWA. This project's goals included compiling and disseminating all curved bridge related research performed previously, as well as addressing weaknesses of the earlier CURT research, specifically the lack of full-scale or field tests with realistic loading and boundary conditions. The CSBRP accomplished its first goal by producing a comprehensive document consisting of nearly 900 references relating to all curved bridge research to date (Zureick et al 1994). The results and conclusions outlined in these references helped build the foundation for the more recent work on curved bridges that has taken place in the last ten years, as well as

AASHTO's most recent publication on the subject, Guide Specifications for Horizontally Curved Steel Girder Highway Bridges 2003 (AASHTO 2003). The CSBRP has led to numerous publications detailing various methods and results that have contributed to the understanding of curved girder bridges. Many of the projects and findings referenced in the following sections are products of the CSBRP, both directly and indirectly.

B.3   AREAS OF STUDY

B.3.1   Structural Stability of Curved I-Girders

Structural stability is an important aspect of curved girders due to the geometrically induced eccentricity commonly exhibited by applied loads from the line of support. A number of papers have been published recently that examine stability issues with horizontally curved I girders. Davidson looked at the effect curvature has on local buckling of curved I-girder flanges (Davidson and Yoo 1996) using finite difference and finite element methods. This study confirmed earlier findings made by CURT (Culver and Frampton 1970), where the buckling behavior of curved steel plates in the elastic range was shown to exhibit no significant difference with behavior observed in rectangular plates within the specified limits for curvature.

Davidson also examined slenderness effects on the webs of curved I-girders to better understand the strength reduction that occurs as a result of the "bulging" effects caused by combined bending and shear (Davidson et al 2000). Jung and White conducted parametric studies to see the effects of residual stresses and geometric imperfections on the shear strength of curved I-girders with the maximum allowable web slenderness ratio permitted by AASHTO (Jung and White 2005).

B.3.2   Cross Frame Behavior in Curved I-Girder Bridge Systems

In addition to individual girder stability issues, publications have focused on more global curved bridge system issues. Specifically, cross-frame behavior and cross frame-girder interaction has seen a notable amount of interest. Maneetes and Linzell conducted parametric studies in which cross frame type, cross section, and spacing were varied to

determine the associated bridge responses (Maneetes and Linzell 2003). It was verified that lateral bracing of the top flange is more beneficial than restraining lateral movement of the bottom flange. Decreasing cross frame spacing leads to an associated decrease in vertical bending stresses and displacements. Davidson performed similar tests using regression analysis techniques (Davidson et al 1996). However, little work has been performed showing cross frame behavior during erection and to what degree it restrains out of plane behavior and effectively transfers the loads between girders, which is the crux of the global stability of the bridge system during erection.

B.3.3 Effectiveness of Analytical Techniques

Numerous papers have reported analytical studies accompanied with laboratory testing giving information on more general curved I-girder behavior. Zureick et al described the large-scale laboratory testing and analytical program started by FHWA. Experimental and analytical efforts involved with testing of a full-scale three girder system are presented (Zureick et al 2000). Continuing the FHWA's CSBRP, Linzell et al collected data from a full scale laboratory setup with a variety of conditions to help test the robustness of currently used analytical tools (Linzell, Leon et al 2004). Erection study tests showed the beneficial effects of providing minimal radial restraint for curved I-girders during construction, as well as the response of removing non-uniform shoring. The comparisons made between experimental and analytical results showed fair predictions of erection behavior, however discrepancies arose due to fabrication and erection sequencing factors, specifically regarding the presence of "locked in" forces and deformations in the experimental bridge.

These problematic effects were unable to be incorporated into analytical models. Issues also arose with inaccurate cross frame connections in analytical models causing unrealistic representations of radial load distributions across the curved steel girder bridge system. It is clear that more research is required to understand the significant interactions taking place between the curved girders and cross frames in the curved

142

bridge system during erection, in order for analytical models to more accurately predict the system's behavior.

B.4   ANALYZING CURVED I-GIRDERS

A paramount challenge when using horizontally curved steel I-girders is how to approach their unique geometry and behavior when modeling them analytically, whether the end is a research effort, or, more commonly, designing a curved girder bridge. No commercial software exists that is able to appropriately model and predict the behavior of curved girders and associated braces during the early stages of erection, due to the uncertainty in the limited amounts of bracing present at various phases, as well as variability of boundary conditions at locations of restraint. Typically, rules of thumb or approximate methods are employed with varying levels of accuracy.

A significant amount of work detailing some of these analysis methods has been performed. Zureick and Naquib classified approximate and refined methods, giving the strengths and weaknesses of each technique. Examples of the approximate methods outlined include the most widely used preliminary analysis method, the V-load method, as well as others such as the plane-grid and space-frame methods. More refined methods covered include the finite element method, finite difference method, and the use of differential equations (Zureick and Naquib 1999).

Fiechtl, Fenves, and Frank summarized and applied the V-load method. The theory behind the method is broken down and applied to single and multiple girder systems. The results of this application are then compared to finite element models to determine the V-load's accuracy. It was shown that a V-load analysis underestimates the torsional stiffness of the bridge system, causing the transfer of too much load from the inner girder to the outer girder (Fiechtl et al 1987). This leads to conservatively high bending stress values on the outer girder, and low, unconservative values reported on the inner girder.

B.5 FIELD TESTING OF CURVED I-GIRDERS

One of the deficiencies noted by the SSRC's report and that the CSBRP recognized was the lack of field tests on curved I-girders, specifically during erection and other construction stages.

The first effort at field testing a curved I-girder bridge was made in 1971 by Beal and Kissane for FHWA Research Project 42-1. In a series of interim reports made to the FHWA and USDOT, Beal and Kissane explored the difficulties and issues with field monitoring and comparisons with analytical results. Their first results were inconclusive due to holes in the data caused by malfunctioning or destroyed gages. Later tests suggested that planar grid analysis is capable of roughly predicting deflections and in-plane bending; however, issues with lateral flange bending and torsional stiffness were unable to be reconciled. Limited experimental information and an inability for the analytical tools at the time to accurately predict out-of-plane behavior led to few solid conclusions from the study (Beal and Kissane 1971, 1972).

More recent literature has been published on field studies of curved I-girders. Galambos et al instrumented a bridge in the field and reported the actual stresses during specific construction stages. These stresses were compared with a finite element program in an effort to better follow and predict the behavior of curved I-girders during construction (Galambos et al 2000). In their study, a four girder, two span bridge was instrumented with vibrating wire strain gages to capture the bending and warping behavior of the girders. When the collected data was compared with the developed finite element program, a number of results were observed. During the first construction stages, experimental data showed little correlation with the model, which was attributed to load levels being so low that fit-up stresses and local eccentricities dominated the data. This situation was present both when shoring towers were employed, as well as when they were removed. Once the concrete deck was poured, collected stress data began to correlate better, since larger loads caused the effect of fit-up stresses to become less prevalent. From the results, it was concluded that all stresses were well below yield

144

during all construction phases, and significant correlation was possible once composite action between the deck slab and girders takes place (Galambos et al 2000).

Chavel and Earls looked at the effects erection sequence can have on maintaining a no-load condition that most girders and cross frames are designed for. A field bridge erection was monitored, with a finite element model predicting results of the erection sequence (Chavel and Earls 2006). After concluding that erection sequence did not lead to fit-up problems observed in the field, Chavel and Earls promoted the awareness of inconsistent detailing as a cause for locked in forces and the difficulties involved in curved I-girder bridge erection and fit-up. In the second part of their 2006 publication, they present multiple detail methods, where girders and cross frames are detailed to be web plumb at various load conditions. Inconsistent detailing with regard to different load conditions can lead to numerous situations not accounted for in design or analytical models, such as locked in stresses and incorrect top of girder elevations that can cause variations in the concrete deck or haunches (Chavel and Earls 2006).

B.6 SUMMARY

The structural engineering field has significantly advanced its knowledge and understanding of curved steel I-girder behavior over the last 40 years. From the efforts by CURT in the late 60s and 70s to more recent work by the CSBRP and others in the 90s and 00s, solid theoretical and analytical research has been conducted and yielded conclusive results. However, there is a visible lack of full scale field monitoring of curved I-girder bridges during critical construction stages like girder lifting, where accurate models of oftentimes incomplete or unpredictable bracing or support conditions are difficult to program and produce representative results. Chapter 2 and 3 of this thesis details field studies and results that attempt to bridge the gap in the current research. Results from these studies were used to validate analytical models to accurately predict curved I-girder behavior during the early stages of construction.

APPENDIX C
Straight vs. Curved Moment Comparison Tables

C.1 INTRODUCTION

The following appendix provides tables documenting the comparison of the moments calculated using straight girder geometry and the moments calculated using the curved girder geometry. The process and information presented in these tables was used to justify the use of the straight girder geometry to calculate moments, as stated in Chapter 1. Figure C.1 gives the variables and equations used in the comparison tables.

$$M_{straight} = \frac{wa^2}{2}$$

$$M_{curved} = wa * x$$

$$where\ x = R\sin\left[\frac{180° * \frac{a}{2}}{\pi * R}\right]$$
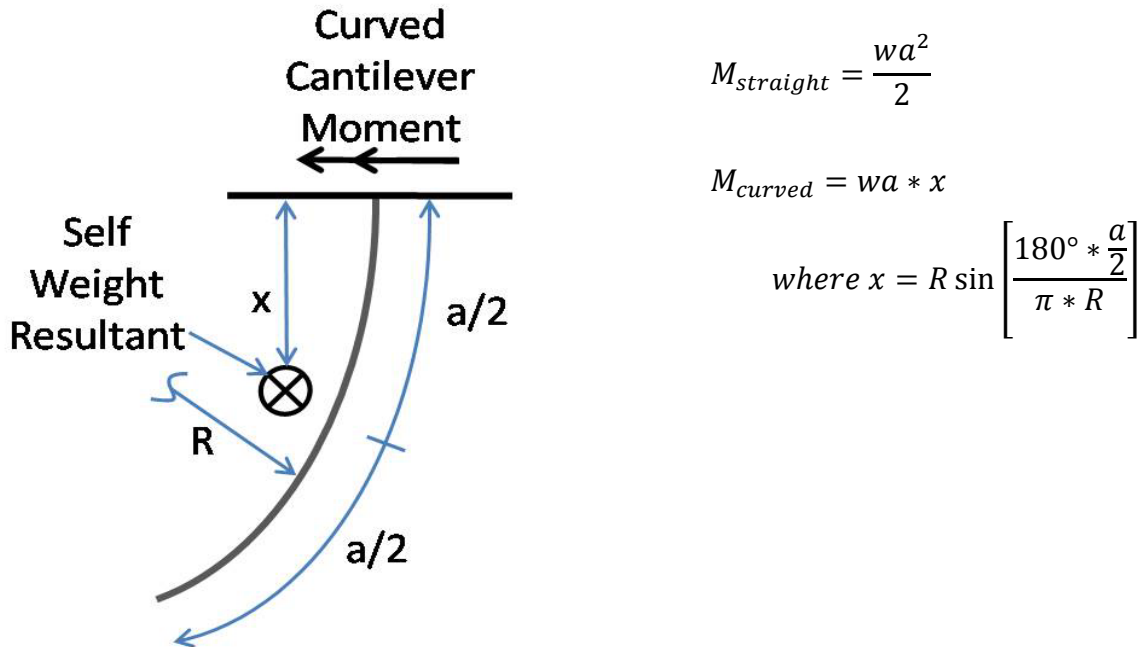
Figure C.1 Straight vs. Curved Girder Moment

C.2 COMPARISON TABLES

Inputs						
w =	0.3598	k/ft	Subtended Angle =		152.79	degrees
L =	120	ft		R =	45	ft

	Straight		Curved			
a/L	a	Moment (k-ft)	a	x	Moment (k-ft)	% Difference
0.1	12	25.9	12	6.0	25.8	0.30
0.15	18	58.3	18	8.9	57.9	0.67
0.2	24	103.6	24	11.9	102.4	1.20
0.225	27	131.1	27	13.3	129.2	1.52
0.25	30	161.9	30	14.7	158.9	1.88
0.275	33	195.9	33	16.1	191.6	2.28
0.3	36	233.2	36	17.5	227.0	2.72
0.35	42	317.3	42	20.2	305.9	3.72
0.4	48	414.5	48	22.9	395.1	4.90

Table C.1 Straight vs. Curved Moment for Subtended Angle of 152 Degrees

Inputs						
w =	0.3598	k/ft	Subtended Angle =		45.84	degrees
L =	120	ft		R =	150	ft

	Straight		Curved			
a/L	a	Moment (k-ft)	a	x	Moment (k-ft)	% Difference
0.1	12	25.9	12	6.0	25.9	0.03
0.15	18	58.3	18	9.0	58.3	0.06
0.2	24	103.6	24	12.0	103.5	0.11
0.225	27	131.1	27	13.5	131.0	0.14
0.25	30	161.9	30	15.0	161.6	0.17
0.275	33	195.9	33	16.5	195.5	0.20
0.3	36	233.2	36	18.0	232.6	0.24
0.35	42	317.3	42	20.9	316.3	0.33
0.4	48	414.5	48	23.9	412.7	0.43

Table C.2 Straight vs. Curved Moment for Subtended Angle of 45 Degrees

Inputs						
w =	0.3598	k/ft	Subtended Angle =		5.85	degrees
L =	124	ft		R =	1215	ft

	Straight		Curved			
a/L	a	Moment (k-ft)	a	x	Moment (k-ft)	% Difference
0.1	12.4	27.7	12.4	6.2	27.7	0.00
0.15	18.6	62.2	18.6	9.3	62.2	0.00
0.2	24.8	110.6	24.8	12.4	110.6	0.00
0.225	27.9	140.0	27.9	13.9	140.0	0.00
0.25	31	172.9	31	15.5	172.9	0.00
0.275	34.1	209.2	34.1	17.0	209.2	0.00
0.3	37.2	249.0	37.2	18.6	248.9	0.00
0.35	43.4	338.9	43.4	21.7	338.8	0.01
0.4	49.6	442.6	49.6	24.8	442.6	0.01

Table C.3 Straight vs. Curved Moment for Subtended Angle of 6 Degrees (14C2)

C.3   SUMMARY

For all practical subtended angles (Table C.2 and Table C.3), the difference between the straight moments and curved moments is negligible. Table C.1 presents the comparison for the subtended angle of 152 degrees, where the difference becomes significant. However, this subtended angle, with a radius of curvature of 45', is not practical for bridge applications.

As stated in Chapter 1, the straight girder geometry was used in the calculation of static moments used in the formulation of the adjustment factor, C_L, and in all other moment calculations for checking the stability of curved I-girders. The tables presented in this appendix justify this assumption.

APPENDIX D
Results from Girder 4 & Girder 3 Web Gage Locations During Erection

D.1 INTRODUCTION

The following appendix presents figures displaying the stress changes recorded by the web gages (Section C) of Girder 4 and Girder 3 during erection. Figure D.1 shows the plan view of the girders, web gage locations given. The web gages were placed with a uniform spacing down the depth of the web, giving a spacing of approximately 1'-9".
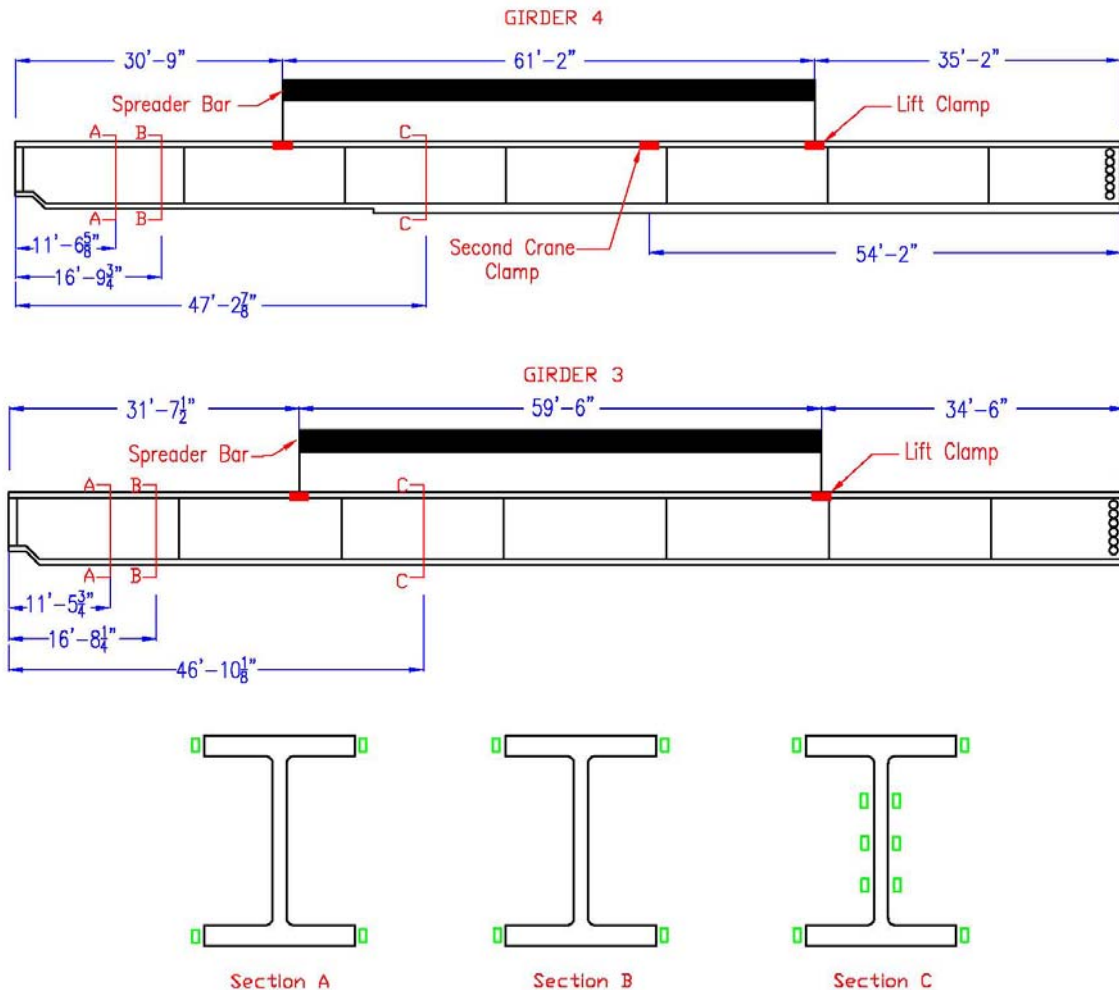
Figure D.1 Girder 4 & 3 Plan View w/ Web Gage Locations

D.2 RESULTS FROM GIRDER WEBS
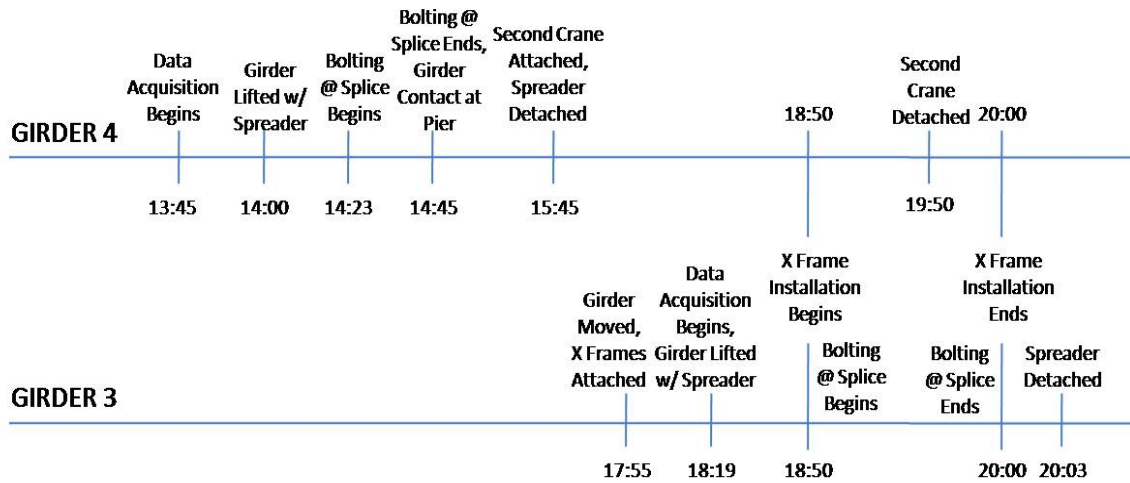
Figure D.2 Erection Timeline for Girder 4 & 3

For reference in the following figures, the erection timeline presented in Chapter 3 is given in Figure D.2. Relevant events are also shown in the figures.
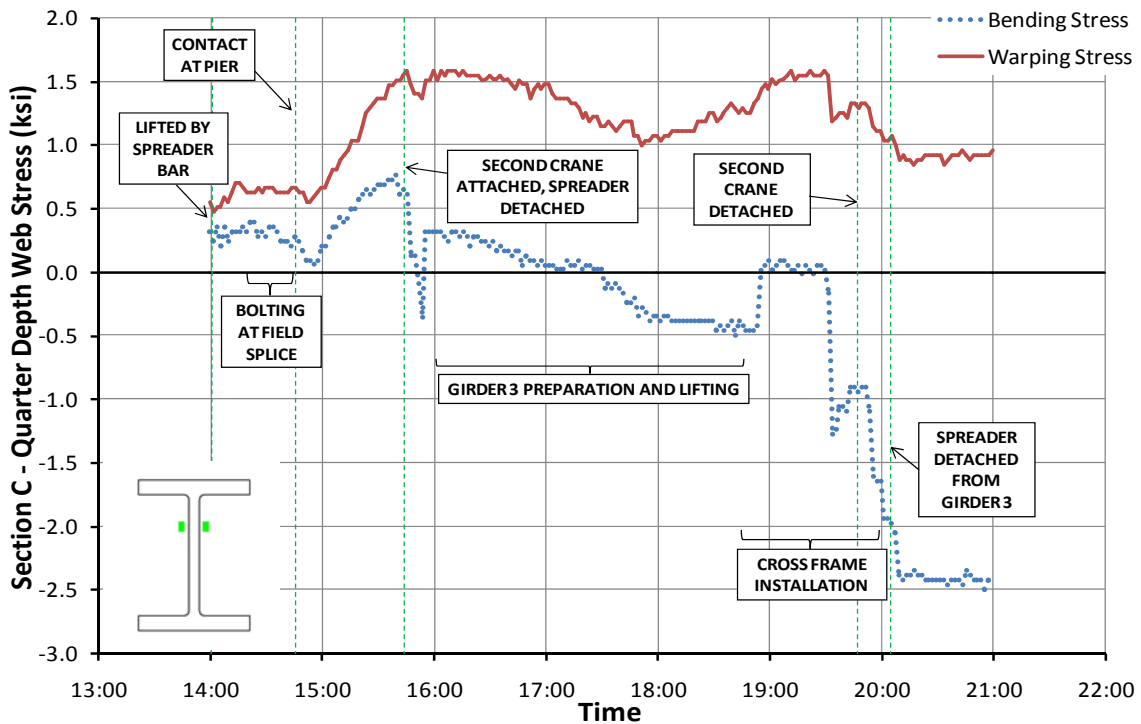
Figure D.3 Girder 4 Stress Change at Section C Quarter Depth of Web
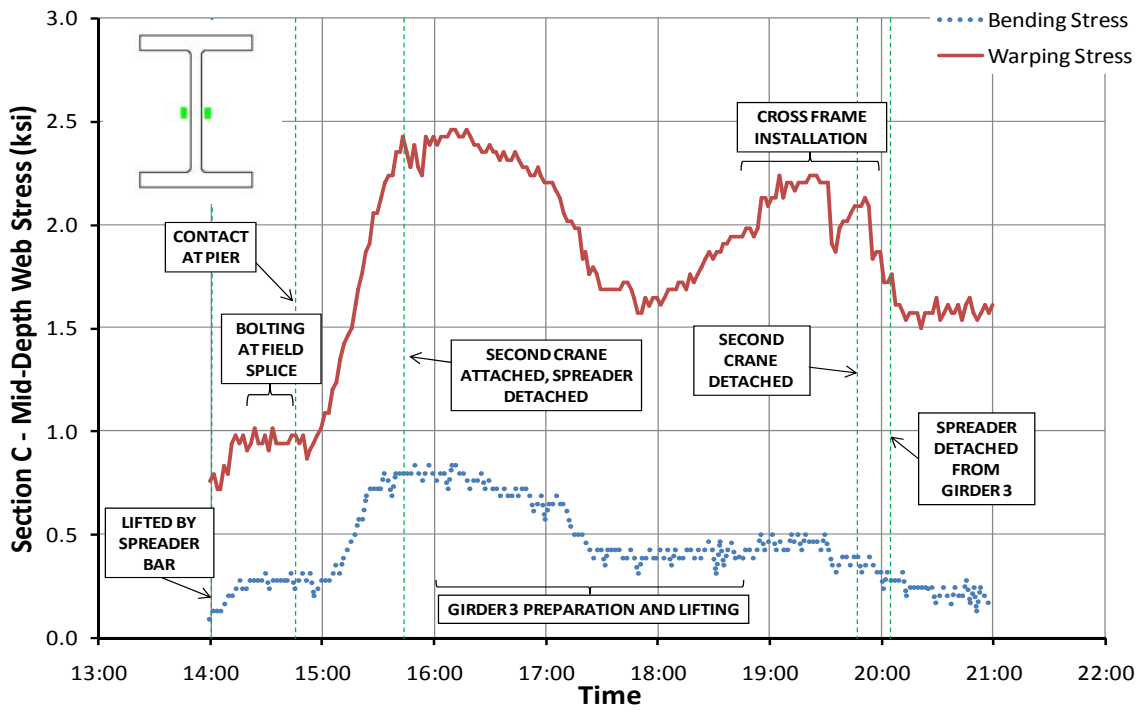
Figure D.4 Girder 4 Stress Change at Section C Mid-Depth of Web
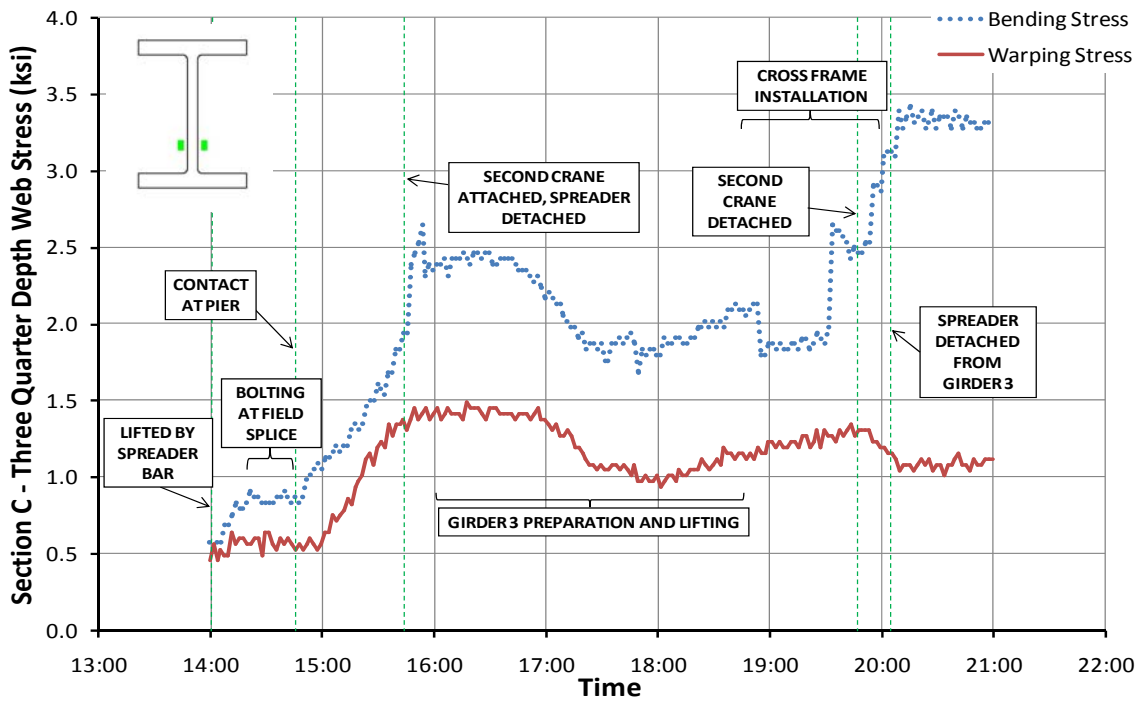
Figure D.5 Girder 4 Stress Change at Section C Three Quarter Depth of Web

151
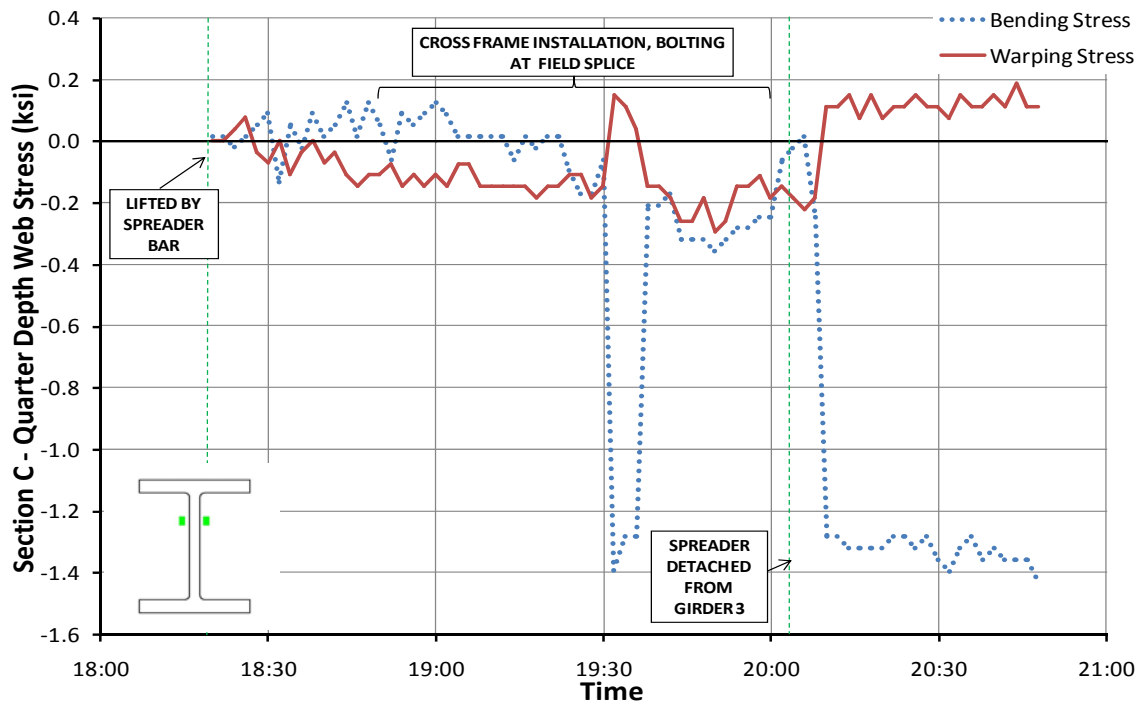
Figure D.6 Girder 3 Stress Change at Section C Quarter Depth of Web
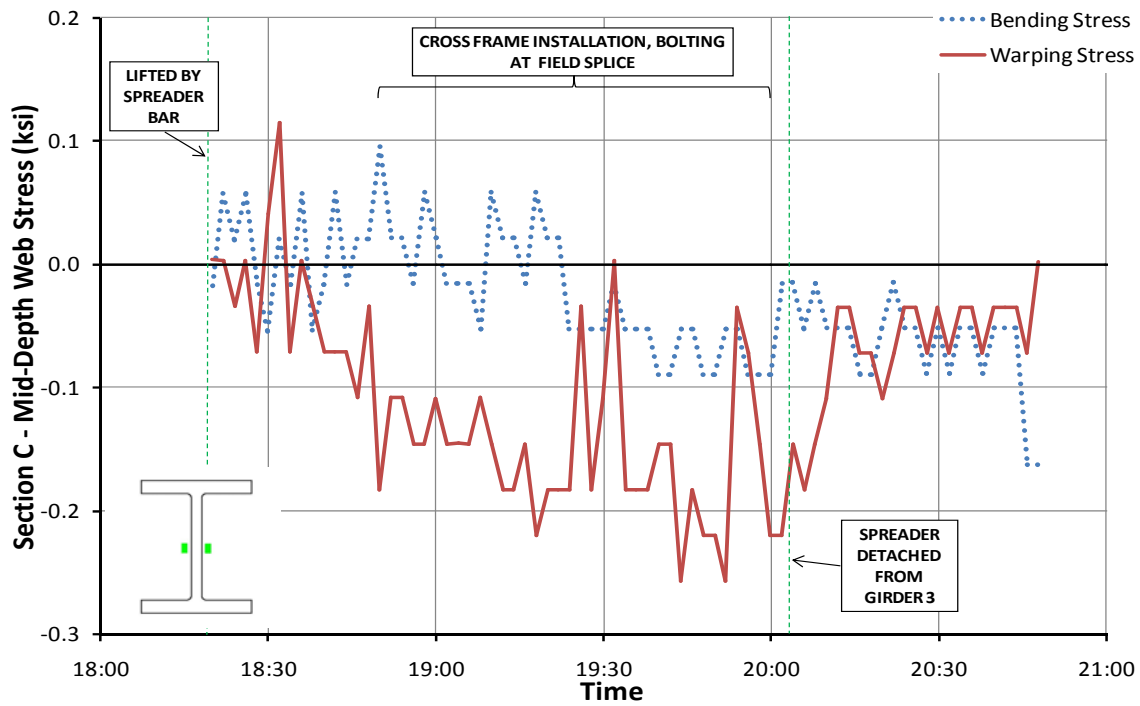
Figure D.7 Girder 3 Stress Change at Section C Mid-Depth of Web

152
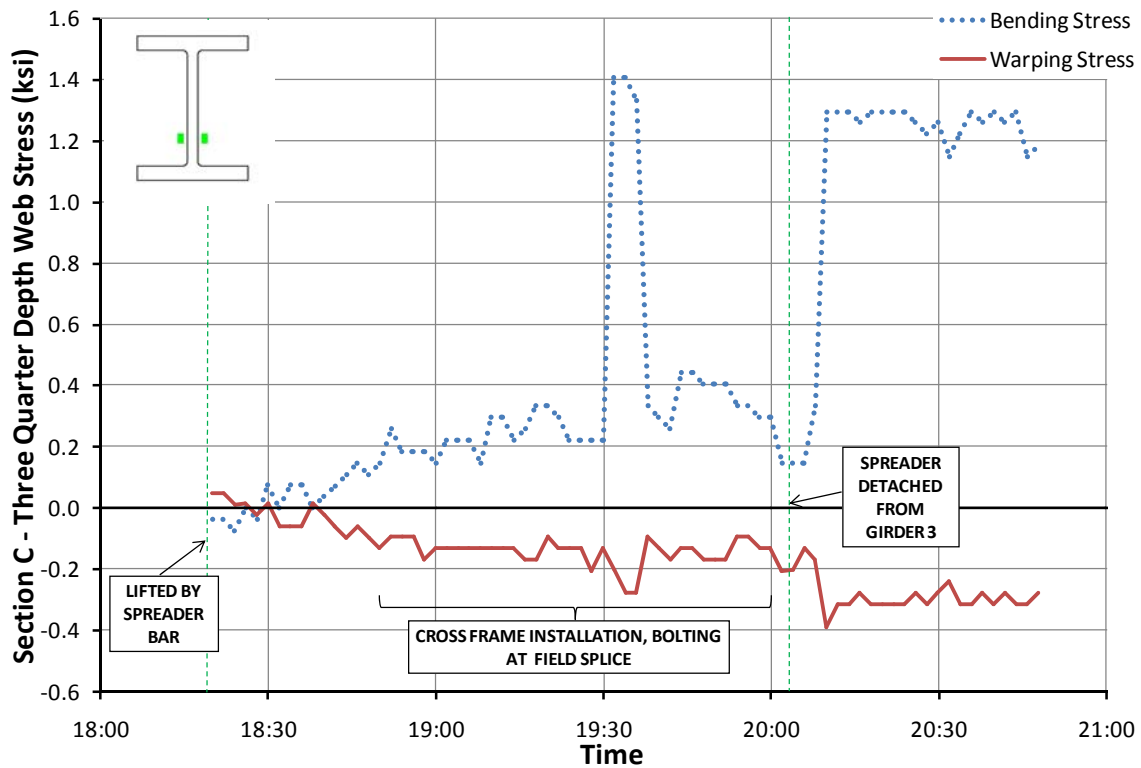
Figure D.8 Girder 3 Stress Change at Section C Three Quarter Depth of Web

D.3 SUMMARY

The stress change trends observed in the figures follow the same trends as the results for the flange gages presented in Chapter 3. As would be expected of a doubly symmetric girder with neutral axis located at mid-depth, the bending stress change at mid-depth of the web of Girder 3 is zero, as shown in Figure D.7. Other relevant trends and values can be seen from the graphs.

APPENDIX E
Parametric Study Tables

E.1 INTRODUCTION

The following appendix provides tables containing the values used to construct the figures showing the results of the parametric study in Chapter 5. Table E.1 and Table E.2 show how the eigenvalue is affected by altering the parameters investigated in the study. Table E.3 through Table E.10 show the effect of lift point location on the eigenvalue, as well as the unbraced length and maximum moment used to calculate C_L which is also shown. These values were calculated using Equation 1.1, Equation 1.5, Equation 1.6, and Equation 1.7.

E.2 PARAMETRIC STUDY TABLES

Effect of Parameters on Eigenvalue w/ Constant a/L = .25					
L/d = 15, b/d = .25		R = 500, b/d = .25		L/d = 15, R = 500	
R	λ	L/d	λ	b/d	λ
250	127.89	10	244.75	0.166667	68.43
300	127.30	15	125.60	0.25	125.60
400	126.22	20	52.48	0.333333	164.60
500	125.60	25	27.98		
600	125.24				
700	125.03				
800	124.89				
900	124.79				
1000	124.72				
1100	124.67				
1200	124.64				
1300	124.61				
1500	124.45				

Table E.1 Effect of Radius of Curvature, Span to Depth Ratio, and Flange Width to Depth Ratio on Eigenvalue

154

R = 500 ft, b/d = .25, L/d = 15, a/L = .1		
H (in)	λ	λ / λ_{30}
6	8.72	0.91
12	9.03	0.95
18	9.26	0.97
24	9.42	0.99
30	9.53	1.00
36	9.62	1.01
42	9.69	1.02
48	9.75	1.02
54	9.80	1.03
60	9.85	1.03

R = 500 ft, b/d = .25, L/d = 15, a/L = .25		
H (in)	λ	λ / λ_{30}
6	125.42	1.00
12	125.53	1.00
18	125.57	1.00
24	125.59	1.00
30	125.60	1.00
36	125.61	1.00
42	125.61	1.00
48	125.60	1.00
54	125.60	1.00
60	125.59	1.00

R = 500 ft, b/d = .25, L/d = 15, a/L = .4		
H (in)	λ	λ / λ_{30}
6	18.08	0.82
12	19.62	0.89
18	20.72	0.94
24	21.52	0.97
30	22.13	1.00
36	22.60	1.02
42	22.97	1.04
48	23.27	1.05
54	23.53	1.06
60	23.74	1.07

R = 500 ft, b/d = .25, L/d = 15, a/L = .2		
H (in)	λ	λ / λ_{30}
6	*	
12	*	
18	*	
24	55.36	1.00
30	55.60	1.00
36	55.78	1.00
42	55.92	1.01
48	56.03	1.01
54	56.11	1.01
60	56.16	1.01

R = 500 ft, b/d = .25, L/d = 15, a/L = .3		
H (in)	λ	λ / λ_{30}
6	52.40	0.93
12	54.13	0.96
18	55.11	0.98
24	55.71	0.99
30	56.12	1.00
36	56.41	1.01
42	56.63	1.01
48	56.80	1.01
54	56.93	1.01
60	57.04	1.02

Table E.2 Effect of Axis of Rotation Height on Eigenvalue

Parameters				
R =	250	ft		
L/d =	15			
b/d =	0.25			
L=	90	ft		

a/L	λ	L_b (ft)	M_{max} (k-ft)	C_L
0.1	9.08	72.0	218.61	0.90
0.15	19.88	63.0	145.74	1.06
0.2	56.71	54.0	72.87	1.17
0.225	115.61	49.5	73.78	2.09
0.25	127.89	45.0	91.09	2.41
0.275	91.42	40.5	110.21	1.73
0.3	61.8	36.0	131.16	1.12
0.35	37.46	31.5	178.53	0.72
0.4	22.86	36.0	233.18	0.74

Table E.3 Parametric Study R = 250'

Parameters				
R =	500	ft		
L/d =	15			
b/d =	0.25			
L=	90	ft		

a/L	λ	L_b (ft)	M_{max} (k-ft)	C_L
0.1	9.53	72.0	218.61	0.94
0.15	19.69	63.0	145.74	1.05
0.2	55.62	54.0	72.87	1.15
0.225	111.71	49.5	73.78	2.02
0.25	125.60	45.0	91.09	2.37
0.275	83.21	40.5	110.21	1.57
0.3	56.09	36.0	131.16	1.02
0.35	35.29	31.5	178.53	0.68
0.4	22.12	36.0	233.18	0.72

Table E.4 Parametric Study R = 500'

Parameters				
R =	1000	ft		
L/d =	15			
b/d =	0.25			
L=	90	ft		

a/L	λ	L_b (ft)	M_{max} (k-ft)	C_L
0.1	9.55	72.0	218.61	0.94
0.15	19.61	63.0	145.74	1.05
0.2	55.51	54.0	72.87	1.15
0.225	110.95	49.5	73.78	2.00
0.25	124.72	45.0	91.09	2.35
0.275	81.72	40.5	110.21	1.55
0.3	55.24	36.0	131.16	1.00
0.35	34.98	31.5	178.53	0.68
0.4	21.99	36.0	233.18	0.71

Table E.5 Parametric Study R = 1000'

Parameters				
R =	∞	ft		
L/d =	15			
b/d =	0.25			
L=	90	ft		

a/L	λ	L_b (ft)	M_{max} (k-ft)	C_L
0.1	9.55	72.0	218.61	0.95
0.15	19.59	63.0	145.74	1.05
0.2	55.49	54.0	72.87	1.15
0.225	110.74	49.5	73.78	2.00
0.25	124.45	45.0	91.09	2.35
0.275	81.38	40.5	110.21	1.54
0.3	55.06	36.0	131.16	1.00
0.35	34.92	31.5	178.53	0.68
0.4	21.96	36.0	233.18	0.71

Table E.6 Parametric Study Straight

	Parameters		
R =	500	ft	
L/d =	20		
b/d =	0.25		
L=	120	ft	

a/L	λ	L_b (ft)	M_max (k-ft)	C_L
0.1	3.50	96.0	388.63	0.94
0.15	7.22	84.0	259.09	1.07
0.2	20.91	72.0	129.54	1.23
0.225	47.24	66.0	131.16	2.44
0.25	52.48	60.0	161.93	2.87
0.275	34.21	54.0	195.93	1.90
0.3	21.10	48.0	233.18	1.14
0.35	12.12	42.0	317.38	0.71
0.4	8.20	48.0	414.54	0.79

Table E.7 Parametric Study L/d = 20

	Parameters		
R =	500	ft	
L/d =	25		
b/d =	0.25		
L=	150	ft	

a/L	λ	L_b (ft)	M_max (k-ft)	C_L
0.1	1.61	120.0	607.24	0.92
0.15	3.34	105.0	404.82	1.06
0.2	10.01	90.0	202.41	1.28
0.225	24.19	82.5	204.94	2.76
0.25	27.98	75.0	253.02	3.41
0.275	16.47	67.5	306.15	2.06
0.3	11.50	60.0	364.34	1.42
0.35	5.43	52.5	495.91	0.73
0.4	4.03	60.0	647.72	0.88

Table E.8 Parametric Study L/d = 25

Parameters				
R =	500	ft		
L/d =	15			
b/d =	0.1666667			
L=	90	ft		
a/L	λ	L$_b$ (ft)	M$_{max}$ (k-ft)	C$_L$
0.1	4.27	72.0	181.40	0.92
0.15	8.80	63.0	120.93	1.05
0.2	25.63	54.0	60.47	1.23
0.225	60.56	49.5	61.22	2.57
0.25	68.43	45.0	75.58	3.10
0.275	35.99	40.5	91.45	1.67
0.3	23.20	36.0	108.84	1.06
0.35	13.84	31.5	148.14	0.68
0.4	8.84	36.0	193.49	0.71

Table E.9 Parametric Study b/d = 1/6

Parameters				
R =	500	ft		
L/d =	15			
b/d =	0.3333333			
L=	90	ft		
a/L	λ	L$_b$ (ft)	M$_{max}$ (k-ft)	C$_L$
0.1	17.01	72.0	255.81	0.93
0.15	34.86	63.0	170.54	1.01
0.2	92.29	54.0	85.27	1.02
0.225	150.67	49.5	86.34	1.44
0.25	164.60	45.0	106.59	1.63
0.275	127.00	40.5	128.97	1.25
0.3	96.65	36.0	153.49	0.90
0.35	67.12	31.5	208.92	0.66
0.4	41.85	36.0	272.87	0.70

Table E.10 Parametric Study b/d = 1/3

E.3 SUMMARY

The calculated values of C_L are given in the presented tables. From observing the trends, Equation 5.2 was formulated to calculate the factor to adjust the Timoshenko critical buckling moment for the effects of girder lifting.

References

1. American Association of State Highway and Transportation Officials (AASHTO). (1980). *Guide specifications for horizontally curved bridges*, Washington, D.C.

2. American Association of State Highway and Transportation Officials (AASHTO). (1993). *Guide specifications for horizontally curved bridges*, Washington, D.C.

3. American Association of State Highway and Transportation Officials (AASHTO). (2003). *Guide specifications for horizontally curved bridges*, Washington, D.C.

4. American Association of State Highway and Transportation Officials (AASHTO). (2007). *AASHTO LRFD Bridge Design Specifications*, Washington, D.C.

5. American Institute of Steel Construction Inc.(AISC). (2005). *Steel construction manual, 13th edition*, The United States of America.

6. ANSYS, Finite element program users' manual, Version 11.0. (2007). ANSYS, Inc.

7. Beal, D. B., and Kissane, R. J. (1971). *First Interim Report on Research Project 42-1*, New York State Department of Transportation, Engineering Research and Development Bureau, Albany, New York.

8. Beal, D. B., and Kissane, R. J. (1971). *Second Interim Report on Research Project 42-1*, New York State Department of Transportation, Engineering Research and Development Bureau, Albany, New York.

9. Beal, D. B., and Kissane, R. J. (1972). *Third Interim Report on Research Project 42-1*, New York State Department of Transportation, Engineering Research and Development Bureau, Albany, New York.

10. Bradford, M. A., Uy, B., and Pi, Y. (2001). "Behaviour of unpropped composite girders curved in plan under construction loading." *Eng. Structures*, 23, 779-789.

11. Brennan, P.J. (1970). "Horizontally curved bridges first annual report: Analysis of horizontally curved bridges through three-dimensional mathematical model and small scale structural testing." *Syracuse Univ., First Annual Rep., Research Project HPR-2(111)*, Syracuse, N.Y.

12. Brennan, P.J. (1971). "Horizontally curved bridges second annual report: Analysis of Seekonk River Bridge small scale structure through three-dimensional mathematical

model and small scale structural testing." *Syracuse Univ., Second Annual Rep., Research Project HPR-2(111)*, Syracuse, N.Y.

13. Brennan, P.J. (1974). "Analysis and structural testing of a multiple configuration small scale horizontally curved highway bridge." *Syracuse Univ., Research Project HPR-2(111)*, Syracuse, N.Y.

14. Chavel, B. W., and Earls, C. J. (2006). "Construction of a horizontally curved steel I-girder bridge: Erection sequence." *J. Bridge Eng.*, 11(1), 81-90.

15. Chavel, B. W., and Earls, C. J. (2006). "Construction of a horizontally curved steel I-girder bridge: Inconsistent detailing." *J. Bridge Eng.*, 11(1), 91-98.

16. "Chapter 1: V-load analysis, an approximate procedure, simplified and extended for determining moments and shears in designing horizontally-curved open-frame highway bridges." (1984). *U.S.S. highway structures design handbook*, Vol. 1, United States Steel Corp., Pittsburgh, Pa.

17. Choo, K. M. (1987), Thesis presented to The University of Texas at Austin, May, "Buckling Program BASP for Use on a Microcomputer".

18. Culver, C. G., and Frampton, R. E. (1970). "Local instability of horizontally curved members." *J. Struct. Div.*, ASCE, 96(2), 245-265.

19. Culver, C. G., and Nasir, N. (1971). "Inelastic flange buckling of curved plate girders." *J. Struct. Div.*, ASCE, 97(4), 1239-1257.

20. Davidson, J. S., and Yoo, C. H. (1996). "Local buckling of curved I-girder flanges." *J. Struct. Engrg.*, ASCE, 122(8), 936-947.

21. Davidson, J. S., and Yoo, C. H. (2000). "Evaluation of strength formulations for horizontally curved flexural members." *J. Bridge Eng.*, 5(3), 200-207.

22. Davidson, J. S., Keller, M. A., and Yoo, C. H. (1996). "Cross-frame spacing and parametric effects in horizontally curved I-girder bridges." *J. Struct. Eng.*, ASCE, 122(9), 1089-1096.

23. Espinoza, O. (2007). *Measurements of Deformations and Stresses Due to Plate Out-of-Flatness in a Steel Twin Box Girder Bridge System.* Thesis, University of Texas.

24. Fiechtl, A. L., Fenves, G. L., and Frank, K. H. (1987). "Approximate analysis of horizontally curved girder bridges." *Final Rep. No. FHWA-TX-91-360-2F*, Center for Transportation Research, Texas Univ., Austin, Austin, Tex.

25. Galambos, T. V., Hajjar, J. F., Huang, W., Pulver, B. E., Leon, R. T., and Rudie, B. J. (2000). "Comparison of measured and computed stresses in a steel curved girder bridge." *J. Bridge Eng.*, 5(3), 191-199.

26. *Guide to Stability Design Criteria for Metal Structures*, 5th Ed. (1998) T. V. Galambos, ed., John Wiley & Sons, Inc., New York, N.Y.

27. Helwig, Todd A., Frank, Karl H., Yura, Joseph A. (1997). "Lateral-torsional buckling of singly symmetric I-beams." *J. of Struct. Eng.*, 123(9), 1172-1179.

28. Jung, S., and White, D. (2005). "Shear strength of horizontally curved steel I-girders – finite element analysis studies." *J. of Constructional Steel Research*, 62, 329-342.

29. Linzell, D., Hall, D., White, D. (2004). "Historical perspective on horizontally curved I-girder bridge design in the United States." *J. of Bridge Eng.*, 9(3), 218-229.

30. Linzell, D., Leon, R. T., and Zureick, A. (2004). "Experimental and analytical studies of horizontally curved steel I-girder bridge during erection." . *J. Bridge Eng.*, 9(6), 521-530.

31. Maneetes, H., and Linzell, D. (2003). "Cross-frame and lateral bracing influence on curved steel bridge free vibration response." *J. of Constructional Steel Research*, 59, 1101-1117.

32. Matchcad, Version 14.0 (2007). Parametric Technology Corporation.

33. McManus, P.F. (1971). "Lateral buckling of curved plate girders." Ph.D. thesis, Carnegie-Mellon Univ., Pittsburgh.

34. Mozer, J., and Culver, C. (1970). "Horizontally curved highway bridges – stability of curved plate girders." *Rep. No. P1, Research Project HPR-2(111),* Carnegie Mellon University, Pittsburgh.

35. Mozer, J., Ohlson, R., and Culver, C. (1971). "Horizontally curved highway bridges – stability of curved plate girders." *Rep. No. P2, Research Project HPR-2(111),* Carnegie Mellon University, Pittsburgh.

36. Mozer, J., Cook, J., and Culver, C. (1973). "Horizontally curved highway bridges – stability of curved plate girders." *Rep. No. P3, Research Project HPR-2(111),* Carnegie Mellon University, Pittsburgh.

37. Nasir, G. A. (1970). "Buckling of stiffened and unstiffened curved plate elements." Ph.D. thesis, Carnegie-Mellon Univ., Pittsburgh.

38. Structural Stability Research Council (SSRC) Task Group 14. (1991). "A look to the future." *Rep. of workshop on horizontally curved girders*, Chicago, 1-18.

39. Texas Department of Transportation (TXDOT). (2007). *Preferred Practices for Steel Bridge Design, Fabrication, and Erection*. Texas Steel Quality Council.

40. Timoshenko, S. P. and Gere, J. M. (1961). *Theory of Elastic Stability*. 2nd Ed., McGraw-Hill Book Company, Inc., New York

41. Yoo, C. H., and Davidson, J. S. (1997). "Yield interaction equations for nominal bending strength of curved I-girders." *J. Bridge Eng.*, 2(2), 37-44.

42. Zureick, A., and Naquib, R. (1999). "Horizontally curved steel I-girders state-of-the-art analysis methods." *J. Bridge Eng.*, 4(1), 38-47.

43. Zureick, A., Linzell, D., Leon, R. T., and Burrell, J. (2000). "Curved steel I-girder bridges: experimental and analytical studies." *Eng. Structures*, 22(2), 180-190.

44. Zureick, A., Naquib, R., and Yadlosky, J. M. (1994). "Curved steel bridge research project. Interim report I: Synthesis." *Rep. No. FHWA-RD-93-129*, HDR Engineering, Inc., Omaha, Neb.